AD_____

Award Number:
W81XWH-06-1-0765

TITLE:
Automation and Preclinical Evaluation of a Dedicated Emission
Mammotomography System for Fully 3-D Molecular Breast Imaging

PRINCIPAL INVESTIGATOR:
Spencer J. Cutler, MS

CONTRACTING ORGANIZATION:
Duke University
Durham, NC 27710

REPORT DATE:
October 2009

TYPE OF REPORT:
Annual Summary

PREPARED FOR: U.S. Army Medical Research and Materiel Command
               Fort Detrick, Maryland 21702-5012

DISTRIBUTION STATEMENT:

    ☑ Approved for public release; distribution unlimited

REPORT DOCUMENTATION PAGE

1. REPORT DATE *(DD-MM-YYYY)*	2. REPORT TYPE	3. DATES COVERED *(From - To)*
01-10-2009	Annual Summary	09-15-2006 to 09-14-2009

4. TITLE AND SUBTITLE	5a. CONTRACT NUMBER
Automation and Preclinical Evaluation of a Dedicated Emission Mammotomography System for Fully 3-D Molecular Breast Imaging	5b. GRANT NUMBER W81XWH-06-1-0765
	5c. PROGRAM ELEMENT NUMBER

6. AUTHOR(S)	5d. PROJECT NUMBER
Spencer J. Cutler	5e. TASK NUMBER
	5f. WORK UNIT NUMBER

7. PERFORMING ORGANIZATION NAME(S) AND ADDRESS(ES)	8. PERFORMING ORGANIZATION REPORT NUMBER
Duke University Office of Sponsored Programs Box 104135 Durham, NC 27708 E-mail: sjc12@duke.edu	

9. SPONSORING / MONITORING AGENCY NAME(S) AND ADDRESS(ES)	10. SPONSOR/MONITOR'S ACRONYM(S)
U.S. Army Medical Research and Materiel Command Fort Detrick, Maryland 21702-5012	11. SPONSOR/MONITOR'S REPORT NUMBER(S)

12. DISTRIBUTION / AVAILABILITY STATEMENT

Approved for public release; distribution unlimited

13. SUPPLEMENTARY NOTES

14. ABSTRACT

The overall objective of this proposal is to automate the acquisition sequences and optimize the performance of a 3-D dedicated SPECT breast imaging system. A retrospective study of 103 clinical MRI uncompressed breast scans was conducted to create surface renderings of the uncompressed breasts and analyze how to adapt existing acquisition orbits for varying breast shapes. Automated laser-guided SPECT contouring hardware and software were implemented. An observer-based study directly comparing 3D dedicated SPECT and 2D planar scintimammography was completed, concluding that statistically significantly ($p<0.05$) more lesions, smaller lesion sizes, and lesion locations were detected with dedicated breast SPECT than with compressed breast scintimammography. As a result of this work, the now fully automated SPECT-CT breast imaging system, with the ability to dynamically contour any sized breast, can potentially improve detection and characterization of small (<1cm) early stage breast cancer and provides a patient-flexible imaging modality ready for clinical testing.

15. SUBJECT TERMS
Nuclear Medicine Imaging, SPECT, Molecular Breast Imaging, Mammotomography

16. SECURITY CLASSIFICATION OF:			17. LIMITATION OF ABSTRACT	18. NUMBER OF PAGES	19a. NAME OF RESPONSIBLE PERSON USAMRMC
a. REPORT U	b. ABSTRACT U	c. THIS PAGE U	UU	63	19b. TELEPHONE NUMBER *(include area code)*

Table of Contents

Introduction

       Early detection of breast cancer significantly increases survival rates of diagnosed women. When a lesion is detected at an early stage there is less chance that the cancer has already spread to other parts of the body, treatments are generally more effective, and more treatment options exist. The current standard breast imaging technique is compressed breast X-ray mammography. This two-dimensional (2-D) imaging technique has several known limitations including patient discomfort from breast compression and the inability to separate overlying tissues, resulting in inconclusive mammograms, especially in women with dense fibroglandular tissue. In an effort to overcome these limitations, our lab has developed a novel single photon emission computed tomography (SPECT) system for uncompressed dedicated emission mammotomography molecular breast imaging. Using a compact, high performance gamma camera, the versatile positioning gantry allows for fully 3-D imaging anywhere within a hemispherical volume about the pendant breast, and overcomes physical proximity restrictions of standard clinical gamma cameras or compact systems without 3-D motion. Because spatial resolution degrades with increasing distance in SPECT, orbits that can closely contour the breast should yield images with the highest resolution. The independent SPECT subsystem has recently been coupled with a low dose cone-beam x-ray CT subsystem to allow co-registration of anatomical information from the CT images with the functional information of the SPECT images (Fig. 1).
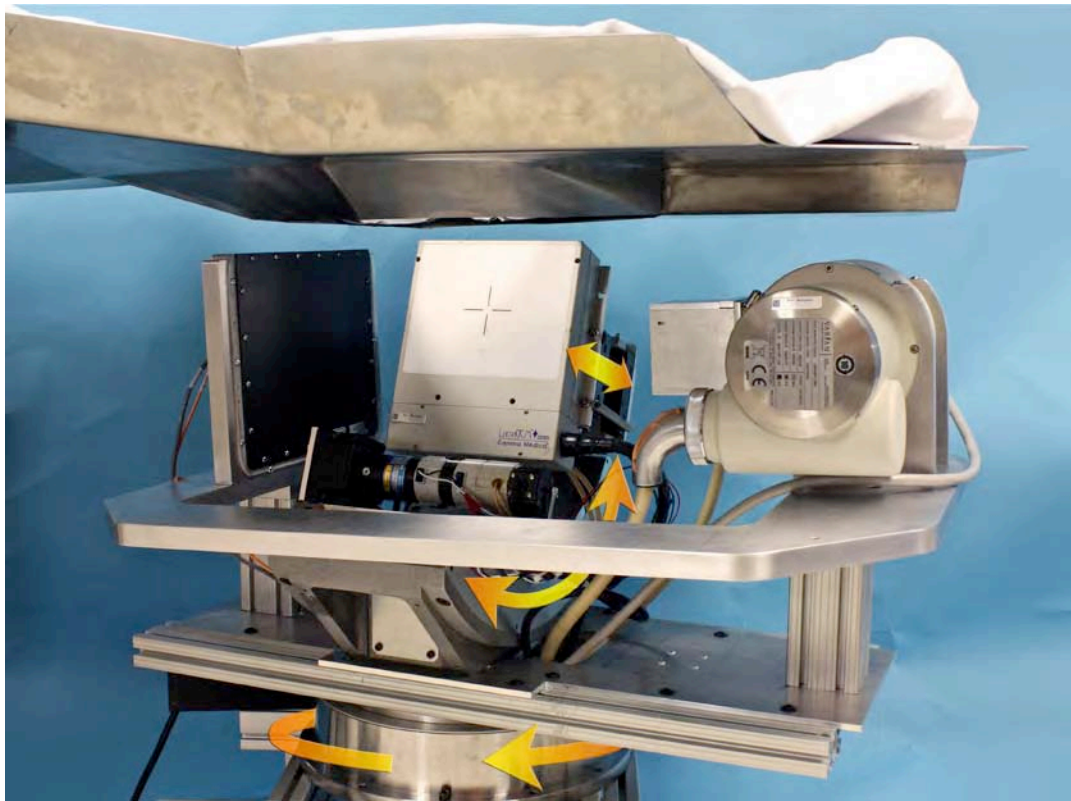

Fig. 1. Photograph of the prototype dual-modality dedicated breast imaging system. The SPECT system (center) is placed orthogonally to the CT tube (right) and digital flat-panel detector (left). The colored arrows illustrate system motions (azimuthal for SPECT and CT, and polar and ROR for the SPECT subsystem). A custom steel bed supports the patient as her pendant breast is imaged in the common field of view of the systems.

       While novel 3-D camera paths (orbits) have already been implemented with the system, the setup for these orbits is time consuming and not quickly adaptable to different breast shapes and sizes, and therefore is impractical for clinical imaging. The *overall objective* of this project is to fully automate and optimize the performance of the current prototype SPECT subsystem for enhanced clinical testing. The first step to automating the system is to better understand the variability in pendant breast shapes and

sizes. A study of existing clinical MRI breast data was conducted to create surface renderings of the uncompressed breast and analyze how to adapt existing orbits for varying breast shapes. Automation of SPECT orbits was achieved by designing and implementing laser sensors on the edge of the camera to maintain a close proximity to the breast while avoiding contact. As the final aim of this work, we compared the 3-D system with current 2-D nuclear medicine imaging techniques by using deformable breast models. 3-D imaging has the benefits of increased contrast, separation of overlapping structures, and patient comfort.

The main hypothesis of this work is that fully automated molecular breast imaging, with the ability to dynamically contour any sized breast, will improve detection and potentially in vivo characterization of small (<1cm) early stage breast cancer and provide a patient-flexible imaging modality ready for clinical testing. This final report of the training grant summarizes the work completed and major outcomes from the entire three-year period.

Body

Task 1. Conduct a retrospective study of breast volumes, shapes, and sizes using existing anonymized bilateral MRI breast data (Refer to Appendix A for original statement of work):

Similar to the SPECT-CT imaging procedure in our lab, clinical MRI images are acquired with patients lying prone, and provide views of a complete 3D uncompressed breast volume. An IRB approved study of 103 unique, existing clinical MRI breast data was conducted to obtain several parameters of uncompressed breasts to categorize shape and size, and in an effort to model an ideal range of contoured orbits that may be used with patients when they would come for a SPECT-CT scan. MRI scans were acquired previously during patients' regular visits to Duke Radiology, and represent a random sampling of high risk breast cancer patients at the Duke University Medical Center. The volumetric data were completely de-identified except for age.

Using open-source *OsiriX* imaging software, breast parameters were obtained for a database consisting of measured pendant breast sizes: nipple-to-chest wall distance, superior-inferior distance, and medial-lateral distance. From the 103 subjects, a total 202 uncompressed breasts were measured (several women had complete unilateral mastectomies and therefore only the remaining intact breast could be measured). Estimated volumes of the breasts were also calculated by first segmenting the images and then using voxel integration of the MRI images. Results are tabulated in Table I and the frequency distributions are displayed in Fig. 2. A weighted mean was calculated from the distributions. Moderate compression did occur for some larger breasts due to the fixed size of the MRI breast coil holes, and thus, true dimensions may have been slightly larger than measured.

A 3D surface rendering of the external breast shape was also generated in order to visualize challenges of contouring the breasts and to generally classify the data according to volumetric shape. These MRI breast image sets can thus be used as the digital "phantoms" when utilizing computer models for system development and orbit optimization purposes.

TABLE I: RESULTS FOR BREAST SIZES OBTAINED FROM MRI STUDIES

	Age (Years)	Nipple-to-Chest (cm)	Medial-Lateral (cm)	Superior-Inferior (cm)	Volume (mL)
Mean	45.8	8.4	10.8	14.3	720
Std Dev	7.6	2.7	2.4	1.6	415
Min	23	2.9	5.5	8	130
Max	66	19.1	16.9	17.3	2970

5

This study was helpful in visualizing the challenging variety of breast shapes and volumes to be contoured during the SPECT-CT scanning procedure. Encouragingly, the polar tilts possible with our current complex orbits will sufficiently sample the majority of the shapes and volumes observed, but the ROR cannot rely on linearly interpolated points to accurately contour the breast, as is currently the protocol.

While the relatively low number of subjects measured prevents us from making any broad statistical classifications for the general population of women, the minimum, maximum, and mean measurements provide a starting estimate of ROR ranges for the gamma camera in our lab. The mean measured volume was ~720mL. With this result, future breast phantom experiments should utilize ~700mL breast volumes as previous experiments in our lab have mainly used phantoms >1000mL in volume, under the assumption that larger breasts are more difficult to image. This work was presented at the both the *2008 DOD Era of Hope Meeting* and at the *2008 IEEE Medical Imaging Conference* in Dresden, Germany (Appendix B).
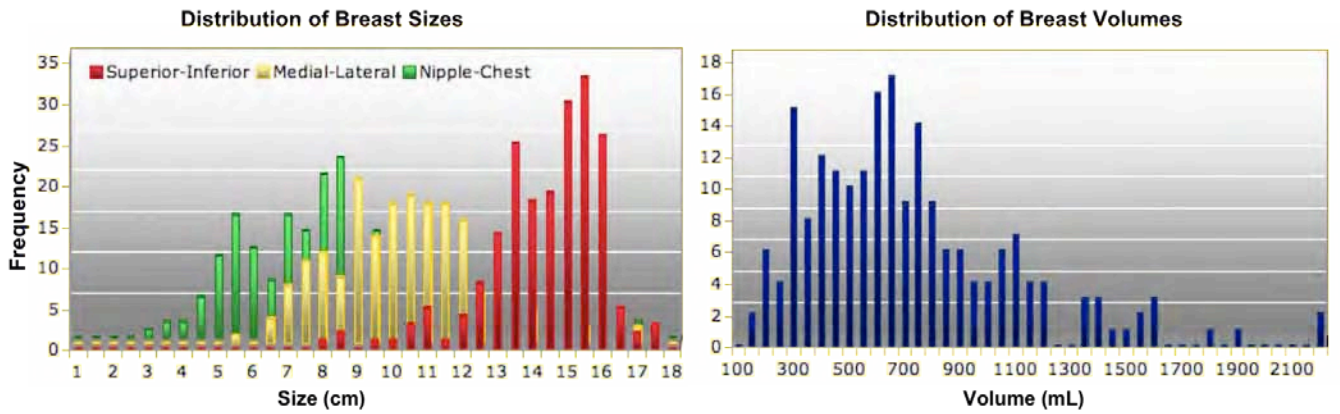

Fig. 2. Frequency distributions of measured breast parameters extracted from 202 individual MRI breast volumes. Breast volumes were estimated using segmentation and mesh volume calculations. The measured MRI breast sizes from this study retrospectively validate the range of shapes and sizes (250 to 1700 mL volumes) of custom shaped pendant breast phantoms available in the MMI Lab at Duke for preclinical research purposes.

Task 2. Implement 3-D fully automated contouring orbits for dedicated SPECT breast imaging (Refer to Appendix A for original statement of work)*:*

The unique pendant breast shapes observed in the MRI study reinforce the need to automate the ROR component of an orbit. We have developed and implemented a prototype dual-layer optical barrier for real-time laser feedback, automated ROR control for arbitrary breast contouring. A single optical barrier only reports that the barrier is compromised, without any knowledge of how close an object (e.g. breast surface) could be. Having a second layer at a known small distance from the camera face provides information that the object has penetrated the first layer, and is therefore within some distance to the camera, but that it has/has-not penetrated the second layer (Fig. 3). Commercially available, low divergence, ribbon laser feedback sensors (*Keyence*, 4cm wide lasers (model LV-51M) and detectors (LV-H300)) were purchased to implement this design. The upper layer consists of independent ribbon lasers that help identify the region on the camera face that has been penetrated, while the lower layer consists of a single, multiply reflected beam defining a virtual plane. In both layers, a receiver senses the signal intensity drop when the path of the beam is interrupted. Therefore, we can know that a breast is within ~1cm of the camera face, but not closer than 0.5 cm, and also at what relative location along the camera face. Changes in ROR to keep the camera close can thus easily be made. In the first year of

study, we successfully bench tested this principle with the ribbon lasers and measured a change in beam intensity even using our clear breast phantoms [1].
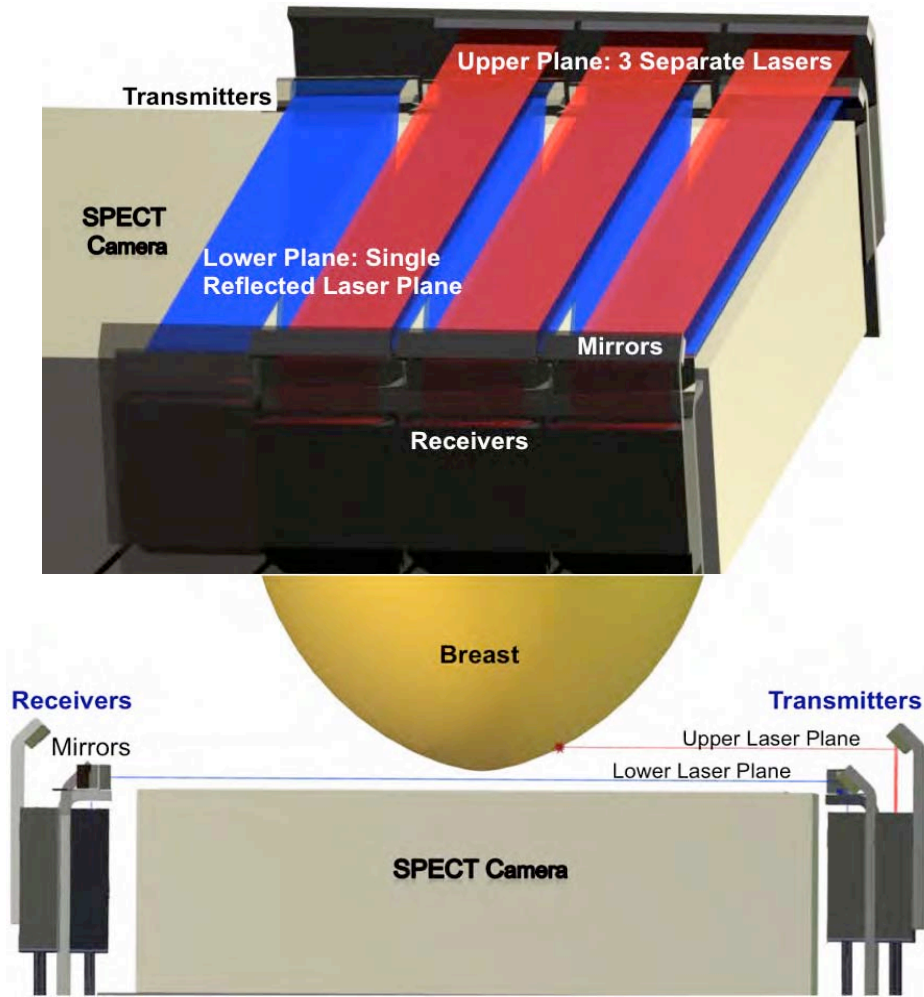

Fig. 3. (TOP) Automated breast surface contouring implementation using a dual-layer, low divergence, ribbon laser feedback sensor system mounted along the edges of the SPECT camera. The upper sensor layer (shown above in red) consists of three laser-detector pairs that identify the region on the camera face that has been penetrated, while the lower layer (shown above in blue) consists of a single, multiply reflected beam defining a virtual plane. (BOTTOM) Side view of the SPECT camera with breast penetrating the upper optical sensor plane.

Next, a working prototype was completed, allowing for dynamic laser-guided contouring for the SPECT system. A circuit was designed and built to power the sensor amplifiers and to channel the output receiver voltages (feedback) into the analog-to-digital converter of the Newport ESP7000 motion controller (Fig. 4). The data acquisition and motion control software were then modified to read in the digitized signals via an RS-232 serial interface, and new algorithms were created to position the camera based on the feedback from the lasers.
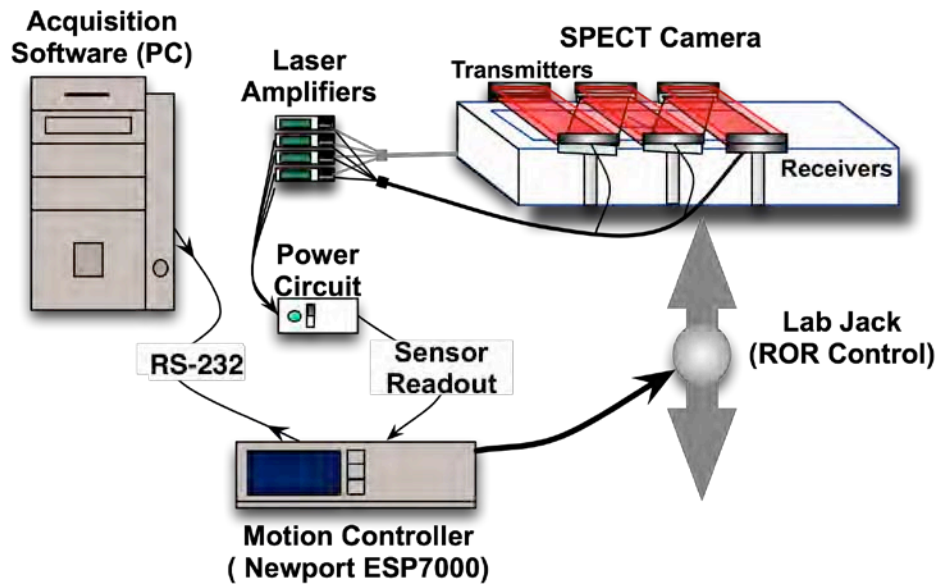
Fig. 4. Illustration of the laser contouring electronics and data flow. Sensors provide feedback to the acquisition software via the motion controller ADC, followed by the computer adjusting the ROR accordingly.

For the initial prototype, a 2x2 array of transmitter-receiver laser pairs were mounted on a thin piece of acrylic plastic, effectively creating two virtual planes with independent upper and lower positional data in each plane (APPENDIX B, Fig. 7, LEFT). After bench-top tests, this plastic sheet was adhered to the face of the SPECT camera, allowing functional scans with small additional attenuation due to the 6 mm thick plastic sheet. Using the functional prototype, we were able to automatically contour a 700 mL breast phantom with no initial setup time (APPENDIX B, Fig. 7, RIGHT). Trajectory repeatability for a fixed breast phantom was found to be very high, with only a few slight differences of less than 1 mm over multiple measurements. Compared to a manually defined contour with the lasers, the automated approach kept the camera significantly closer during the scan.

Automated orbits both simplify and significantly expedite the overall SPECT imaging process (Table II). Contoured acquisition times take slightly longer due to longer gantry motion times from the increased range of ROR motion. This should be improved combining the gantry's physical capability of moving faster, and smarter software algorithms to "anticipate" the next ROR position based on positional information from the upper sensor plane and the current polar tilt of the system. The elimination of manual orbit setup time, however, more than makes up for the minimally increased scan time.

TABLE II: EFFECT OF AUTOMATED CONTOURING ON TOTAL IMAGING TIME

	Setup Time	Acquisition Time	Total
Without Lasers	6-8 min	11 min	*17-19 min*
With Lasers	0 min	11-13 min	*11-13 min*

At the end of year 3, a second, more compact, vertically mounted laser hardware implementation was also designed and constructed, in an effort to reduce obstruction of the protruding mirrors and sensors. The hardware was first precisely modeled using 3D computed aided design software (Autodesk Inventor 2010, Autodesk, Inc.). I completed all of the fabrication myself in the newly opened Duke student machine shop. This proved to be much larger project than I had anticipated, but very educational and rewarding. The majority of the parts were manufactured from acrylic using a computer guided Universal Laser System (Fig. 5). Aluminum braces to mount the lasers to the system, and

8

housings for the electronics were made on a milling machine. First, surface reflecting mirrors (*Edmund Scientific*, Tonawanda, NY) were cut by hand and adhered to the acrylic. The assembled hardware was first tested on the bench-top and, after several iterations, secured permanently to then SPECT camera (Figs. 6-8). In this design the height of the mirrors can easily be adjusted to change the desired patient-camera separation distance. Further testing and optimizations of this design are still in progress and initial patient tests are planned in the near future.

      Overall we have successfully implemented a working dynamic contouring system, which both simplifies and expedites the overall SPECT imaging process. Automated orbits are highly robust, repeatable, and improve overall image quality. Future modifications will also focus on adjusting the polar tilt of the camera based on the positional information from the upper plane of sensors, as well as potentially adding ranging sensors to the tip of the SPECT camera to allow polar-tilts to dynamically contour a patient's protruding shoulder and chest area.

Fig. 5. A computer aided universal laser system was used to fabricate the vertical mounts and mirror supports from acrylic with a high degree of accuracy.

Fig. 6. Top-down photo of the finished system with anthropomorphic breast penetrating both planes of lasers. The top plane consists of three independent ribbon lasers, while the bottom plane uses a single transmitter/receiver pair to create a virtual plane through a series of reflections ~5-7mm above the camera surface.

Fig. 7. (LEFT) Side view of the breast penetrating separate 35 mm wide top-layer ribbon laser beams. (RIGHT) The height of the mirrors can be adjusted to vary the separation between the camera and breast.
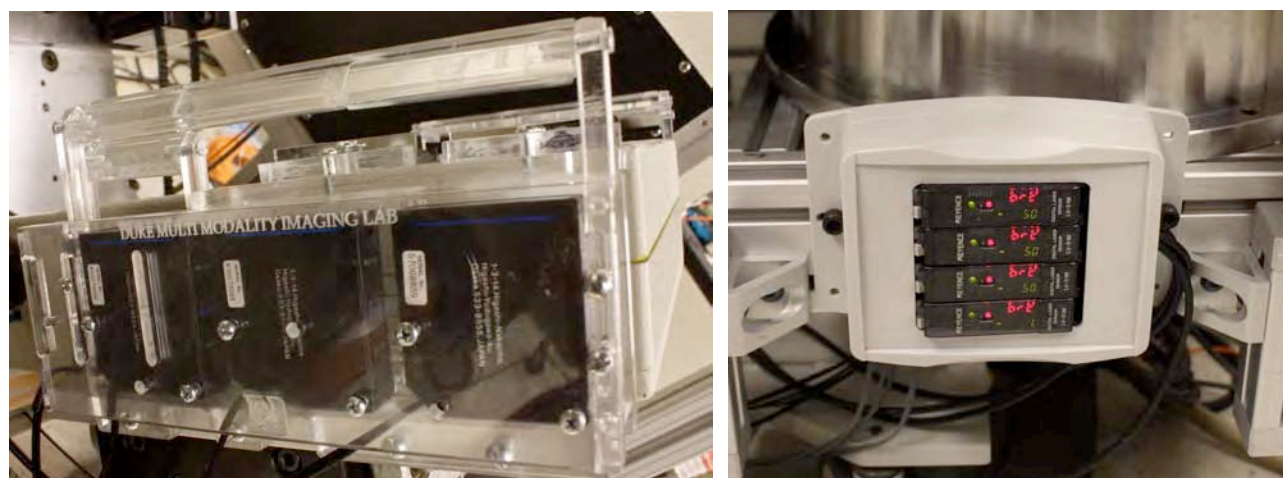

Fig. 8. (LEFT) Clear acrylic vertical laser supports with laser engraved lab logos. (RIGHT) A custom housing encasing the amplifiers is mounted at the bottom of the camera, providing beam intensity measurements.

Task 3. Compare performance of the fully automated 3-D SPECT system with 2-D scintimammography:

Scintimammography, a nuclear medicine planar acquisition technique, was one of the first dedicated breast imaging alternatives to mammography. Sometimes known as molecular breast imaging (MBI) or breast specific gamma imaging (BSGI), scintimammography utilizes a dedicated gamma camera to image concentrations of injected tumor-avid compounds that are usually ^{99m}Tc radiolabeled, such as the FDA approved imaging agent ^{99m}Tc-miraluma. Early scintimammography studies using conventional whole-body gamma cameras found a sensitivity and specificity of approximately 85% [2, 3], but sensitivity dropped significantly for tumors smaller than 1 cm [4]. To overcome this, several groups have investigated higher resolution, small field-of-view cameras for planar scintimammography [5-8]. Given the increased image information content and improved image characteristics, it is believed that the diagnostic accuracy of nuclear medicine images may further be improved when using 3D tomographic techniques [9].

Breast SPECT has been investigated for both traditional, contemporary clinical cameras [10-13] and dedicated camera systems [14, 15]. Breast imaging with clinical SPECT cameras is limited by the bulkiness of the large whole body cameras, which results in a larger ROR. Because spatial resolution degrades with increasing distance in SPECT, the larger ROR results in a fall-off in contrast and image

quality. The superiority of SPECT over planar scintimammography has been controversial with several studies showing less sensitivity for SPECT [16-18], potentially due to the non-optimized nature of the SPECT cameras, acquisitions, and simple back projection reconstruction algorithms.

The overall goal of Task 3 was to quantitatively and qualitatively compare 2D planar scintimammography (SCINTI) imaging of the breast under various degrees of compression with uncompressed, dedicated 3D SPECT using contoured acquisition trajectories through a limited observer study. The results of this study were presented at the *Fourth International Workshop on the Molecular Radiology of Breast Cancer (MRBC)* in Dresden, Germany, Oct 21-22, 2008. A Conference Proceedings publication containing the full methods and results is included in Appendix C, but an abbreviated summary follows.

A custom-built 500mL compressible anthropomorphic breast phantom (*Radiology Support Devices, Inc.,* Newport Beach, CA) containing small lesions was utilized to compare 2D and 3D breast imaging. Thin walled, latex based lesions (*Harvard Apparatus*, Holliston, MA), from 40 to 500uL volume, were arranged and suspended on a thin plastic sheet placed in the breast phantom were used to mimic breast lesions undergoing different degrees of compression (Appendix C, Fig. 2). Using our $16x20cm^2$ CZT-based gamma camera, ^{99m}Tc-scintimammography was performed for 10min imaging times for compression thicknesses of 6 (compressed) and 12cm (fully uncompressed) using a single mediolateral view. Dedicated breast SPECT was then performed for 10min using the uncompressed breast acquired with a simple tilted parallel beam (TPB) rotational acquisition and a complex 3D acquisition trajectory (PROJSINE). A total of 72 images were created with experimental variables including background breast composition, and low count (clinically relevant) and high count (low noise) images (Fig. 9). The radioactivity Lesion:Background concentration ratio was varied from 12:1 down to 3:1. A comparison between the two modalities was made in a limited observer study with 6 independent observers (2 nuclear medicine physicians and 4 medical physicists) analyzing reconstructed images for the smallest detectable lesion in these signal-known-exactly (SKE) cases. Image quality, based on lesion SNRs and contrasts, and sampled breast volume were also evaluated.
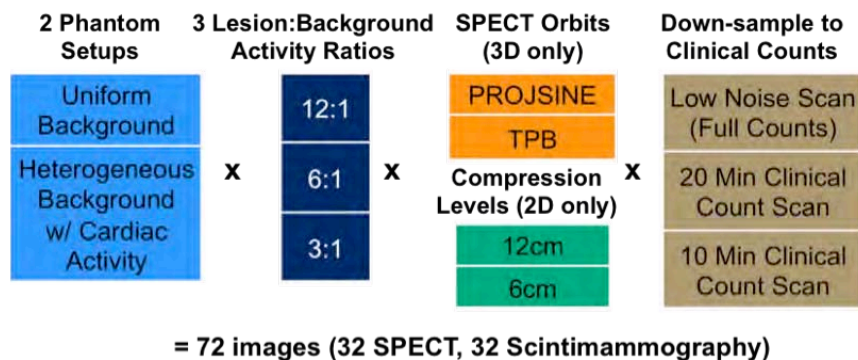

Fig. 9. Summary of the 72 different imaging parameters analyzed in this study.

The results of the observer study (see Appendix C) provide compelling motivation to continue development of 3D dedicated SPECT imaging. SPECT was able to both image a larger breast volume and view the anterior chest wall, where tumors may be otherwise missed in 2D imaging. SPECT and scintimammography were generally statistically equivalent at the highest lesion:background concentrations (12:1), except that chest wall lesions were detected in SPECT that were not in the field of view of scintimammography. At 6:1 and 3:1 simulated uptake, SPECT overall statistically outperformed scintimammography, seeing more and smaller lesions. In the heterogeneous compressed breast, scintimammography was equivalent to SPECT only at 6:1, but this could be explained by the overall higher noise.

Clinically equivalent count data indicate that with the current system, a 20 min SPECT scan may be preferable to 10 min in order to lower noise and boost sensitivity. A TPB SPECT acquisition trajectory generally outperformed PROJSINE despite conical distortion, with the caveat that this was a SKE observer study. Future random lesion placement observer studies are warranted to determine overall sensitivity in lesion detection. Under a wide range of measurement conditions, statistically significantly more lesions, smaller lesion sizes, and lesion locations can be detected with dedicated breast SPECT than with compressed breast scintimammography. Furthermore, whereas for scintimammography, few physical features or improvements can be further employed in the planar acquisition process, ongoing development to improve breast contouring (Task 2), as well as implementation of resolution modeling, attenuation and scatter correction for the SPECT imaging, we would expect SPECT image quality and observer detectability of smaller lesions to improve.

Task 4. Complete other aspects of breast cancer training program:
    As part of the training program I spent multiple days shadowing clinicians in the mammography, nuclear medicine, and breast oncology divisions at Duke University. I gained valuable insight into current clinical breast cancer detection and treatment methods. With the awarded funds, I had the opportunity to present this research at numerous international conferences as described in the Reportable Outcomes.
    In addition to the research in this proposal, I participated with other members of my lab in investigating absolute SPECT quantification, limited angle acquisition techniques, determining the effect of background contamination, and implementing non-traditional SPECT-CT acquisition trajectories. Abstracts describing this research are listed in the Reportable Outcomes and abstracts not attached in Years 1 and 2 are included in Appendices E-I.
    During the third year of this grant, I interviewed for and was invited to take a special two-semester course "Invention to Application," a combined venture by the Duke Biomedical Engineering Department and Fuqua School of Business at Duke. In the class, I worked with a small team of MBA and PhD students to commercialize biomedical technologies being developed at Duke. I learned about market research, the regulatory process, and gained valuable experience writing a business plan. Our team won the Duke Grand Engineering Challenge business plan competition and 1st place in the health track of the 2009 Duke Start-up Challenge. While the technologies we were given to pursue for the class were not related to breast cancer, the experience gained in transitioning research from the lab to a commercial application are directly applicable to the translation of the research in this proposal.
    In the second year of funding, I successfully passed my preliminary exam using much of the research from this predoctoral award as the basis of my proposed thesis. The preliminary exam consisted of submitting a 30-page NIH grant-format proposal and research summary, and then a three-hour oral examination discussing the proposed work. I also received a Master of Engineering degree in biomedical engineering independent of the process of the examination. I am currently compiling the research conducted in this proposal into my dissertation, "Evaluation of a Dedicated SPECT-CT Mammotomography System for Quantitative Hybrid Breast Imaging." With the aims of this proposal successfully completed, I am scheduled to defend my thesis in August of 2010, supported until then by funding from the renewed NIH grant (R01-CA96821-06) of my advisor, Martin Tornai.

Key Research Accomplishments

Summary: All tasks in this proposal have been completed. Sub tasks were completed in their entirety with the exception of subtask E of Task 4 (Prepare for and defend thesis), with a defense set in August of 2010.

Accomplishments:
- The MRI study proposed in Task 1, analyzing 103 uncompressed breast subjects, was completed with the approval of the Duke IRB. Breast metrics including nipple-chest wall distance, superior-inferior distance, medial-lateral distance, and total breast volumes were tabulated into a database (Appendix B).

- A fully functional dynamic laser-guided contouring system for the SPECT system was completed and found to significantly simplify the acquisition of 3D imaging trajectories (Task 2). Automated contouring has greatly simplified the SPECT imaging process and improved image quality. A portion of this research was presented at the *2008 IEEE Nuclear Science Symposium & Medical Imaging Conference*, Dresden, Germany, Oct. 2008 (Appendix B)*,* and a peer-reviewed paper is in progress.

- A phantom-based comparison of 3D dedicated breast SPECT and 2D scintimammography using embedded lesions of varying sizes and activity concentrations was successfully investigated. Results indicated that SPECT may be more sensitive than scintimammography at clinically low activity concentrations. This research was presented at the *Fourth International Workshop on the Molecular Radiology of Breast Cancer*, Dresden, Germany, Oct. 2008 (Appendix C)*,* and a peer-reviewed paper is in peer-review.

- The molecular SPECT imaging system was successfully coupled with an x-ray computed tomography system to create the world's first dual-modality SPECT/CT dedicated breast imaging system.

- The first observer based 3D contrast-detail study of the SPECT system was conducted and results were presented at the *2006 IEEE Nuclear Science Symposium and Medical Imaging Conference*, San Diego, CA, 29 Oct. - 4 Nov. and published in *Physics and Medicine and Biology* (Appendix D).

- The first successful SPECT patient and world's first dedicated breast SPECT-CT patient scans were conducted on the prototype mammotomography system during this grant period, with promising results, and further studies are planned under the renewed NIH grant (R01-CA96821-06).

- As part of the training program I shadowed clinicians in the mammography, nuclear medicine, and breast oncology divisions at Duke University, gaining valuable insight into current clinical breast cancer detection and treatment methods.

- In addition to the research outlined in this proposal, I collaborated with other members of my lab in investigating absolute SPECT quantification, determining the effect of background contamination, and implementing non-traditional SPECT-CT acquisition trajectories. A comprehensive list of presentations and publications is included in the Reportable Outcomes and abstracts from Year 3 (not previously included in annual reports) are included in Appendices E-I.

Reportable Outcomes

Peer Reviewed Publications:

- CN Brzymialkiewicz, MP Tornai, RL McKinley, **SJ Cutler**, JE Bowsher. "Performance of Dedicated Emission Mammotomography for Various Breast Shapes and Sizes." Phys. Med. Biol. **51**:5051-5064, 2006.

- P Madhav, JE Bowsher, **SJ Cutler**, and MP Tornai. "Characterizing the MTF in 3D for a Quantized SPECT Camera Having Arbitrary Trajectories," *Nuclear Science, IEEE Transactions on,* **56**: 661-670, 2009.

- **SJ Cutler**, KL Perez, MP Tornai. "Observer Detection Limits for a Dedicated SPECT Breast Imaging System." *Phys. Med. Biol.,* **55**:1903-1916, 2010.

Presentations, Published Abstracts, and Published Proceedings:

- **SJ Cutler**, KL Perez, MP Tornai. "3-D Contrast-Detail Analysis for Dedicated Emission Mammotomography." Presented at the *2006 Nucl. Sci. Symp. & Med. Imag. Conf.*, San Diego, CA, 29 Oct. – 4 Nov. 2006, and published in *2006 IEEE Nuclear Science Symposium & Medical Imaging Conference Record*, **5**:2954 – 2958.

- DJ Crotty, P Madhav, KL Perez, **SJ Cutler**, RL McKinley, T Wong, PK Marcom, MP Tornai. "3D molecular breast imaging with dedicated emission mammotomography: results of the first patient study." Presented at the *Duke University Center for Molecular and Biomolecular Imaging Meeting*, Durham, NC, 11-13 March, 2007 and *Duke Frontiers 2007*, Durham, NC, 14 May, 2007.

- P Madhav, DJ Crotty, **SJ Cutler**, KL Perez, RL McKinley, MP Tornai. "A novel dual-modality SPECT-CT system dedicated to 3D volumetric breast imaging." Presented at the *Duke University Center for Molecular and Biomolecular Imaging Meeting*, Durham, NC, 11-13 March, 2007 and *Duke Frontiers 2007*, Durham, NC, 14 May, 2007.

- MP Tornai, P Madhav, **SJ Cutler ,** DJ Crotty, RL McKinley, KL Perez, JE Bowsher. "Initial hybrid SPECT-CT system for dedicated fully-3D breast imaging." Presented at *The Society of Nucl. Med. 54th Annual Meeting*, Washington, DC, 2-6 June 2007, and published in *J. Nucl. Med.* **48**(5), 2007.

- MP Tornai, P Madhav, DJ Crotty, **SJ Cutler**, RL McKinley, KL Perez, JE Bowsher. "Application of volumetric molecular breast imaging with a dedicated SPECT-CT mammotomograph." Presented at the *49th Annual Meeting of the American Association of Physicists in Medicine*, Minneapolis, MN, 22-26 July 2007, and published in *Med. Phys.* **34**(6):2597.

- **SJ Cutler**, DJ Crotty, P Madhav, KL Perez, MP Tornai. "Comparison of reduced angle and fully 3D acquisition sequencing and trajectories for dual-modality mammotomography." Presented at the *2007 IEEE Nucl. Sci. Symposium & Med. Imaging Conference*, Honolulu, Hawaii, 28 Oct.-3 Nov. 2007 and published in *IEEE Conference Record NSS/MIC*, 6:4044-4050.

- KL Perez, **SJ Cutler**, and MP Tornai, "Empirical effects of angular sampling and background content on image quality in dedicated breast SPECT," Presented at the *2007 IEEE Nucl. Sci. Symposium & Med. Imaging Conference*, Honolulu, Hawaii, 28 Oct.-3 Nov. 2007 and published in *IEEE Conference Record NSS/MIC*. 4:3065-3069.

- P Madhav, DJ Crotty, KL Perez, **SJ Cutler**, RL McKinley, TZ Wong, MP Tornai. "Initial patient study with dedicated dual-modality SPECT-CT mammotomography." Presented at the *2007 IEEE Nucl. Sci. Symposium & Med. Imaging Conference*, Honolulu, Hawaii, 28 Oct.-3 Nov. 2007 and published in *IEEE Conference Record NSS/MIC*, 5:3781-3787.

- P Madhav, **SJ Cutler**, DJ Crotty, KL Perez, RL McKinley, MP Tornai. "3D volumetric breast imaging with a dedicated dual-modality SPECT-CT system." Presented at the *2007 Duke Biomedical Engineering Retreat*, Myrtle Beach, SC, 7-9 Oct. 2007.

- DJ Crotty, P Madhav, **SJ Cutler**, KL Perez, RL McKinley, MP Tornai, "Performance of a new dual-modality molecular-anatomical imaging system dedicated to breast cancer." Presented at the *2008 Duke Cancer Center Annual Meeting*, Durham, NC, 10 Mar. 2008.

- P Madhav, **SJ Cutler**, DJ Crotty, KL Perez, RL McKinley, PK Marcom, TZ Wong, MP Tornai. "Dedicated molecular and anatomical breast imaging - initial patient studies." Presented at the *2008 Duke Cancer Center Annual Meeting*, Durham, NC, 10 Mar. 2008.

- **SJ Cutler**, MP Tornai. "Automation and Preclinical Evaluation of a Dedicated Emission Mammotomography System for Fully 3-D Molecular Breast Imaging." Presented at the 2008 DOD Era of Hope Conference on Breast Cancer, Baltimore, MD, 25-28 Jun. 2008.

- P Madhav, **SJ Cutler**, DJ Crotty, KL Perez, RL McKinley, PK Marcom, T Wong, MP Tornai. "Pilot Patient Studies Using a Dedicated Dual-Modality SPECT-CT System for Breast Imaging." Presented at the *50th Annual Meeting of the American Association of Physicists in Medicine*, Houston, TX, 27-31 Jul. 2008.

- **SJ Cutler**, KL Perez, P Madhav, MP Tornai. "Comparison of 2D Scintimammography and 3D Dedicated Breast SPECT Using A Compressible Breast Phantom and Lesions of Varying Size and Tracer Uptake." Presented at the *Fourth International Workshop on the Molecular Radiology of Breast Cancer (MRBC),* Dresden, Germany, 20 - 21 Oct. 2008, and published in 2008 IEEE Nuclear Science Symposium & Medical Imaging Conference Record, 5640-5646.

- DJ Crotty, **SJ Cutler**, P Madhav, KL Perez, RL McKinley, MP Tornai. "Improved Chest Wall Imaging through Combined Complex Trajectories in Dedicated Dual Modality SPECT-CT Breast Molecular Imaging." Presented at the *Fourth International Workshop on the Molecular Radiology of Breast Cancer (MRBC),* Dresden, Germany, 20 - 21 Oct. 2008, and published in 2008 IEEE Medical Imaging Conference Record, 5650-5665.

- KL Perez, **SJ Cutler**, P Madhav, MP Tornai "Novel Patient Acquisition Trajectories for Optimized Dedicated Breast SPECT Imaging." Presented at the *Fourth International Workshop on the Molecular Radiology of Breast Cancer (MRBC),* Dresden, Germany, 20 - 21 Oct. 2008, and published in 2008 IEEE Medical Imaging Conference Record, 5629-5634.

- **SJ Cutler**, DJ Crotty, MP Tornai. "Dynamic Laser-Guided Contouring for Dedicated Emission Mammotomography." Presented at the *2008 IEEE Nuclear Science Symposium & Medical Imaging Conference*, Dresden, Germany, 19-25 Oct. 2008, and published in 2008 IEEE Nuclear Science Symposium & Medical Imaging Conference Record, 4789-4793.

- DJ Crotty, RL McKinley, P Madhav, **SJ Cutler**, MP Tornai. "Initial Investigation of Novel Trajectories to Improve Chest Wall Imaging in a Dedicated Breast Computed Tomography System." Presented at the 2009 SPIE Medical Imaging Conference, Orlando, FL, and published in 2009 Proc. SPIE: Physics of Medical Imaging, 72585L-10.

- KL Perez, **SJ Cutler**, P Madhav, MP Tornai "Towards Quantification of Dedicated Breast SPECT Using Non-Traditional Acquisition Trajectories." Presented at the *2009 Duke Cancer Center Annual Meeting*, Durham, NC, 05 Oct. 2009.

Awards/Honors

- IEEE 2006, 2007, 2008 Medical Imaging Conference Student Travel Awards (awarded on scientific merit of the submitted abstracts).

- This technology, as part of a dedicated breast SPECT-CT system, was chosen by Readers Digest (Mar 2008) as one of the top medical breakthroughs for 2008.

Conclusions

In an effort to characterize a range of breast shapes and sizes anticipated in the dedicated, uncompressed breast imaging paradigm, a retrospective study of breast shapes, sizes, and volumes provided useful guidelines for system and orbit optimization. Obtained parameters included measured nipple-to-chest wall (mean=8.4cm), superior-inferior (mean=10.8cm), medial-lateral distances (mean=14.3cm), and estimated breast volume (mean=720mL). The range of pendant breast shapes observed in the MRI study reinforce the need to automate the radius of rotation component of the dedicated breast SPECT orbit to closely contour to the wide variety of individual breast shapes. The published measurements (Appendix B) have proven useful numerous times in development of the prototype hybrid breast SPECT-CT gantry and bed, and are generally useful to all researchers designing systems for uncompressed breast imaging.

Dynamic laser-guided SPECT contouring hardware and software were successfully implemented. This straightforward, but effective dual-plane method for automated breast contouring has been shown to both simplify and expedite the overall SPECT imaging process. Automated orbits created using this prototype system are highly robust, repeatable, and improve overall image quality. The implementation of dynamic laser-guided contouring facilitates a smoother scanning process for ongoing clinical patient studies in the Duke Multi-modality Imaging Laboratory.

An observer-based study directly comparing 3D dedicated SPECT and 2D planar scintimammography was completed, concluding that statistically significantly (p<0.05) more lesions, smaller lesion sizes, and lesion locations were detected with dedicated breast SPECT than with compressed breast scintimammography. These results provide support the main hypothesis of this work that fully automated 3D molecular breast imaging has the potential to improve detection and potentially in vivo characterization of small (<1cm) early stage breast cancer.

The aims of this pre-doctoral proposal were successfully completed, and I'm scheduled to defend my thesis in August of 2010, supported until then by funding from the renewed NIH grant (R01-CA96821-06) of my advisor. I'm grateful to the DOD for funding me in this research, and I look forward to continuing a career in breast cancer imaging research. Conducting the research in this

proposal has proven to be worthwhile both scientifically and professionally. Many scientifically significant outcomes have resulted from this funding and the first clinical tests have shown initial promise of improving detectability of breast cancer, ultimately leading to increased survival.

References

[1]   MP Tornai, RL McKinley, SJ Cutler, DJ Crotty, and CN Brzymialkiewicz. "Anthropomorphic breast phantoms for preclinical imaging evaluation with emission or transmission imaging," *2005 Proc SPIE: Phys Med Imag,* vol. 5746, pp. 825-834, 2005.

[2]   R Taillefer. "The role of 99mTc-sestamibi and other conventional radiopharmaceuticals in breast cancer diagnosis," *Semin Nucl Med,* vol. 29, pp. 16-40, 1999.

[3]   AD Waxman. "The role of (99m)Tc methoxyisobutylisonitrile in imaging breast cancer," *Semin Nucl Med,* vol. 27, pp. 40-54, 1997.

[4]   A Tofani, R Sciuto, A Semprebene, A Festa, R Pasqualoni*, et al.* "99Tcm-MIBI scintimammography in 300 consecutive patients: factors that may affect accuracy," *Nucl Med Commun,* vol. 20, pp. 1113-21, 1999.

[5]   RF Brem, JA Rapelyea, G Zisman, K Mohtashemi, J Raub*, et al.* "Occult Breast Cancer: Scintimammography with High-Resolution Breast-specific Gamma Camera in Women at High Risk for Breast Cancer," *Radiology,* vol. 237, pp. 274-280, 2005.

[6]   CB Hruska, SW Phillips, DH Whaley, DJ Rhodes, and MK O'Connor. "Molecular breast imaging: use of a dual-head dedicated gamma camera to detect small breast tumors," *Ajr,* vol. 191, pp. 1805-15, 2008.

[7]   A Spanu, P Cottu, A Manca, F Chessa, D Sanna*, et al.* "Scintimammography with dedicated breast camera in unifocal and multifocal/multicentric primary breast cancer detection: a comparative study with SPECT," *Int J Oncol,* vol. 31, pp. 369-77, 2007.

[8]   MJ More, PJ Goodale, S Majewski, and MB Williams. "Evaluation of Gamma Cameras for Use in Dedicated Breast Imaging," *IEEE Trans. Nucl. Sci.,* vol. 53, pp. 2675-2679, 2006.

[9]   PJ La Riviere, X Pan, and BC Penney. "Ideal-observer analysis of lesion detectability in planar, conventional SPECT, and dedicated SPECT scintimammography using effective multi-dimensional smoothing," *IEEE Trans. Nucl. Sci.,* vol. 45, pp. 1273-1279, 1998.

[10]   H Wang, C Scarfone, KL Greer, RE Coleman, and RJ Jaszczak. "Prone breast tumor imaging using vertical axis-of-rotation (VAOR) SPECT systems: an initial study," *IEEE Trans. Nucl. Sci.,* vol. 44, pp. 1271-1276, 1997.

[11]   BC Pieper, JE Bowsher, MP Tornai, J Peter, and RJ Jasczak. "Breast tumor imaging using tiltable head SPECT cameras," *IEEE Trans Med Imaging,* vol. 48, pp. 1477-1492, 2001.

[12]   A Seret, M Defrise, and D Blocklet. "180 degree pinhole SPET with a tilted detector and OS-EM reconstruction: phantom studies and potential clinical applications," *European journal of nuclear medicine,* vol. 28, pp. 1836-41, 2001.

[13]   O Schillaci, R DanieIi, L Filippi, P Romano, E Cossu*, et al.* "Scintimammography with a Hybrid SPECT/CT Imaging System," *Anticancer research,* vol. 27, pp. 557-562, 2007.

[14]   M Singh and E Mumcuoglu. "Design of a CZT based breast SPECT system," *IEEE Trans. Nucl. Sci.,* vol. 45, pp. 1158-1165, 1998.

[15]   MP Tornai, JE Bowsher, CN Archer, J Peter, RJ Jaszczak*, et al.* "A 3D gantry single photon emission tomograph with hemispherical coverage for dedicated breast imaging," *Nucl. Instr. Meth. Phys. Res. A,* vol. 497, pp. 157-167, 2003.

[16]   R Tiling, K Tatsch, H Sommer, G Meyer, M Pechmann*, et al.* "Technetium-99m-sestamibi scintimammography for the detection of breast carcinoma: comparison between planar and SPECT imaging," *J Nucl Med,* vol. 39, pp. 849-56, 1998.

[17]   A Spanu, F Chessa, D Sanna, P Cottu, A Manca, *et al.* "Scintimammography with a high resolution dedicated breast camera in comparison with SPECT/CT in primary breast cancer detection," *Q J Nucl Med Mol Imaging,* vol. 53, pp. 271-80, 2009.

[18]   D Kieper, S Majewski, B Kross, V Popov, AG Weisenberger, *et al.* "Optimization of breast imaging procedure with dedicated compact gamma cameras," *Nucl. Instr. and Meth. A,* vol. 497, pp. 168-173, 2003.

Appendices

<div align="center">APPENDIX A
STATEMENT OF WORK</div>

Task 1   Conduct a retrospective study of breast volumes, shapes, and sizes using existing anonymized bilateral MRI breast data (Months 1-4):

    a. Acquire IRB approval to use already acquired MRI uncompressed breast data sets for 50-100 patients (Month 1).

    b. Extract the pendant breast sizes: nipple-chest wall distance, superior-inferior distance, medial-lateral distance, skin thickness, and obtain a rendering of external breast surface shape (Months 1-4).

    c. Tabulate metrics of distance measurements and classify the varying spectrum of pendant breast surfaces (Month 4).

Task 2   Implement 3-D fully automated contouring orbits for dedicated SPECT breast imaging (Months 3-16):

    a. Based on the results of Task 1, modify the existing basis set of orbits to account for challenges imposed by non-uniform breast shapes (Month 4).

    b. Develop and implement a series of optical or ultrasonic feedback sensors on the camera for dynamic contouring. Update software interface to implement real-time feedback from sensors (Months 3-12).

    c. Investigate dynamic acquisition robustness using anthropomorphic breast phantoms of varying size and shape, and compare reconstructed image quality to images acquired previously using manually defined orbits (Months 13-15).

Task 3   Compare performance of the fully automated 3-D SPECT system with 2-D scintimammography (Months 15-36):

    a. Characterize and optimize 3-D system using geometric phantoms and anthropomorphic breast and torso phantoms, acquiring data under various lesion-to-background concentration conditions, with and without patient shielding, and for a variety of automated complex orbits (Months 15-21).

    b. Assess reconstructed images for contrast, signal-to-noise ratio, artifacts, and lesion detectability for both low noise and clinical high noise count rates (Months 22-25).

    c. Utilize compressible breast phantom containing various lesions and in varying lesion-to-background ratios to acquire 2-D planar data under varying compressions for scintimammography as well as uncompressed breast 3-D tomographic imaging (Months 26-30).

    d. Conduct a limited observer study to evaluate reconstructed images for smallest lesion detectability under varying contrasts, noise levels, background uniformity, and patient shielding conditions (Months 31-36).

Task 4   Complete other aspects of breast cancer training program (Months 1-36):

    a. Clinical shadowing patients having breast cancer management (Nuclear Medicine Clinic, Mammography Clinic) (Months 1-12)

    b. Publish research work in peer-reviewed journals. (Months 1-36)

    c. Attend and present at local Duke Medical Center lectures and medical seminars related to breast cancer (Months 1-36)

    d. Attend and present work at international conferences: *DOD BCRP Era of Hope Meeting, IEEE Medical Imaging, Society of Nuclear Medicine, Radiological Society of North America,* and *San Antonio Breast Cancer Symposium*. (Months 1-36).

    e. Prepare for and defend thesis (Months 30-36)

IEEE 2008 Nuclear Science Symposium and Medical Imaging Conference
Conference Record

Dynamic Laser-Guided Contouring for Dedicated Emission Mammotomography

Spencer J. Cutler, *Member, IEEE*, Dominic J. Crotty, Martin P. Tornai, *Senior Member, IEEE*

Abstract–**The dedicated breast CZT-based SPECT imaging system in our lab implements novel 3D camera trajectories that can minimize breast-detector separation, thus improving resolution and image quality. Current trajectories are manually customized for each patient by measuring breast-detector separations at several positions and interpolating. This study seeks to transition from this manual method to an automated contouring solution for routine patient SPECT imaging, given the vast array of uncompressed breast shapes in women.**

In the initial effort to model "typical" SPECT camera trajectories for patients, a sub-study was conducted of 103 MRI breast data sets to categorize the shape and size of uncompressed, pendant breasts. Obtained parameters include measured nipple-to-chest wall (mean=8.4cm), superior-inferior (mean=10.8cm), medial-lateral distances (mean=14.3cm), and estimated breast volume (mean=720mL). These images will be used as digital "phantoms" when utilizing computer models for orbit optimization and system development purposes.

Automated breast surface contouring is implemented using a dual-layer, low divergence, ribbon laser feedback sensor system mounted along the edge of the SPECT camera. The upper and lower sensor layers consist of two laser-detector pairs that identify the region on the camera face that has been penetrated, defining a virtual plane. In both layers, receivers sense reduced signal intensity when the beam path is interrupted by the breast surface. The ROR can then be automatically adjusted such that the breast is within ~1cm of the camera face, but no closer than 0.5cm, thus safely keeping the camera face as close to breast as possible. Robustness of the contouring system is assessed using flexible anthropomorphic breast phantoms to model various pendant breast shapes and sizes. Initial results indicate that dynamic contouring both improves image quality and potentially adds comfort to the patient by shortening scan setup time.

I. INTRODUCTION

Our lab has developed a novel single photon emission computed tomography (SPECT) system that is now coupled with a CT system, allowing for uncompressed 3D dedicated SPECT-CT molecular breast imaging or "mammotomography" [1, 2]. The current prototype system includes a cadmium zinc telluride (CZT) based compact gamma camera (*LumaGEM^{TM} 3200S, Gamma Medica,* Northridge, CA) with 2.5 mm discrete pixels, a measured mean energy resolution of 6.8 % FWHM at 140 keV, and sensitivity of 37.9 cps/MBq [3]. The gantry consists of a goniometric cradle, providing polar tilt; a motorized laboratory jack for radius-of-rotation (ROR) control; and a rotational stage for azimuthal positioning. Image acquisition and gantry movement are synchronized and precisely computer controlled. This versatile positioning gantry allows for fully 3D imaging anywhere within a hemispherical volume about the pendant breast and overcomes physical proximity restrictions of standard clinical gamma cameras or compact systems without 3D motion [4].

Novel acquisition orbits are currently defined by creating a file listing the ROR, polar tilt angle, and rotation degree for each desired projection. Polar tilt and rotation angles have limits mostly defined by the patient bed and can be quickly defined using existing software algorithms developed in the lab for a number of complex orbits. The ROR measurements essential for close contouring, however, are more complex to define for a non-uniform object. To closely contour a non-uniform uncompressed breast currently requires first manually moving the camera to several positions around the breast, taking measurements, and interpolating the points around the breast. Even for a stationary phantom this process can become time consuming, and any movement of the system or phantom requires adjustments to the orbit file. This study seeks to transition from this manual method to an automated contouring solution for routine patient SPECT imaging, given the vast array of uncompressed breast shapes in women.

This work is divided into two parts. First, in an effort to model "ideal" SPECT camera trajectories for patients, a study was conducted of retrospective MRI breast data to analyze the shape and size of uncompressed, pendant breasts. Second, a prototype automated breast surface contouring is implemented using a dual-layer, low divergence, ribbon laser feedback sensor system mounted along the edge of the SPECT camera.

II. MRI STUDY

Similar to the SPECT-CT imaging procedure in our lab, clinical MRI images are acquired with patients lying prone, and provide views of a complete 3D uncompressed breast volume. An IRB approved study of 103 unique, existing clinical MRI breast data was conducted to obtain several parameters of uncompressed breasts to categorize shape and size, and in an effort to model an ideal range of contoured orbits that may be used with patients when they would come
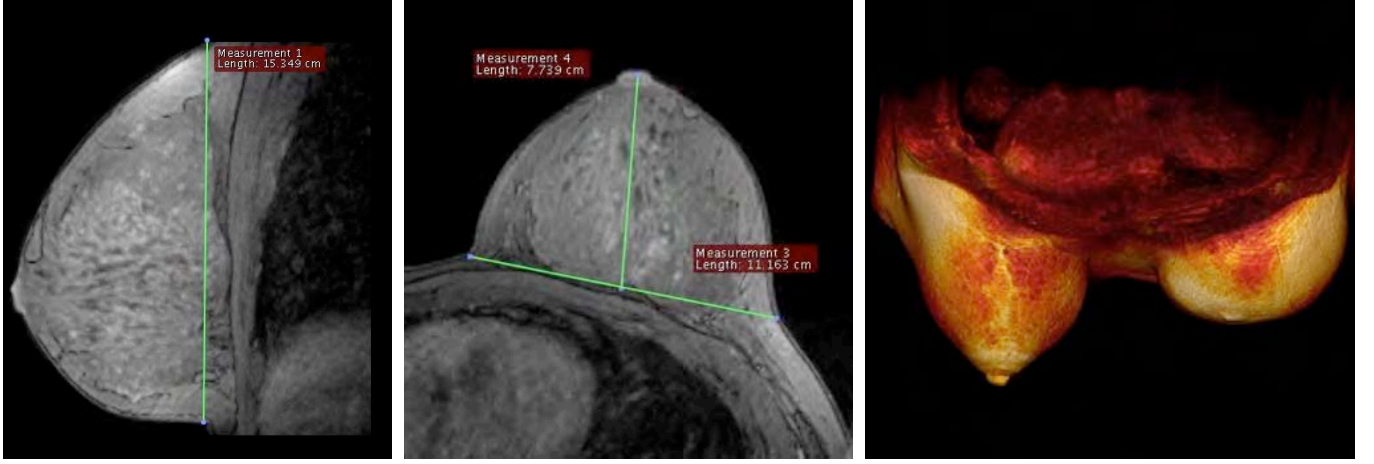
Fig. 1. Sample breast MRI sagittal (LEFT) and transverse (MIDDLE) slices with illustrated superior-inferior, nipple-chest, and medial-lateral measurements. A volumetric rendering (RIGHT) was also created for each subject.

for a SPECT-CT scan. MRI scans were acquired previously during patients' regular visits to Duke Radiology, and represent a random sampling of high risk breast cancer patients at the Duke University Medical Center. The volumetric data were completely de-identified except for age.

Using open-source *OsiriX* imaging software [5], breast parameters were obtained for a database consisting of measured pendant breast sizes: nipple-to-chest wall distance, superior-inferior distance, and medial-lateral distance (Fig. 1). From the 103 subjects, a total 202 uncompressed breasts were measured (several women had complete unilateral mastectomies and therefore only the remaining intact breast could be measured). Estimated volumes of the breasts were also calculated by first segmenting the images and then using voxel integration of the MRI images. Results are tabulated in Table I and the frequency distributions are displayed in Fig. 2. A weighted mean was calculated from the distributions. Moderate compression did occur for some larger breasts due to the fixed size of the MRI breast coil holes, and thus, true dimensions may have been slightly larger than measured.

A 3D surface rendering of the external breast shape was also generated in order to visualize challenges of contouring the breasts (Fig. 1, RIGHT) and to generally classify the data

according to volumetric shape (Fig. 3). These MRI breast image sets can thus be used as the digital "phantoms" when utilizing computer models for system development and orbit optimization purposes (Fig. 4).

TABLE I: RESULTS FOR BREAST SIZES OBTAINED FROM MRI STUDIES

	Age (Yr)	Nipple-to-Chest (cm)	Medial-Lateral (cm)	Superior-Inferior (cm)	Vol. (mL)
Mean	45.8	8.4	10.8	14.3	720
Std Dev	7.6	2.7	2.4	1.6	415
Min	23	2.9	5.5	8	130
Max	66	19.1	16.9	17.3	2970

This study was helpful in visualizing the challenging variety of breast shapes and volumes to be contoured during the SPECT-CmT scanning procedure. Encouragingly, the polar tilts possible with our current complex orbits (Fig. 4) will sufficiently sample the majority of the shapes and volumes observed, but the ROR cannot rely on linearly interpolated points to accurately contour the breast, as is currently the protocol.
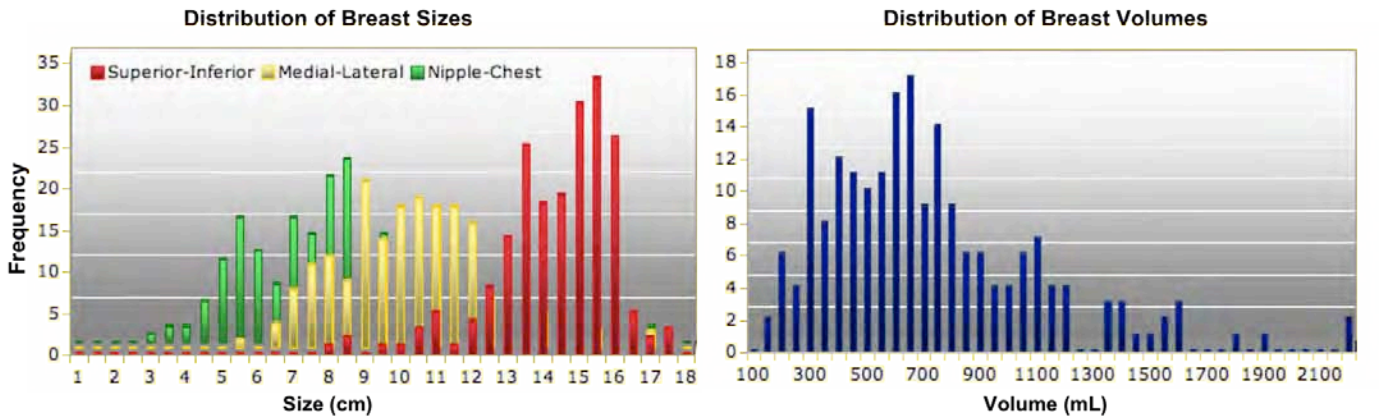

Fig. 2. Frequency distributions of measured breast parameters extracted from 202 individual MRI breast volumes. Breast volumes were estimated using segmentation and mesh volume calculations.
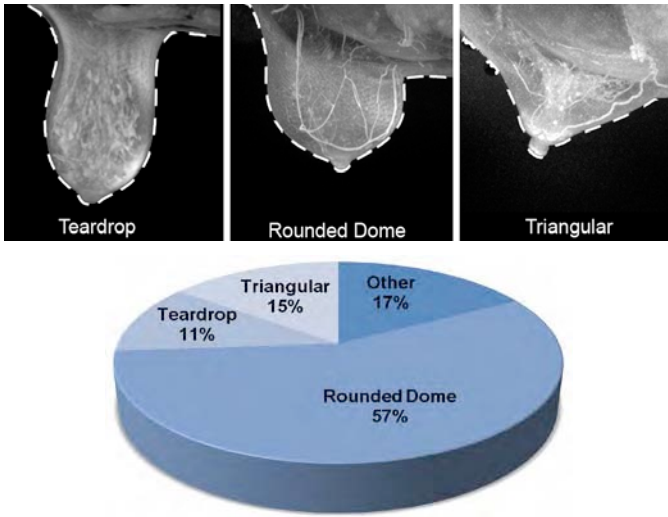
Fig. 3. (TOP) Representative examples of shape labels used to classify each subject. (BOTTOM) Distribution of general breast shapes over the 103 subjects. The "Other" category includes mastectomy and miscellaneous shaped breasts that didn't fit into the other three general classifications.
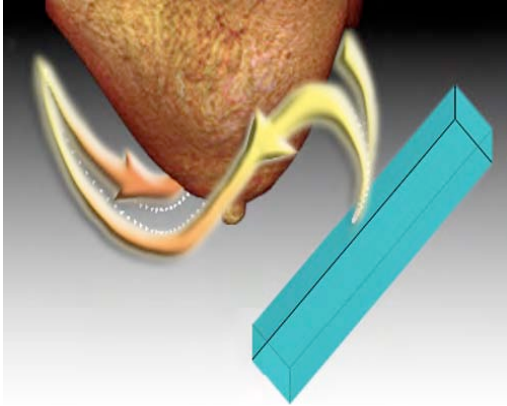

Fig. 4. A complex projected sine wave (PROJSINE) imaging acquisition orbit shown about a volume rendered digital breast "phantom"

While the relatively low number of subjects measured prevents us from making any broad statistical classifications for the general population of women, the minimum, maximum, and mean measurements provide a starting estimate of ROR ranges for the gamma camera in our lab.

Prior to this study, one compressible and six incompressible breast phantoms were fabricated to our general specifications at *Radiology Support Devices, Inc.* (*RSD, Inc.*, Newport Beach, CA) [6]. These phantoms vary in shape and overall fillable volume, and were molded to resemble prone or pendant breasts. The measured MRI breast sizes from this study retrospectively validate the range of shapes and sizes of these custom shaped pendant breast phantoms. The compressible phantom dimensions are close to the mean value measurements of the MRI subjects, and the incompressible phantoms allow us to physically test from minimum to maximum extremities.

III. DYNAMIC LASER-GUIDED CONTOURING IMPLEMENTATION

The unique pendant breast shapes observed in the MRI study reinforce the need to automate the ROR component of an orbit. We have developed and implemented a prototype dual-layer optical barrier for real-time laser feedback, automated ROR control for arbitrary breast contouring. A single optical barrier only reports that the barrier is compromised, without any knowledge of how close an object (e.g. breast surface) could be. Having a second layer at a known small distance from the camera face provides information that the object has penetrated the first layer, and is therefore within some distance to the camera, but that it has/has-not penetrated the second layer (Fig. 5). Commercially available, low divergence, ribbon laser feedback sensors (*Keyence*, 4cm wide lasers (model LV-51M) and detectors (LV-H300)) were purchased to implement this design. The upper layer consists of independent ribbon lasers that help identify the region on the camera face that has been penetrated, while the lower layer consists of a single, multiply reflected beam defining a virtual plane. In both layers, a receiver senses the signal intensity drop when the path of the beam is interrupted. Therefore, we can know that a breast is within ~1cm of the camera face, but not closer than 0.5 cm,
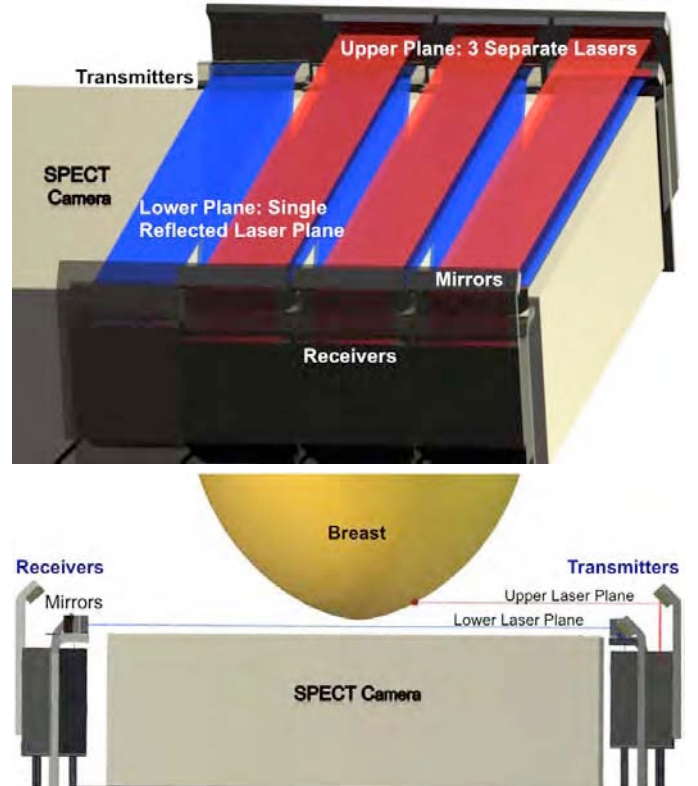

Fig. 5. (TOP) Automated breast surface contouring implementation using a dual-layer, low divergence, ribbon laser feedback sensor system mounted along the edges of the SPECT camera. The upper sensor layer (shown above in red) consists of three laser-detector pairs that identify the region on the camera face that has been penetrated, while the lower layer (shown above in blue) consists of a single, multiply reflected beam defining a virtual plane. (BOTTOM) Side view of the SPECT camera with breast penetrating the upper optical sensor plane.

and also at what relative location along the camera face. Changes in ROR to keep the camera close can thus easily be made. We successfully bench tested this principle with the ribbon lasers and measured a change in beam intensity even using our clear breast phantoms [6].

Next, a working prototype was completed, allowing for dynamic laser-guided contouring for the SPECT system. A circuit was designed and built to power the sensor amplifiers and to channel the output receiver voltages (feedback) into the analog-to-digital converter of the Newport ESP7000 motion controller (Fig. 6). The data acquisition and motion control software were then modified to read in the digitized signals via an RS-232 serial interface, and new algorithms were created to position the camera based on the feedback from the lasers.
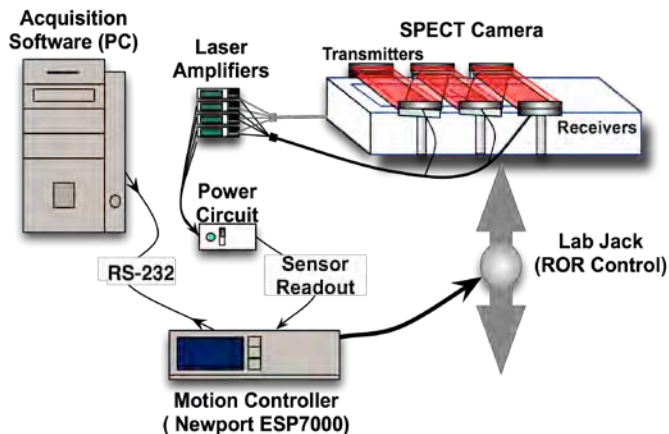
Fig. 6. Illustration of the laser contouring electronics and data flow. Sensors provide feedback to the acquisition software via the motion controller ADC, followed by the computer adjusting the ROR accordingly.

For the initial prototype, a 2x2 array of transmitter-receiver laser pairs were mounted on a thin piece of acrylic plastic, effectively creating two virtual planes with independent upper and lower positional data in each plane (Fig. 7, LEFT). After bench-top tests, this plastic sheet was adhered to the face of the SPECT camera, allowing functional scans with small additional attenuation due to the 6 mm thick plastic sheet.
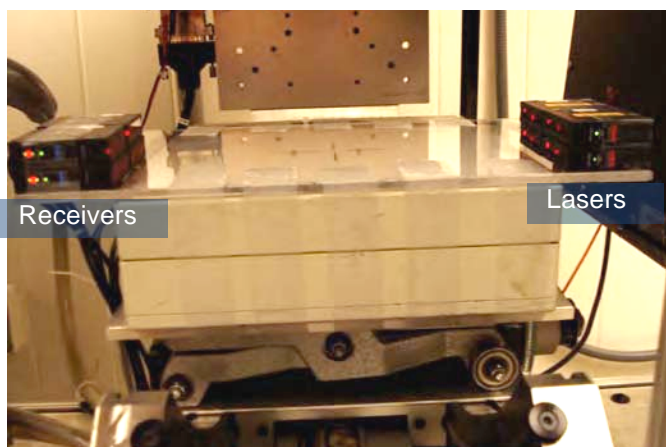
Using the functional prototype, we were able to automatically contour a 700 mL breast phantom with no initial setup time (Fig. 7, RIGHT). Trajectory repeatability for a fixed breast phantom was found to be very high, with only a few slight differences of less than 1 mm over multiple measurements. Compared to a manually defined contour with the lasers, the automated approach kept the camera significantly closer during the scan (Fig. 8).
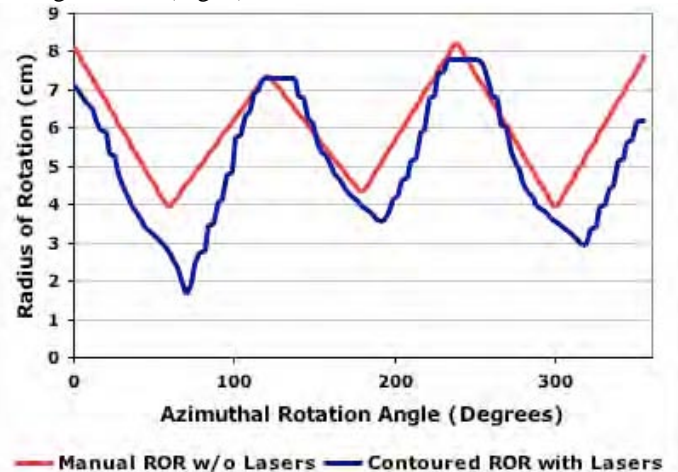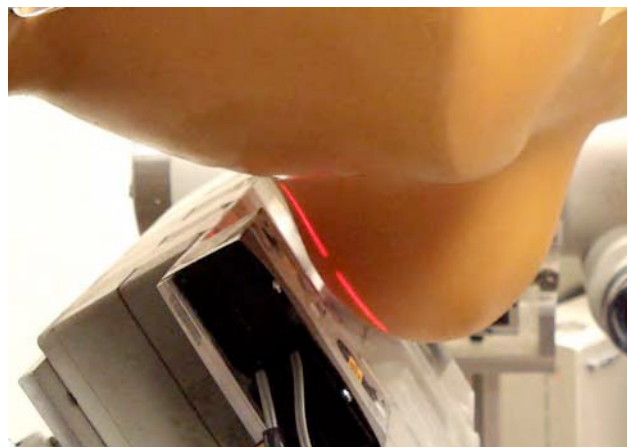

Fig. 8. 360° SPECT radius-of-rotation (ROR) trajectories about a 700 mL breast phantom. Laser guided contouring (blue) keeps the camera significantly closer to the breast (smaller ROR is better) during the scan compared to the manually created orbit (red)

Mini-cold rod image data, acquired prior to the sensor implementation, illustrate the proof-of-principle distance-dependant fall-off in spatial resolution with varying the radii-of-rotation. The 2.6 cm long rods were arranged in six sectors of equal diameters of 4.7, 3.9, 3.1, 2.3, 1.5, and 1.1 mm, on a pitch of twice their diameters. 15 mCi of 99mTc in water filled the interstitial spaces. The phantom was suspended vertically with the mini-rods in the center of the camera's field of view and parallel to the camera surface. The cold rods were first imaged as close as possible to the camera (4.4 cm constant ROR), and then with the camera backed away to a 7

Fig. 7. (LEFT) Dual-layer prototype ribbon laser *(Keyence* Model HV300*)* contouring system attached to face of the SPECT camera. Sensor outputs are channeled through an ADC into the gantry motion controller (*Newport* ESP7000) that monitors and adjusts the ROR accordingly. (RIGHT) Separate 35 mm wide top-layer ribbon laser beams are seen on the breast phantom skin, as the camera dynamically contours at a minimal radius of rotation to improve resolution and image quality.

cm ROR. Spatial resolution and contrast degradation are evident with increasing ROR (Fig. 9). The 4.7 and 3.9mm rods are visible in both cases, but the 3.1 mm rods are distinguishable only with the closest contouring (4.4 cm) ROR. Thus we anticipate that automated close contouring will improve spatial resolution, especially with concomitant incorporation of resolution modeling using the feedback ROR data.
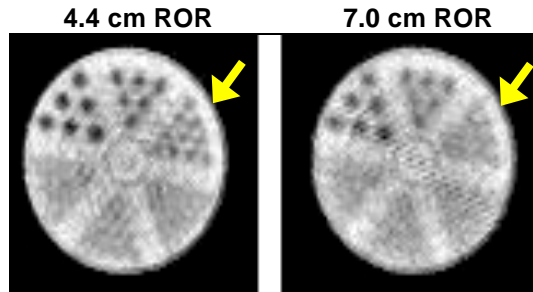

4.4 cm ROR   **7.0 cm ROR**

Fig. 9. Proof-of-principle reconstructed mini-cold rod image data illustrating the distance-dependant fall-off in spatial resolution with ROR that differ by only 2.6 cm. The largest 4.7 and 3.9 mm rods are visible in both cases, but the 3.1 mm rods (yellow arrow) are distinguishable only with the closest contouring (4.4 cm) ROR.

Automated orbits have been shown to both simplify and significantly expedite the overall SPECT imaging process (Table II). Contoured acquisition times take slightly longer due to longer gantry motion times from the increased range of ROR motion. This should be improved combining the gantry's physical capability of moving faster, and smarter software algorithms to "anticipate" the next ROR position based on positional information from the upper sensor plane and the current polar tilt of the system. The elimination of manual orbit setup time, however, more than makes up for the minimally increased scan time.

TABLE II: EFFECT OF AUTOMATED CONTOURING ON TOTAL IMAGING TIME

	Setup Time	Acquisition Time	Total
Without Lasers	6-8 min	11 min	*17-19 min*
With Lasers	0 min	11-13 min	*11-13 min*

A permanent fixed hardware design is in progress with the sensors mounted vertically on the sides of the camera (Fig. 5) and then reflected across the face in order to minimize obstructing area of the protruding sensors. This is important to avoid contact with the patient or obscuring the CT-cone beam mounted orthogonal to the SPECT system. Future modifications will also focus on adjusting the polar tilt of the camera based on the positional information from the upper plane of sensors, as well as potentially adding ranging sensors to the tip of the SPECT camera to allow polar-tilts to dynamically contour a patient's protruding shoulder and chest area.

IV. CONCLUSIONS

In an effort to characterize a range of breast shapes and sizes anticipated in the dedicated, uncompressed breast imaging paradigm, a retrospective study of breast shapes, sizes, and volumes provided useful guidelines for system and orbit optimization. The range of pendant breast shapes observed in the MRI study reinforce the need to automate the radius of rotation component of the dedicated breast SPECT orbit to contour to the wide variety of individual breast shapes. A simple, but effective method for automated dynamic laser-guided contouring system has been shown to both simplify and expedite the overall SPECT imaging process. A dual-layered system was implemented to allow modest determination of breast distance in addition to utilizing the optical barrier for safety (i.e. collision avoidance) concerns. Automated orbits created using this prototype system are highly robust, repeatable, and potentially improve overall image quality. More in-depth image quality comparisons will be undertaken once the final mounting hardware is fixed and software acquisition software is fully optimized. The implementation of dynamic laser-guided contouring will facilitate a smoother scanning process for ongoing clinical patient studies in the Duke Multi-modality Imaging Laboratory.

REFERENCES

[1] P. Madhav, D. J. Crotty, R. L. McKinley, and M. P. Tornai, "Initial development of a dual-modality SPECT-CT system for dedicated mammotomography," *2006 IEEE Nucl Sci Symp & Med Imag Conf,* vol. 4, pp. 2382 - 2386, 2006.

[2] M. P. Tornai, J. E. Bowsher, C. N. Archer, J. Peter, R. J. Jaszczak, L. R. MacDonald, B. E. Patt, and J.S. Iwanczyk, "A 3D gantry single photon emission tomograph with hemispherical coverage for dedicated breast imaging," *Nucl. Instr. Meth. Phys. Res. A,* vol. 497, pp. 157-167, 2003.

[3] C. N. Brzymialkiewicz, M. P. Tornai, R. L. McKinley, and J. E. Bowsher, "Evaluation of fully 3D emission mammotomography with a compact cadmium zinc telluride detector," *IEEE Trans. Med. Imag.,* vol. 24, pp. 868-877, 2005.

[4] C. N. Archer, M. P. Tornai, J. E. Bowsher, S. D. Metzler, B. C. Pieper, and R. J. Jaszczak, "Implementation and initial characterization of acquisition orbits with a dedicated emission mammotomograph," *IEEE Trans. Nucl. Sci.,* vol. 50, pp. 413-420, 2003.

[5] A. Rosset, L. Spadola, and O. Ratib, "OsiriX: An Open-Source Software for Navigating in Multidimensional DICOM Images," *Journal of Digital Imaging,* vol. 17, pp. 205-216, 2004.

[6] M. P. Tornai, R. L. McKinley, S. J. Cutler, D. J. Crotty, and C. N. Brzymialkiewicz, "Anthropomorphic breast phantoms for preclinical imaging evaluation with emission or transmission imaging," *2005 Proc SPIE: Phys Med Imag,* vol. 5746, pp. 825-834, 2005.

Fourth International Workshop on the Molecular Radiology of Breast Cancer
Conference Record

Comparison of 2D Scintimammography and 3D Dedicated Breast SPECT Using A Compressible Breast Phantom and Lesions of Varying Size and Tracer Uptake

Spencer J. Cutler, *Member, IEEE*, Kristy L. Perez, *Member, IEEE*, Priti Madhav, *Member, IEEE*, Martin P. Tornai, *Senior Member, IEEE*

Abstract– **This study aims to qualitatively and quantitatively compare 2D planar scintimammography imaging of the breast under various degrees of compression with uncompressed, dedicated 3D SPECT using dedicated acquisition trajectories. A 700mL compressible anthropomorphic breast phantom containing small lesions was developed to compare 2D and 3D breast imaging. Thin walled, deformable lesions ranging from 40 to 500uL volume suspended on a thin plastic sheet in the phantom were used to mimic breast lesions undergoing different degrees of compression. Using a 16x20cm^2 CZT-based gamma camera, ^{99m}Tc-scintimammography was performed for 10min imaging times for compression thicknesses of 6 and 12cm (fully uncompressed) using a single mediolateral view. Dedicated breast SPECT was then performed for 10min using the uncompressed breast acquired with a simple tilted rotation, and a complex 3D acquisition trajectory. Experimental variables include: (1) background torso contamination; (2) (in)homogeneous breast composition; and (3) low count (clinically relevant) and high count (low noise) images. The radioactivity lesion:background concentration ratio was varied from 12:1 down to 3:1. A comparison between the two modalities was made in a limited observer study with independent observers evaluating reconstructed images for the smallest detectable lesion and total number of lesions. Image quality, based on lesion SNRs and contrasts were also evaluated. SPECT images appear to yield observation of smaller and more simulated lesions than those seen in scintimammography, additionally with more than twice the SNR and contrast. Due to greater positioning flexibility of the SPECT system gantry, under a wide range of measurement conditions, statistically significantly (p<0.05) more lesions, smaller lesion sizes, and (3D) lesion locations were detected with dedicated breast SPECT than with compressed breast scintimammography.**

I. INTRODUCTION

THE overall goal of this work was to qualitatively and quantitatively compare breast lesion imaging using 2-dimensional (2D) planar scintimammography imaging of the breast under various degrees of compression with fully uncompressed, dedicated 3-dimensional (3D) breast SPECT using contoured acquisition trajectories. An initial study was conducted in our lab comparing 2D scintimammography using a compact, high performance gamma camera and partial compression, also known as molecular breast imaging (MBI) or breast specific gamma imaging (BSGI), with dedicated breast SPECT [1]. Two important results from this low noise study were that (1) dedicated SPECT images showed over twice the simulated lesion contrast and signal to noise ratios (SNR) compared to scintimammography for equal counting times, and (2) all distributed lesions, even those on the chest wall, were visible with dedicated SPECT. Further studies were warranted as the results were not comprehensive due to a leak in the compressible breast phantom, and those studies focused only on low noise, non-clinical count densities. The phantom can now be used for compression in its full range, and we have included moldable components in the breast phantom allowing for non-uniform activity distributions as observed in some clinical SPECT images in our lab and in scintimammograms by others [2, 3]. In this broader yet more specific observer-study based comparison we compare 3D SPECT with 2D scintimammography by investigating detectability limits of various sized lesions under the following imaging conditions: (1) different lesion:background activity concentrations, (2) low noise vs. high noise (clinical count densities) (3) 10-minute vs. 20-minute clinical acquisition times, and (4) uniform vs. heterogeneous breast backgrounds.

II. Materials & Methods

A. Gamma Camera

A 16 x 20 cm^2 area cadmium zinc telluride (CZT) based compact gamma camera (*LumaGEM 3200S*, *Gamma Medica*, Northridge, CA) with 2.5 mm discrete pixels, a measured mean energy resolution of 6.7 % FWHM at 140 keV, and sensitivity of 37.9 cps/MBq was used for all imaging studies [4]. A low energy collimator with 1.22 mm (flat-to-flat) hexagonal hole openings, 0.2 mm septa, and 2.54 cm height was used in both series of 2D and 3D measurements.

B. Breast and Lesion Phantoms

A specialized compressible phantom (*Radiology Support Devices, Inc.,* Newport Beach, CA) was previously developed as described in [1] (Fig. 1). It accommodates 2D and 3D emission and/or transmission imaging, and the chest plate also introduces physical hindrances similar to those encountered on a human torso. In this study, the phantom was filled with 500mL of water.
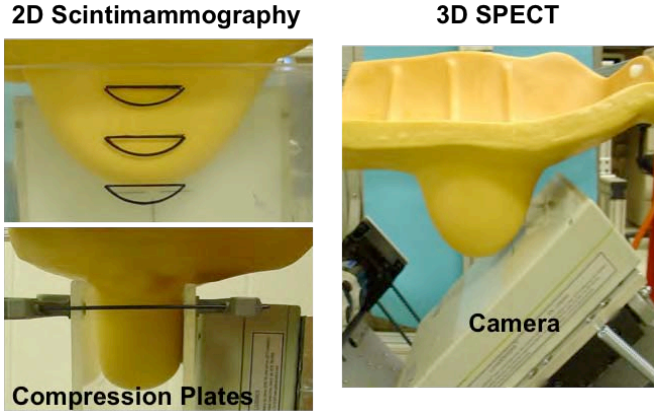

Fig. 1. (LEFT) Compressed breast phantom containing known lesions, and (RIGHT) Uncompressed SPECT set-up.

Thin walled, latex based lesions were adapted from animal catheterization balloons (*Harvard Apparatus*, Holliston, MA) and filled with radioactive fluids. The filled volumes (axis diameters) were 70 (5x9 mm), 140 (6x10 mm), 300 (8x12 mm), and 500 (10x14 mm) microL. The thin walled, refillable lesions benefit from minimal cold (non-radioactive) material around them, which might otherwise provide a signal enhancement. These lesions were not spherically symmetric, so we refer to their volumes rather than effective "diameters." A total of eight balloons, two balloons of each volume, were distributed at roughly equal spacing through small holes made in a thin transparency film cut in a semicircle (Fig. 2). The film was bonded to the fill cap of the breast phantom with clear silicone, such that the plane of lesion phantoms could be suspended vertically near the center of the breast. This lesion holder helped gauge the amount of breast volume within the field of view as well as the smallest lesion detectable under various imaging approaches.
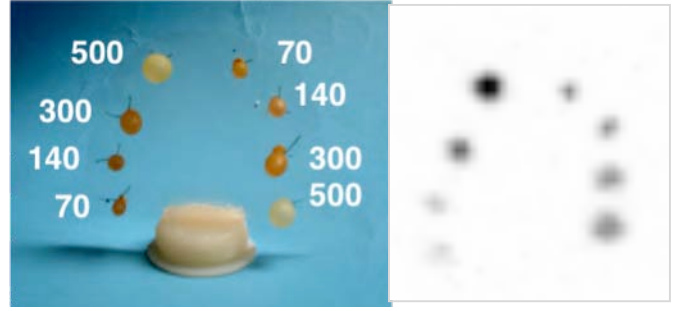

Fig. 2. (LEFT) Transparency film with distributed 70 to 500 microL balloon lesions (RIGHT) Reconstructed SPECT maximum intensity projection (MIP) of the lesions acquired with no additional background.

C. Scintimammography (2D) Acquisition Parameters

For the planar imaging, two 6 mm thick acrylic plates were used to compress the breast. The standard marks seen on mammography compression plates were transcribed onto the plates used here. The thinner plates used in x-ray mammography could not be adapted for use here since their modification resulted in severe bending while attempting to uniformly compress the breast phantom across the entire field. The drawback of the thicker plates is the calculated ~11% attenuation, which potentially degrades the count-limited clinical studies while barely affecting the scatter profile.

The plates were secured at each corner by an adjustable slider-clamp used to hold the plates at fixed separation or compression thicknesses (Fig. 1, LEFT). Image acquisitions were each for 10 min (increased compensated times with radioactive decay) for both an uncompressed 12cm plate separation, similar to that in "standard" scintimammography, and a compressed 6 cm plate separation, similar to that for MBI or BSGI acquisitions. Since the lesions were nearly coplanar and centered along the compression dimension, the distance between the camera face and lesions was nominally 3-4 cm under compression. The views were in a mediolateral orientation with respect to the chest plate of the phantom, with the camera placed as close as possible to the chest wall.

D. Dedicated Breast SPECT (3D) Acquisition Parameters

The main difference in these studies was that the breast was always completely uncompressed, and the camera system orbited the suspended breast in a contoured fashion. orbits were investigated (described in more detail in [5]) including a tilted parallel beam (TPB) and a 3-lobed sinusoid projected onto a hemisphere (PROJSINE) (Fig. 3). For each orbit, the camera system always used 360∘ azimuthal rotation. The TPB acquisition with 45∘ tilt has a constant polar deflection with varying azimuth, while PROJSINE varies polar and azimuthal angles simultaneously. Each angular increment was ≤2.8∘ over the 10 min acquisition period.
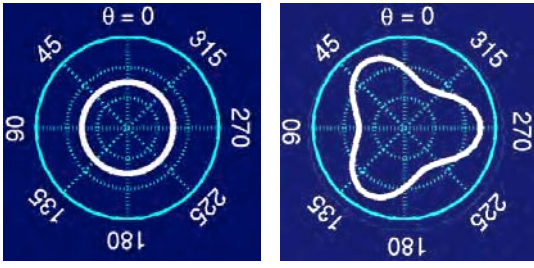
Fig. 3. Inverse polar projection plots of the orbital paths TPB 45∘ (LEFT) and PROJSINE 15-45∘ (RIGHT). The camera trajectory is shown in solid white, azimuthal camera angle is in polar direction, and polar camera angle is an inverted radius (90∘ is at center, and 0∘ tilt is at max radius) [5].

E. Reconstruction and Post-Processing

A previously described, ray driven OSEM algorithm was used to reconstruct the acquired data, with up to 3 iterations and 8 subsets [4-6]. Scintimammograms and reconstructed SPECT images were filtered with a simple Gaussian blur with increased pixel blur for clinical count images. Image grayscale window and leveling was also normalized between data sets in an effort to provide unbiased images to the observers. Image data was shown at the 1st iteration to maximize SNR. In order to more easily view all the lesion image data, the maximum intensity projection (MIP) images were used here for display, but in the observer study, single lateral slices of the original 3D data set were viewed.

F. Lesion Activity Concentrations

The absolute lesion activity concentration was 36 microCi/mL, which is roughly a factor of 18 greater than that observed clinically or used in other studies [7-10]. This concentration ensures low noise quality in the final obtained images. Lesion-to-background concentration ratios using aqueous ^{99m}Tc pertechnetate (140 keV) were varied from 12:1 to 6:1 to 3:1 by adding additional activity to the background. This method is much simpler than refilling and potentially moving the lesions. The full list-mode data for 6:1 and 3:1 were therefore down-sampled such that the total counts per projection were approximately the same for each simulated biological uptake variation. A ±6% energy window was used in all acquisitions [11].

G. Clinical Count Densities

A sub-aim of this study was to investigate the effect of a 10-min equivalent versus a 20-min equivalent patient scan time on lesion detection for various concentrations. For ongoing dedicated breast SPECT human subject studies in our lab, we have been imaging for 10 minutes per breast. Scintimammography is often conducted for 10 minutes per view for a total of 20 minutes per breast [7]. We examine here the potential benefits of adjusting our clinical protocol for an increased scan time. The full list-mode emission data from both 2D and 3D modalities were down-sampled such that the lesion activity concentration was effectively ~2 microCi/mL. Two independent "clinical count" projection data sets were created from each complete "low noise" data set: the first with count levels of a 10 min clinical acquisition, and the second the count levels of a 20 min clinical acquisition.

H. Breast Composition

^{99m}Tc-based 2D breast imaging techniques generally appear to have fairly uniform uptake throughout the normal tissue "background" [2, 3, 7]. In our initial 3D SPECT images of patients with confirmed cancer, we have observed some patients with areas of apparent non-uniform, patchy uptake in the breast background. To simulate this effect in the breast phantom, small ($<1cm^2$) randomly cut pieces of acrylic plastic were embedded in various-sized sponges. The sponges, while not seen in the emission images, allowed the plastic pieces to float at various heights in the breast in addition to pooling at the bottom without the sponges, and compressed nicely in the scintimammograms because of their otherwise loose arrangement. With this method we were able to simulate patches of heterogeneous uptake in the breast background.

Dedicated breast SPECT and scintimammograms were acquired first with a uniform aqueous background with previously described imaging acquisition parameters and lesion-to-background concentration ratios. The same experiments were then repeated with added material for the heterogeneous breast background. The added material did displace water further into the chest wall, but the total activity remained the same for both uniform and heterogeneous breast background scenarios. Additionally, for the heterogeneous breast experiments, an anthropomorphic activity-filled heart was placed above the chest wall to simulate additional cardiac contamination. The heart-to-lesion concentration ration was 1 : 1.

I. Observer study

Seven independent observers, including 2 nuclear medicine physicians and 5 medical physicists participated in a signal known exactly (SKE) contrast-detail observer study. Scintimammograms and contiguous 13-slice SPECT image sets were randomly displayed in a controlled viewing room. The observers marked which of the lesions were visualized for each of the 72 data sets, collected as summarized in Fig 4.
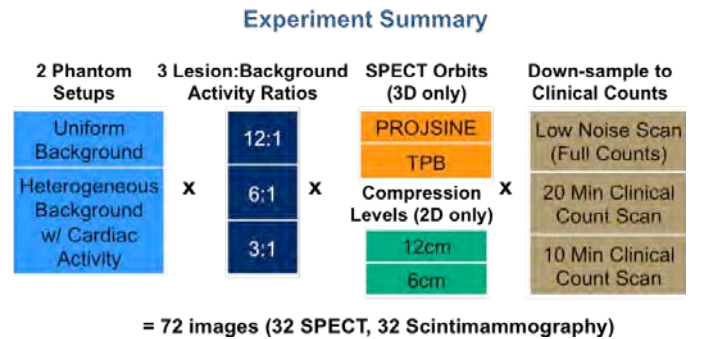

Fig. 4. Summary of the 72 different imaging parameters analyzed in this study.

Basic tests of statistical significance comparing the observer results were computed using paired Student T-tests. Image

analysis to extract region of interest (ROI) data from the images was performed using *ImageJ* freeware. Equally-sized ROIs were drawn within the boundaries of the visible lesions, and larger background ROIs were obtained. Signal was considered as the mean of an ROI, and noise was the pixel standard deviation about the mean measured in the background region. Thus, contrast was determined as the signal and background difference, divided by the background, while SNR was the signal and background difference, divided by the standard deviation of the background.

III. Results & Discussion

A. Low Noise Uniform Breast Results

Qualitative side-by-side analysis of the low noise SPECT MIPs and scintimammography projections in Fig. 5 illustrate that scintimammography is more limited in its ability to image the entire breast volume and near chest wall activity, which can be more reliably imaged with full breast SPECT. The largest 500 microL lesion in the upper left hand corner of the breast is truncated and the 70 microL lesion in the upper right corner is completely out of the field of view in the scintimammograms. Comparing PROJSINE and TPB SPECT images, PROJSINE images are a more faithful reproduction of the real breast shape, and fewer visible distortions are apparent in the lesions as observed previously [1, 6]. Often, this is more clear in individual SPECT slices, not the MIPs.
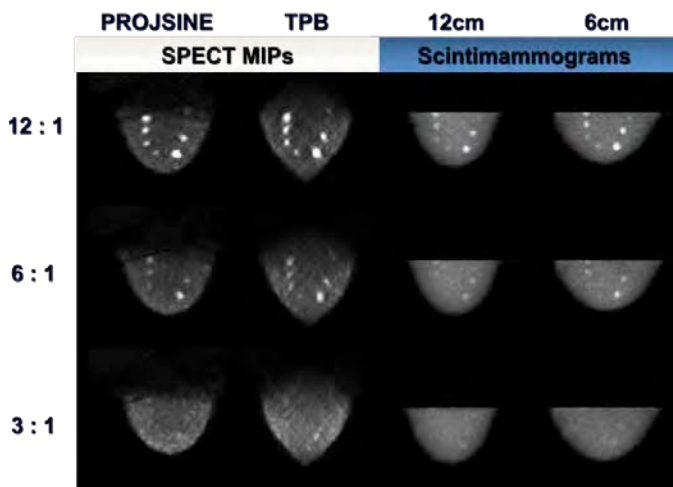
Fig. 5. SPECT MIPs for TPB and PROJSINE orbits shown together with uncompressed (12cm) and compressed (6cm) scintimammograms acquired of the same breast phantom for varying lesion to background concentrations.

Quantitative observer study results are given in Fig. 6. The standard deviation between observers was relatively small for the low noise case as may be expected. For both SPECT orbits, observers saw a significantly greater ($p<0.05$) number of lesions at 12:1 and 6:1 than for scintimammography. The TPB trajectory was more sensitive at 3:1. For the 12:1 case, SPECT most likely outperforms scintimammography due to its ability to see more lesions closer to the chest wall. SPECT and scintimammography were generally equivalent at 12:1 for lesions within the field of view for both systems, while more and smaller lesions were seen in both of the lower contrast

SPECT cases. SPECT's advantage in this SKE observer study appears to correlate to its significantly increased measured SNR and contrast for each lesion (Fig. 7). Scintimammography compression had no significant impact on observer performance in the low noise uniform breast.
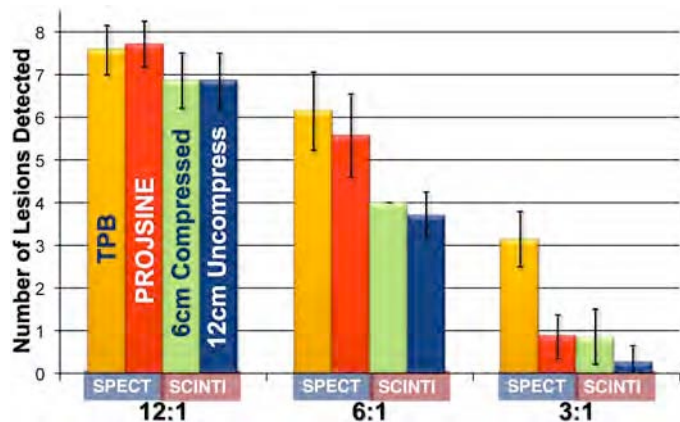
Fig. 6. Low noise, uniform breast background observer results. Error bars represent one standard deviation across the 7 observers.
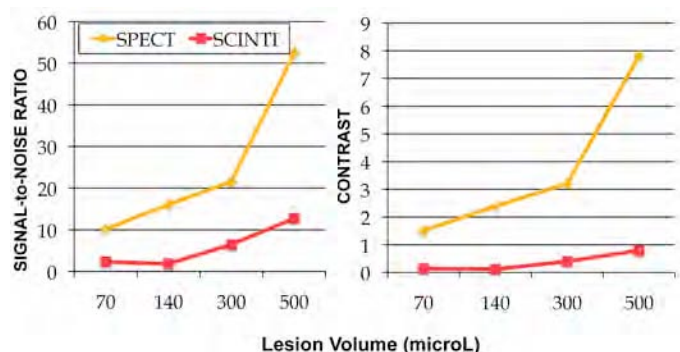
Fig. 7. SNR and Contrast measurements for each lesion volume, measured for the low noise uniform breast study with a 12:1 lesion : background activity ratio for PROJSINE (SPECT in orange) and 6cm compressed (scintimammography in red) acquisitions.

B. Clinical Count Uniform Breast Results

The down-sampled "clinical" count-level image results for a simulated 20 and 10 min scans are shown in Figs. 8 and 9 respectively. These MIP images have been smoothed with a Gaussian filter, but the increased noise is apparent, especially in the 10 min SPECT MIPs (Fig. 10). Scintimammograms benefit from the line integral of all counts projected into a single projection. Without smoothing or other noise reduction, small lesion detection is much more challenging and could result in more false positives, especially in the count starved individual SPECT slices.
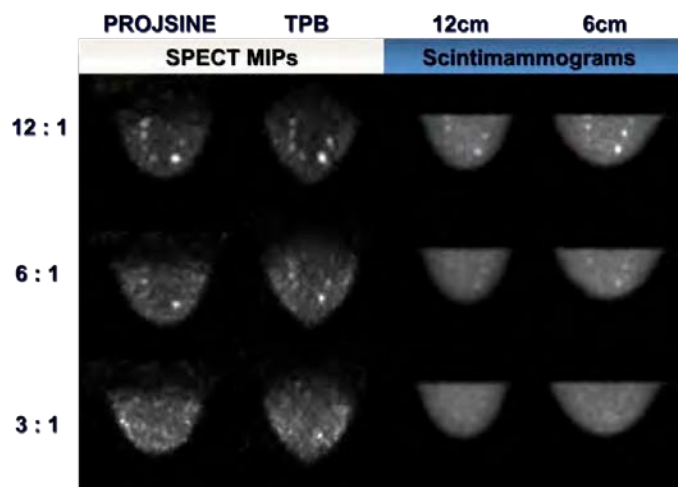
Fig. 8. Clinical 20-min scan SPECT MIPs and scintimammograms acquired of the same uniform breast phantom.
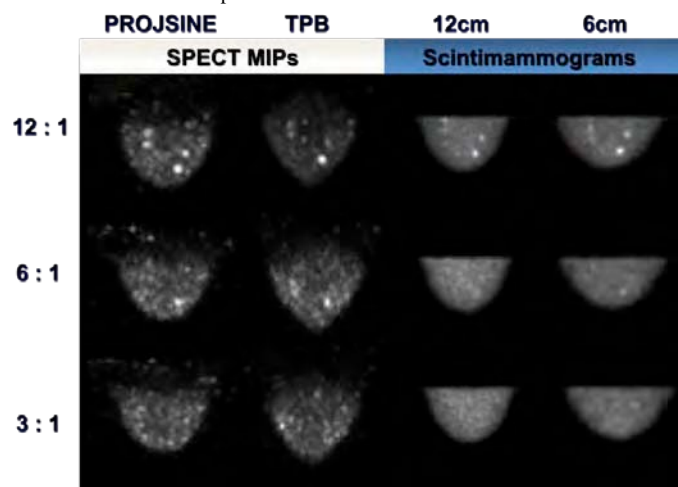

Fig. 9. Clinical 10-min scan SPECT MIPs and scintimammograms acquired of the same uniform breast phantom.

Overall, there was a significant loss in observer performance between the 20-minute and 10-minute scans (Figs. 10-11). One surprising result from the 10-minute clinical scan was that the detection performance on the uncompressed (12cm) breast at a 12:1 concentration was actually highest, significantly better than TPB ($p<0.05$). The two scans were sub-sampled from different sections of the same original complete list-mode spectrum. Also unexpected, the measured SNR and contrast showed moderately increased SNR and contrast for several lesions in the 10-minute SPECT scan versus the 20-minute scans (Fig. 12). This may be indicative of the high noise and variability at low count rates. SNR and contrast were nearly identical for scintimammography. These results suggest that a 20-minute scan may be beneficial for future patient studies in our lab.
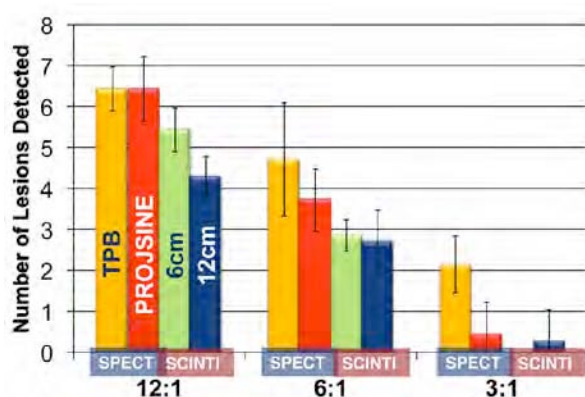

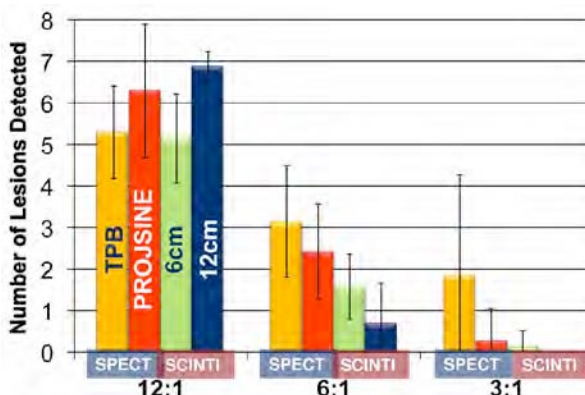Fig. 10. Clinical 20-minute scan, uniform breast background observer results.

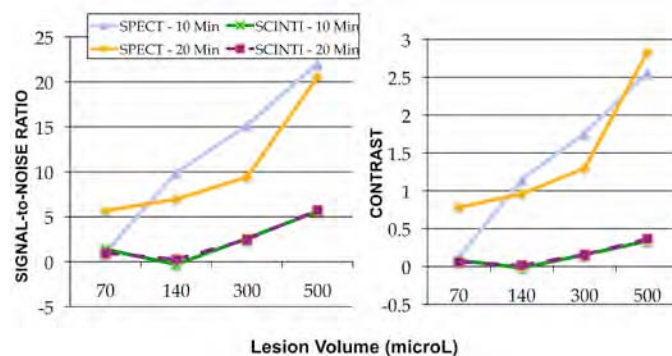Fig. 11. Clinical 10-minute scan, uniform breast background observer results.

Fig. 12. SNR and Contrast measurements for each lesion volume, measured for the clinical count high noise uniform breast studies with a 12:1 lesion : background activity ratio for the PROJSINE SPECT and 6cm compressed scintimammography acquisitions.

C. Low Noise Heterogeneous Breast Results

The addition of sponge-embedded floating cold spots simulates "patchy" radiotracer uptake in the heterogeneous image results (Fig. 13). The cardiac phantom may have been placed too high above the chest wall, and so cardiac activity is only faintly visible at the top of the SPECT images. Plastic pieces also pooled at the bottom of the breast phantom, creating the heterogeneously "cold" area near the nipple region. ^{99m}Tc appears to have concentrated in the 1.6 mm polyethylene-based malleable skin, resulting in an abnormally "hot" rim, most pronounced in the 3:1 images acquired later in the scan sequence.
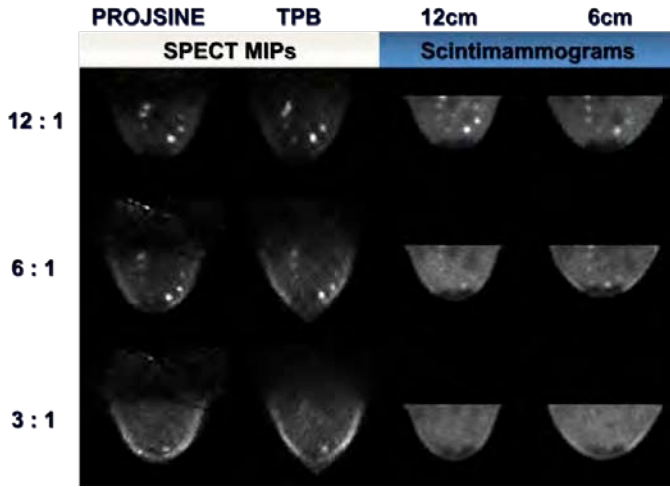
Fig. 13. SPECT MIPs for TPB and PROJSINE orbits shown together with uncompressed (12cm) and compressed (6cm) scintimammograms acquired of the same heterogeneous breast phantom for varying lesion to background concentrations.

For both SPECT orbits, lesions were significantly ($p<0.05$) more detectable at 12:1, and 3:1 than for scintimammography (Fig. 14). Compression had a more notable effect in the heterogeneous breast. At 6:1, there was no significant difference between SPECT and compressed breast scintimammography. With compression, the most likely explanation for the improved performance was that the added plastic pieces were compressed closed to the lesions thus raising the relative contrast and lesion visibility. However, at 3:1 concentration uptake, even compressed breast scintimammography significantly underperformed SPECT. TPB and PROJSINE orbits were more comparable in the low noise heterogeneous studies.
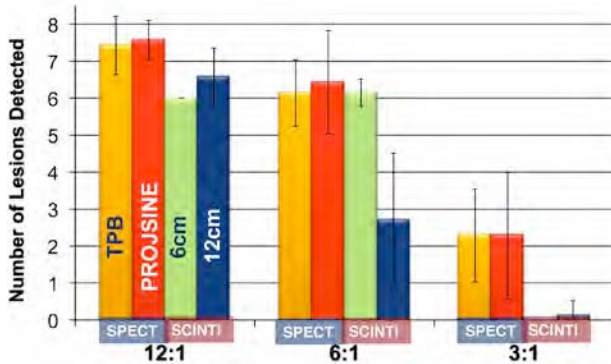

Fig. 14. Low noise, heterogeneous breast background observer results. Error bars represent one standard deviation across 7 observers.

D. Clinical Count Heterogeneous Breast Results

Images from the clinical count heterogeneous breast studies (Figs. 15-16) follow similar qualitative trends as the uniform clinical images. The 20-minute images had improved noise quality compared to the 10-minute images.
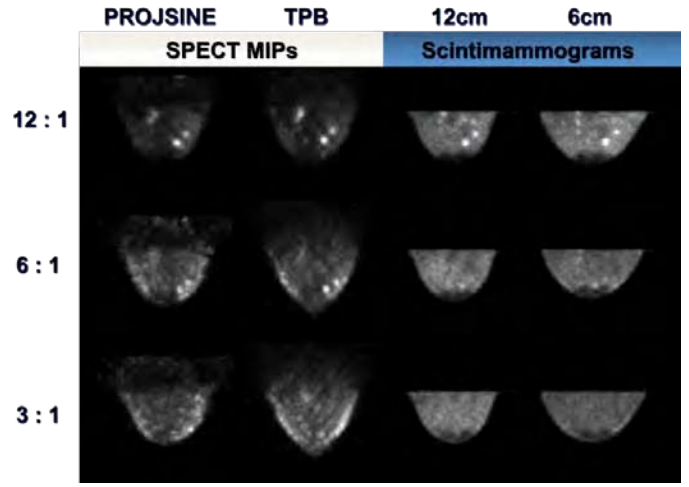

Fig. 15. Clinical 20-min scan SPECT MIPs and scintimammograms acquired of the same heterogeneous breast phantom.
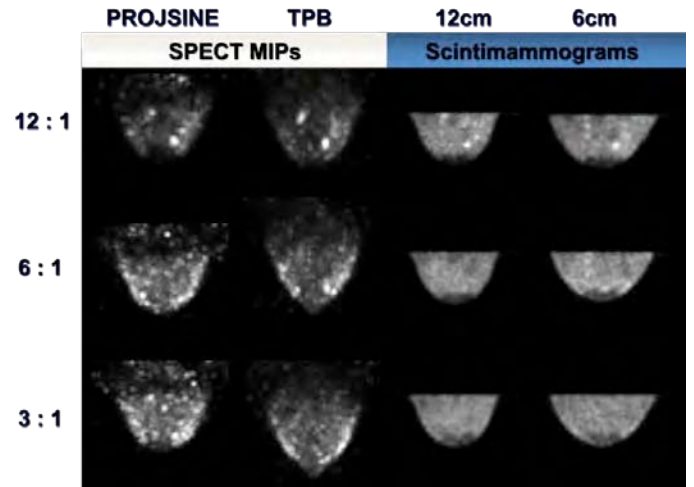

Fig. 16. Clinical 10-min scan SPECT MIPs and scintimammograms acquired of the same heterogeneous breast phantom.

The observer study results are shown in Figs. 17-18. As before with the uniform breast case, the 10-minute scan has considerably larger error bars and overall poorer performance. There was no statistically significant difference between the 20-minute and 10-minute scans for either the 6 cm compressed breast scintimammograms or SPECT PROJSINE. These results suggest that our SPECT patient acquisition may again benefit from an increased 20-minute scan time, while in this case, scintimammograms with compression could be acquired for 10-minutes with less of a performance drop (allowing for two 10-minute views of the breast).
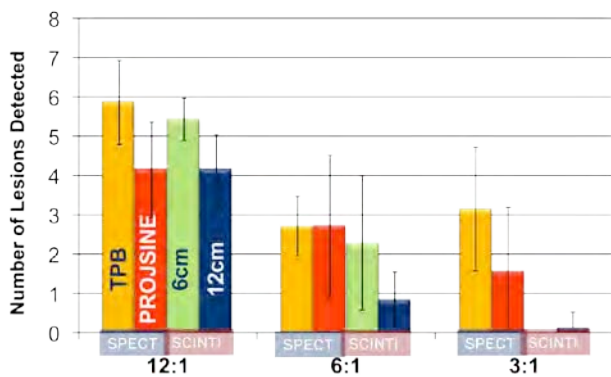
Fig. 17. Clinical 20-minute scan, heterogeneous breast background observer results.
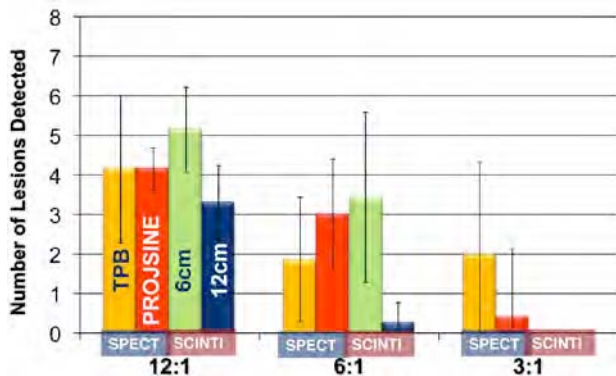

Fig. 18. Clinical 10-minute scan, heterogeneous breast background observer results.

IV. CONCLUSIONS

An observer-based direct comparison of 3D dedicated breast SPECT and 2D scintimammography using a single-headed high-resolution gamma camera was completed. SPECT benefits from overall greater SNR and contrast compared to uncompressed or compressed breast scintimammography. Scintimammograms were much quicker for the observers to read. Due to greater positioning flexibility of the system gantry, dedicated SPECT was able to both image a larger breast volume and view the anterior chest wall, where tumors may be otherwise missed in 2D imaging. SPECT and scintimammography were generally statistically equivalent at the highest lesion:background (12:1), except that chest wall lesions were detected in SPECT that were not in the field of view of scintimammography. At 6:1 and 3:1 simulated uptake, SPECT overall statistically outperformed scintimammography, seeing more and smaller lesions. In the heterogeneous compressed breast, scintimammography was equivalent to SPECT only at 6:1, but this could be explained by the overall higher noise.

Clinically equivalent count data indicate that a 20 min SPECT scan would be preferable to 10 min in order to lower noise and boost sensitivity. A TPB SPECT acquisition trajectory generally outperformed PROJSINE despite conical distortion, with the caveat that this was a SKE observer study. Future random lesion placement observer studies are warranted to determine overall sensitivity in lesion detection. Under a wide range of measurement conditions, statistically

significantly: more lesions, smaller lesion sizes, and (3D) lesion locations can be detected with dedicated breast SPECT than with compressed breast scintimammography. Furthermore, whereas for scintimammography, few physical features or improvements can be further employed in the planar acquisition process, ongoing development to improve breast contouring [12], as well as implementation of resolution modeling and attenuation and scatter correction for the SPECT imaging, we would expect SPECT image quality and observer detectability of smaller lesions to improve.

REFERENCES

[1] M. P. Tornai, C. N. Brzymialkiewicz, and R. L. McKinley, "Comparison of scintimammography and dedicated emission mammotomography," *2004 IEEE Nucl. Sci. Symposium & Med. Imaging Conference*, Rome, Italy, 2004, pp. 2818-2822.

[2] L. R. Coover, G. Caravaglia, and P. Kuhn, "Scintimammography with dedicated breast camera detects and localizes occult carcinoma," *J Nucl Med,* vol. 45, pp. 553-558, 2004.

[3] M. K. O'Connor, S. W. Phillips, C. B. Hruska, D. J. Rhodes, and D. A. Collins, "Molecular Breast Imaging: Advantages and Limitations of a Scintimammographic Technique in Patients with Small Breast Tumors," *Breast J,* vol. 13, pp. 3-11, 2007.

[4] C. N. Brzymialkiewicz, M. P. Tornai, R. L. McKinley, and J. E. Bowsher, "Evaluation of fully 3D emission mammotomography with a compact cadmium zinc telluride detector," *IEEE Trans. Med. Imag.,* vol. 24, pp. 868-877, 2005.

[5] C. N. Brzymialkiewicz, M. P. Tornai, R. L. McKinley, and J. E. Bowsher, "3D data acquisition sampling strategies for dedicated emission mammotomography for various breast sizes," *2004 IEEE Nucl Sci Symp & Med Imag Conf,* vol. 4, pp. 2596-2600, 2004.

[6] C. N. Brzymialkiewicz, M. P. Tornai, R. L. McKinley, S. J. Cutler, and J. E. Bowsher, "Performance of dedicated emission mammotomography for various breast shapes and sizes," *Phys Med Biol,* vol. 51, pp. 5051-64, 2006.

[7] C. B. Hruska and M. K. O'Connor, "Quantification of lesion size, depth, and uptake using a dual-head molecular breast imaging system," *Med Phys,* vol. 35, pp. 1365-1376, 2008.

[8] J. Maublant, M. de Latour, D. Mestas, A. Clemenson, S. Charrier*, et al.*, "Technetium-99m-Sestamibi Uptake in Breast Tumor and Associated Lymph Nodes," *J Nucl Med,* vol. 37, pp. 922-925, 1996.

[9] F. J. Wackers, D. S. Berman, J. Maddahi, D. D. Watson, G. A. Beller*, et al.*, "Technetium-99m Hexakis 2-Methoxyisobutyl Isonitrile: Human Biodistribution, Dosimetry, Safety, and Preliminary Comparison to Thallium-201 for Myocardial Perfusion Imaging," *J Nucl Med,* vol. 30, pp. 301-311, 1989.

[10] M. B. Williams, M. J. More, D. Narayanan, S. Majewski, B. Welch*, et al.*, "Phantom study of radiotracer concentration quantification in breast scintigraphy," *Nuclear Science, IEEE Transactions on,* vol. 50, pp. 433-438, 2003.

[11] S. J. Cutler, C. N. Brzymialkiewicz, and M. P. Tornai, "Investigating the effects of energy resolution in dedicated emission mammotomography," *2005 IEEE Nucl Sci Symp & Med Imag Conf,* vol. 5, pp. 2537-2541, 2005.

[12] S. J. Cutler, K. L. Perez, P. Madhav, and M. P. Tornai, "Dynamic Laser-Guided Contouring for Dedicated Emission Mammotomography," *2008 IEEE Nucl Sci Symp & Med Imag Conf*, Dresden, Germany, 2008.

Observer detection limits for a dedicated SPECT breast imaging system

S J Cutler[1,2], K L Perez[2,3], H X Barnhart[4] and M P Tornai[1,2,3]

[1] Department of Biomedical Engineering, Duke University, Durham, NC 27708, USA
[2] Department of Radiology, Duke University Medical Center, Durham, NC 27710, USA
[3] Medical Physics Graduate Program, Duke University Medical Center, Durham, NC 27710, USA
[4] Department of Biostatistics and Bioinformatics, Duke University, Durham, NC 27715, USA

E-mail: spencer.cutler@duke.edu

Abstract

An observer-based contrast-detail study is performed in an effort to evaluate the limits of object detectability using a dedicated CZT-based breast SPECT imaging system under various imaging conditions. A custom geometric contrast-resolution phantom was developed that can be used for both positive ('hot') and negative contrasts ('cold'). The 3 cm long fillable tubes are arranged in six sectors having equal inner diameters ranging from 1 mm to 6 mm with plastic wall thicknesses of <0.25 mm, on a pitch of twice their inner diameters. Scans of the activity filled tubes using simple circular trajectories are obtained in a 215 mL uniform water filled cylinder, varying the rod:background concentration ratios from 10:1 to 1:10 simulating a large range of biological uptake ratios. The rod phantom is then placed inside a non-uniformly shaped 500 mL breast phantom and scans are again acquired using both simple and complex 3D trajectories for similarly varying contrasts. Summed slice and contiguous multi-slice images are evaluated by five independent readers, identifying the smallest distinguishable rod for each concentration and experimental setup. Linear and quadratic regression is used to compare the resulting contrast-detail curves. Results indicate that in a moderately low-noise 500 mL background, using the SPECT camera having 2.5 mm intrinsic pixels, the mean detectable rod was ∼3.4 mm at a 10:1 ratio, degrading to ∼5.2 mm with the 2.5:1 concentration ratio. The smallest object detail was observed using a 45° tilted trajectory acquisition. The complex 3D projected sine wave acquisition, however, had the most consistent combined intra- and inter-observer results, making it potentially the best imaging approach for consistent results.

(Some figures in this article are in colour only in the electronic version)

1. Introduction

Nuclear medicine breast imaging is a promising complementary molecular imaging technique to x-ray mammography and computed tomography (CT) because of its ability to provide functional information that can help distinguish malignant from benign tissue. Small concentrations of injected compounds that are ^{99m}Tc radiolabeled are imaged, providing functional information about the metabolic activity of the lesion. To date, there is one FDA-approved compound (^{99m}Tc-sestamibi) for breast cancer imaging. Combining planar x-ray mammography and planar single photon scintimammography (both 2D imaging techniques) has been shown to increase the accuracy of diagnosis of primary breast cancers (Buscombe *et al* 2001). Studies have also indicated that the accuracy of scintimammography alone is unaffected by breast density and that women with dense breasts may benefit most from this complementary imaging technique (Coover *et al* 2004, Khalkhali *et al* 2002).

Early scintimammography studies using conventional whole-body gamma cameras found a sensitivity and specificity of scintimammography in the detection of malignant breast tumors of approximately 85% (Taillefer 1999, Waxman 1997), but sensitivity dropped significantly for tumors smaller than 1 cm (Tofani *et al* 1999). To overcome this, several groups have investigated higher resolution, small field-of-view cameras for planar scintimammography (Brem *et al* 2005, Hruska *et al* 2008, Spanu *et al* 2007, More *et al* 2006). Given the increased image information content, it is believed that the diagnostic accuracy may further be improved when using 3D tomographic techniques.

Thus, our lab has developed a dedicated single photon emission computed tomography (SPECT) breast imaging system that allows for fully 3D imaging of a hemispherical volume about a pendant breast (Archer *et al* 2003, Tornai *et al* 2003, Brzymialkiewicz *et al* 2005, 2006). The patient lies prone on a customized table, while the system images about her pendant, uncompressed breast (figure 1). The independent SPECT subsystem has recently been coupled with a low dose cone-beam x-ray CT subsystem, also developed in our lab, but CT data were not acquired in this study. The compact SPECT gamma camera and flexible camera gantry allow for innovative 3D imaging trajectories, as opposed to simple circular orbits, using a camera tilt to image a greater volume of the breast and lesions close to the chest wall. Breast imaging with clinical SPECT cameras is limited by the bulkiness of the large whole body cameras, which results in a larger radius of rotation (ROR). Spatial resolution degrades with increasing distance from the collimator in SPECT, and therefore, the larger ROR additionally results in degradation in image quality. Our compact gamma camera and computerized motion system gantry overcome the physical proximity restrictions of clinical gamma cameras, allowing close contouring of the pendant breast while potentially avoiding high-activity background regions outside the breast volume of interest.

With the implementation of this 3D dedicated breast SPECT imaging system, it is necessary to evaluate and characterize system performance to provide tangible motivation for further clinical testing of this paradigm. In previous studies, lesion detectability for varying lesion sizes and contrast ratios has been evaluated using the quantitative signal to noise ratio and lesion to background contrast measurements (Archer *et al* 2003, Brzymialkiewicz *et al* 2005, Tornai *et al* 2005a). However, an observer study is desirable to further characterize the system for an object detection imaging task.

Contrast-detail observer studies are commonly used for comparing varying imaging systems and techniques and have been regularly used for nuclear medicine tomographic and planar imaging systems (Faulkner and Moores 1986, More *et al* 2006). The goal of this initial phantom-based study is to compare multiple 3D SPECT imaging trajectories possible with our system, and evaluate the minimum object size under a variety of 'hot' and 'cold' signal to
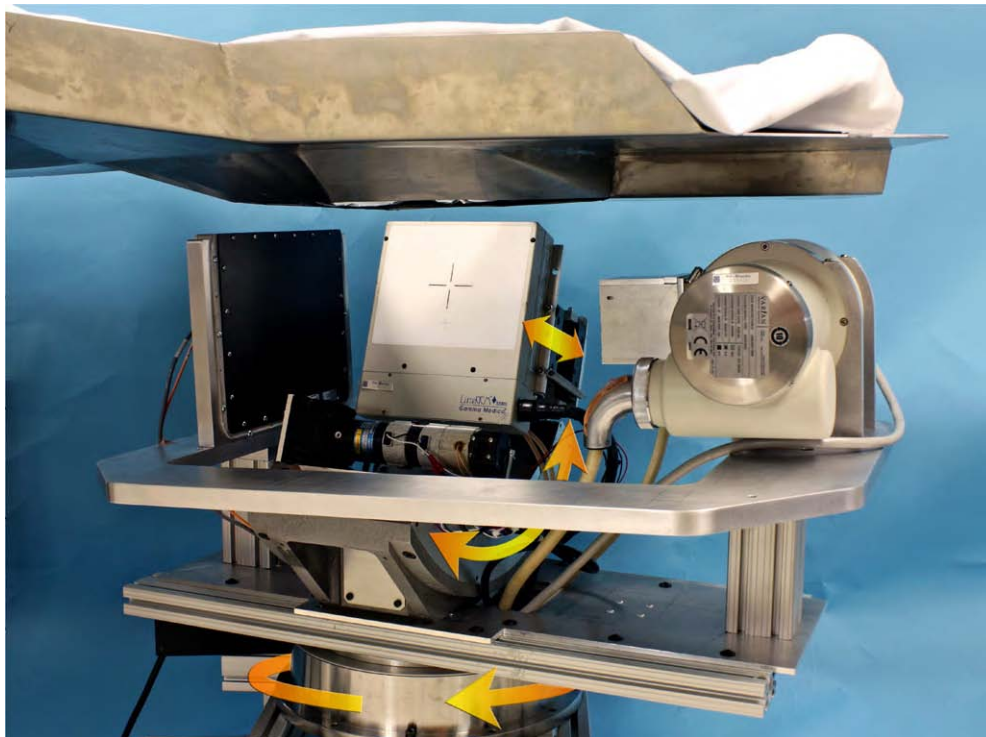
Figure 1. Photograph of the prototype dual-modality dedicated breast imaging system. The SPECT system (center) is placed orthogonally to the CT tube (right) and digital flat-panel detector (left). The colored arrows illustrate system motions (azimuthal for SPECT and CT, and polar and ROR for the SPECT subsystem). A custom steel bed supports the patient as her pendant breast is imaged in the common field of view of the systems.

background contrast ratios since early and later stage, and more and less aggressive cancers take up varying amounts of tracer compounds (Maublant *et al* 1996, Wackers *et al* 1989). Imaging 'hot' objects is appropriate because most cancerous lesions are more metabolically active than the surrounding normal tissue. 'Cold' imaging is also appropriate because, as cancers become more advanced, they may contain necrotic cores that do not uptake or concentrate radioactive tracers. Object size (detail) is also important as early detection of smaller lesions potentially increases survival rates along with patient treatment options.

2. Materials and methods

2.1. Gamma camera

A 16×20 cm^2 area cadmium zinc telluride (CZT)-based compact gamma camera (LumaGEM 3200S, Gamma Medica, Northridge, CA) with $2.3 \times 2.3 \times 5$ mm discrete crystals spaced on a 2.5 mm pitch was used for all imaging studies. The camera has a measured mean energy resolution of 6.7% FWHM at 140 keV and sensitivity of 37.9 cps MBq^{-1}. A low energy collimator with 1.22 mm (flat-to-flat) hexagonal hole openings, 0.2 mm septa and 2.54 cm height was used. The gamma camera is attached to a laboratory jack (model M-EL120, Newport Corp., Irvine, CA) and a goniometer (model BGM200PE, Newport Corp., Irvine,
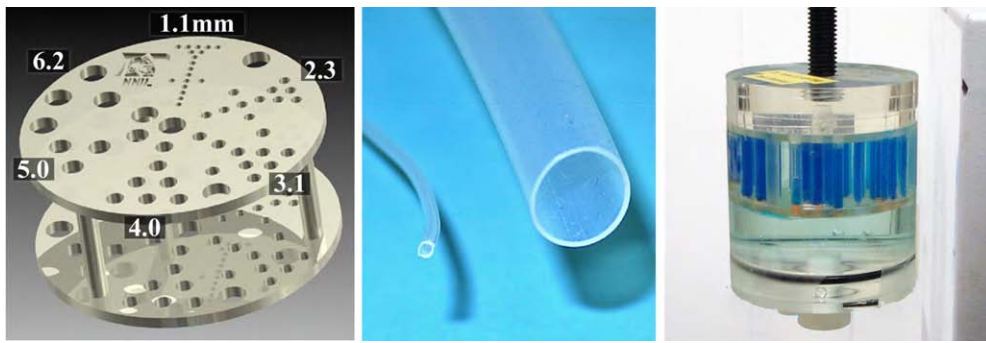
Figure 2. (Left) 3D rendered design of the contrast-detail phantom frame with rod diameters (mm). (Middle) Thin-walled PTFE tubing showing two different diameters. (Right) Contrast-detail phantom in water-filled cylinder imaged using a simple circular scan at a close radius of rotation. Food coloring was added to the fluid inside the tubes for better visibility.

CA), which provide the maneuverability for flexible, 3D trajectories traversing a hemisphere about the pendant breast. The hybrid SPECT-CT system is united on a common gantry (model RV350CCHL, Newport Corp., Irvine, CA), which rotates the system about the breast's central axis (figure 1). The overall performance characteristics and breast imaging capabilities of this specific camera system have been previously described (Brzymialkiewicz *et al* 2005).

2.2. Contrast-detail phantom design

A custom geometric contrast-resolution phantom was developed that can be used for both positive ('hot') and negative contrasts ('cold') (figure 2). The frame was designed using Autodesk Invento*r* software and then constructed using 3D stereolithography (American Precision Prototyping, Tulsa, OK) using a water-resistant resin (DSM Somos® 11120, density ~1.12 g cm^{-3}). The 3 cm long thin-walled polytetrafluoroethylene (PTFE, density ~2.2 g cm^{-3}) plastic tubes (Small Parts, Inc., Miami Lakes, FL) of varying inner diameters (6.2, 5.0, 4.0, 3.1, 2.3 and 1.2 mm with equal wall thicknesses of <0.25 mm), on a pitch of twice their inner diameter were arranged in six sectors. For the three smallest diameter sectors, two additional tubes were added, spaced at three times their inner diameter, in order to evaluate if rods would be visible at all, regardless of satisfying Nyquist's criteria. Tubes were independently filled using equal concentrations of radioactivity and then sealed on their open ends with thin plastic tape.

Though loosely based on a commercially available mini-cold rod phantom we have used in the past (model ECT/DLX-MP, Data Spectrum Corp., Hillsborough, NC), this newly developed phantom can be used for any combination of concentrations, both for hot and cold spot imaging, while also varying the background activity and (fluid density) composition. The thin wall of the tubes is intended to minimize scatter and partial volume sampling effects due to the minimal introduction of a 'cold' region between the tube interstitial space and the remainder of the phantom. The phantom can be used for a variety of other applications, such as for SPECT-CT multi-modality imaging and co-registration, by placing aqueous activity in the tubes and replacing the background liquid with fluids of varying density to modify the CT contrast along with simulated biological uptake of radioactive compounds.

Table 1. Parameters used for acquisitions over a 360° azimuthal range (θ).

| Orbit	No of projections	Polar tilt, ϕ (range, min:max)	ROR (range, min:max (cm))
VAOR	128	0°	4.3
TPB	128	45°	6.3
PROJSINE	128	15–45°	3.3–7.6

2.3. Contrast-detail observer study

Imaging experiments with geometric and anthropomorphic phantoms were designed. The first set of experiments was designed to optimally image the cylindrical geometric rod phantom using a close ROR of 4.3 cm and low scatter conditions. The phantom was placed in a 7.7 cm inner diameter cylinder, and the background volume was filled with 215 mL of water (figure 2, RIGHT). The tubes were individually filled with aqueous ^{99m}Tc-pertechnetate radioactivity with an absolute concentration of 10 μCi mL^{-1}, approximately five times the lesion uptake found in biodistribution data obtained via pharmaceutical uptake studies (Maublant *et al* 1996, Wackers *et al* 1989). The background concentration was varied, resulting in tube:background ratios of infinite:1, 10:1, 5:1, 2.5:1, 0.4:1, 0.2:1, to 0.1:1 (with ~5% error due to variations intrinsic to the dose calibrator). The varying contrast ratios in this study are modeled after clinical findings that ^{99m}Tc-sestamibi concentrates in breast tumors with a mean contrast ratio of ~5.6:1 compared to the surrounding normal tissue, varying from ~2.6:1 up to ~8.7:1 (Maublant *et al* 1996).

A vertical axis of rotation (VAOR) 360° circular acquisition orbit was used to acquire a total of 128 projections. Scan times were initially 10 min and subsequently lengthened to account for radioactive decay. The initial count rate was ~300 counts per second (cps) for the 10:1 contrast ratio, thereafter increasing proportionally with the added background activity. Taking advantage of the excellent energy resolution of the semiconductor-based CZT gamma camera, an 8% (±4%) window about the 140 keV photopeak was used for this and all of the following studies.

In the second set of experiments, the contrast-detail phantom was removed from the cylinder and placed inside a non-uniformly shaped breast phantom (Tornai *et al* 2005b), giving more clinically realistic attenuation and scatter characteristics. The dimensions of the phantom were approximately 7 × 14 × 17 cm (nipple-to-chest depth, superior-inferior height, medial-lateral width, respectively). The breast phantom was only partially filled with 500 mL of water in order to avoid paralyzing the detector with the continually added activity to vary concentration ratios, but sufficient to completely submerge the contrast-detail rod phantom. Scans were obtained using both a simple tilted parallel beam (TPB) and a complex projected sine wave (PROJSINE) 3D trajectory (Brzymialkiewicz *et al* 2006) (table 1, figure 3). Absolute activity was again 10 μCi mL^{-1} in the tubes, and activity was continually added to the background to generate the same contrast ratios as for the cylinder experiments. Scan times were initially 10 min and then subsequently adjusted during the acquisition sequences to account for radioactive decay. The initial count rate was ~480 cps for the 10:1 contrast ratio, which was increased compared to the cylinder experiments due to the added volume in the breast background.

During data acquisition, the expected emission counts from the tubes was kept constant for each contrast ratio by adjusting the scan times for radioactive decay, yielding constant noise quality from the tubes in reconstructed images. The continuously added activity
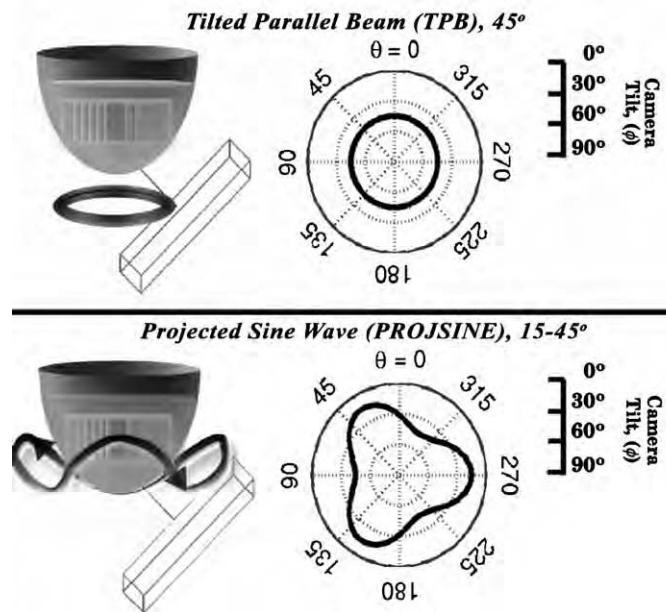
Figure 3. Acquisition orbits, TPB and PROJSINE used for the phantom in breast studies. To the left are visual representations of the 3D orbits, and to the right are polar plots of the camera tilt as a function of an azimuthal angle, where the radius refers to polar tilt, and in-plane angular displacement represents azimuth.

to the background, however, results in a greater number of overall acquired counts, and therefore increases the emitted events from the background overall, especially for the cold tube:background contrast ratios (0.4:1, 0.2:1, 0.1:1, which correspond to 1:2.5, 1:5 and 1:10, respectively), therefore yielding improved noise quality for the background. To account for this in the observer study, a separate set of count-normalized 'high noise' images was generated by randomly down-sampling the breast projection data such that the background noise quality was approximately uniform for each concentration ratio. The total targeted counts in each down-sampled projection image were randomly determined using a Poisson distribution with a mean based on the number of counts in each corresponding 10:1 concentration ratio projection image. Two down-sampled projection data sets were created for each concentration ratio to account for sample variation in the count skimming process.

An iterative, ray-driven implemented ordered subsets expectation maximization (OSEM) algorithm, with eight subsets and five iterations was used to accurately model the 3D acquisitions and reconstruct the data. Calculated attenuation correction was applied, assuming a uniform emission volume. A 3D Hann smoothing filter with a cutoff of 0.7 times the Nyquist frequency was then applied to the reconstructed data. For the phantom breast images, the reconstructed volume was rotated in 3D slightly so that the tubes were vertical in the sagittal plane and therefore multiple slices could be combined to enhance image quality. Single planar images were generated for each experiment set by summing planes where rods where present (fourteen 2.5 mm thick slices).

The resulting summed slice and contiguous 14-slice SPECT image sets were evaluated in random order, in a controlled environment by five independent observers (four medical physicists and one nuclear medicine radiologist). The observers were tasked with identifying

the smallest distinguishable rods (details) for all concentrations, noise levels, experimental setups and acquisitions. In this signal-known-exactly (SKE) study, the observers were shown the location and pattern of the rods prior to viewing the study. Three training images were shown prior to beginning the study. One challenge for the reader was to determine whether the randomized images had 'hot' (10:1, 5:1, or 2.5:1 ratios) or 'cold' contrast (e.g. 0.4:1, 0.2:1 and 0.1:1 ratios). Ambient lighting remained low and the observers could not adjust the window and leveling during the study. Summed images were read three times in randomized presentation order to assess intra-observer variability. For each test, results were averaged over the multiple readings.

Intra-observer variability was examined by computing the repeatability coefficient (RC) and intraclass correlation coefficient based on the one-way ANOVA model (ICC1). The RC provides the difference expected for 95% of the contrasts between any two replicated readings. Inter-observer variability was examined by the intraclass correlation coefficient from the two-way ANOVA model with interaction (ICC3 from Barnhart *et al* 2007). The ICC3 value describes the inter-observer agreement between the five observers based on their single readings and it takes intra-observer variability into account. The resulting data were examined by plotting contrast versus the average results by experimental setups. If the reader could not see any rod at all, a value of 7.0 mm was assigned for analyses below. Depending on the best fit to the averaged data (over the multiple readings) from the five observers, linear or quadratic regression was used to model the data from the five observers. The linear lines or quadratic curves were compared between experimental setups by testing the equality of the coefficients from the linear or quadratic functions. Hot and cold contrast curves were analyzed separately. All statistical tests were computed using SAS (version 9.2) statistical analysis software, and a p-value less than or equal to 0.05 is considered as statistically significant.

3. Results and discussion

Contrast-detail analysis has known limitations as it is, by nature, subjective and can be susceptible to observer bias. The SKE setup represents the best-case scenario where visualization of the rods should be obvious to the casual observer. Since nuclear images are routinely filtered and smoothed in the clinic, a modest amount of smoothing was used on all image sets. This study did not account for false positives that may be expected to increase in high noise SPECT images. Readers did not give confidence levels for their decisions as in a full ROC observer study. The following results provide a quantitative measure of observer variability in defining the detection limits, comparing varying orbit techniques possible with a fully 3D acquisition-positioning system as well as hot versus cold imaging for a dedicated breast imaging system.
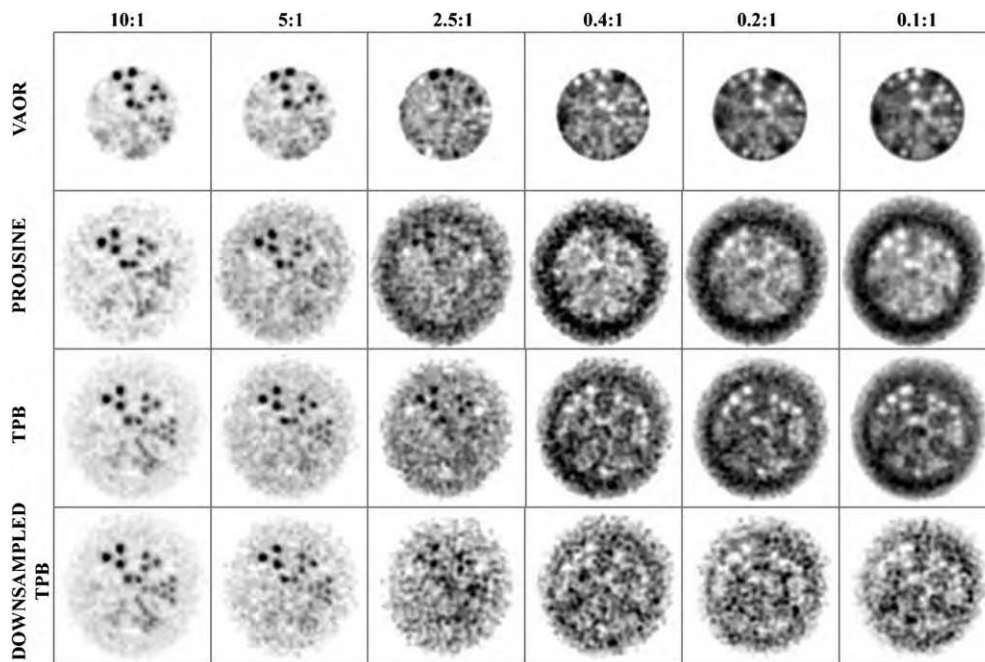
3.1. Summed slice images

Reconstructed images of low noise infinite:1 and 1:10 rods illustrate the best case examples of visualization of rods for these experiments (figure 4). Due to the vertical geometry and axial symmetry of the phantom, the vertical axis of rotation scan optimizes distance-dependent spatial resolution for the rods at all acquisition angles. The increased background volume of the breast phantom creates an additional and non-uniformly varying scatter medium about the rods, visually apparent in the reconstructed images (figure 5).

Contrast-detail observer study results demonstrate an expected trend that finer resolution is observed for higher contrasts (figure 6). For the phantom in the cylinder using the VAOR trajectory, the mean observed detail ranges from ~2.8 mm in the infinite:1 case, which degrades
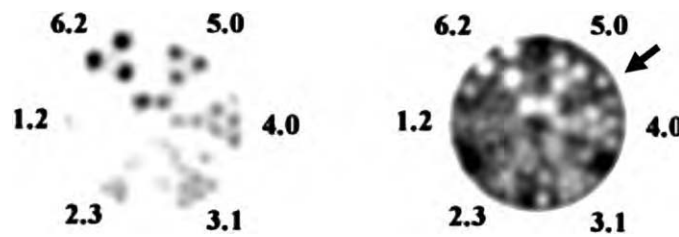
Figure 4. Reconstructed images (5th iteration, 8 subsets, 14 summed slices, calculated attenuation correction, post-reconstruction Hann smoothing applied at 0.7*Nyquist to reduce noise) of the phantom in the cylinder for infinite:1 (left) and 1:10 (right) concentration ratios. Rod sizes are indicated in mm. Note that three additional cold spots are seen on the right (2 (at the arrow tip), 6 and 10 o'clock) due to the 5 mm diameter posts holding the tube alignment layers together.

Figure 5. Reconstructed summed coronal slice images for rod:background concentration ratios ranging from 10:1 down to 0.1:1 (effectively 1:10) for VAOR scans about the cylinder, and two trajectories about the breast phantom. Downsampled reconstructions for the TPB orbit (only) are shown on the bottom row, where projection count densities were normalized to the 10:1 concentration case.

to ~5.2 mm for the 2.5:1 setup. The inverse then occurs from ~3.8 mm for the 0.4:1 case improving to ~3.0 mm for the 0.1:1 concentration ratio. The mean detectable rod size over all the breast acquisitions was ~3.5 mm at the 10:1 concentration ratio, which degraded to ~5.5 mm at the 2.5:1 concentration ratio. For cold contrasts, the average rod detected was ~4.5 mm at 0.4:1, improving to ~3.5 mm. Hot and cold contrasts (e.g. 5:1 versus 0.2:1) generally agreed within ±0.75 mm from each other, except for the lowest contrast ratios where 0.2:1 was significantly better than 2.5:1. The mean system detection limits observed
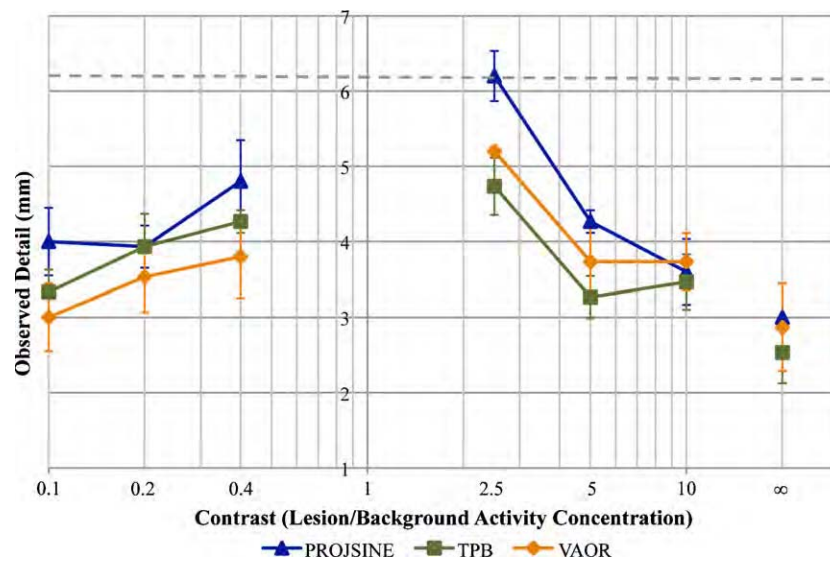
Figure 6. Contrast-detail plots illustrating mean and standard deviation values of independent observers comparing the rod phantom imaged in a cylinder using a standard VAOR trajectory and in a breast using PROJSINE and TPB acquisition trajectories. The upper limit of the phantom (6.2 mm) is indicated with a dotted line.

in this study are approximately in line with the calculated and previously measured spatial resolution for the SPECT system (Brzymialkiewicz *et al* 2005, Madhav *et al* 2009). The system in-plane spatial resolution is determined heavily by the distance-dependent collimator resolution, as well as the intrinsic resolution of the camera, in this case the size of the individual 2.5 mm CZT detector elements.

Comparative test results for statistical significance are summarized in table 2. For cold rod imaging, VAOR exhibited the best results of the three acquisition trajectories. For hot contrasts, TPB outperformed both VAOR and PROJSINE. Observer performance for the contrast-detail phantom in the non-uniformly shaped breast filled was overall close to that of the rod phantom in the uniform cylinder. These studies may have benefitted from the placement of the contrast-detail phantom near to the nipple, thus decreasing the camera ROR and improving resolution, in contrast to placement near the chest wall. A larger breast having increased scatter and attenuation, and a necessarily larger imaging ROR would likely degrade the images and the observer results more.

Intra- and inter-observer results are summarized in table 3, with the average and range of RC and ICC1 values over the five observers for intra-observer variability, and ICC3 values for inter-observer variability. If a repeatability coefficient is 0.7 mm, you expect to see a −0.7 to 0.7 mm difference between any two replicates for 95% of the time. For ICC values, 1.0 indicates perfect agreement and, generally, an ICC value of 0.8 or greater is considered as very good agreement. VAOR scans in the cylinder had the average lowest repeatability coefficient as might be expected. The intra-observer ICC1 values averaged between 0.8 and 0.9 for all of the methods except for the noisy downsampled TPB data. Generally, the complex PROJSINE orbit had the best overall agreement among and within observers for all of these studies.

Table 2. Summary of linear/quadratic regression tests for statistical significance ($p > 0.05$ higlighted)

Methods		Summed Slices			Original versus Downsampled			
		TPB versus PROJSINE	VAOR versus PROJSINE	TPB versus VAOR	PROJSINE (summed)	TPB (summed)	PROJSINE (slices)	TPB (slices)
p value	Cold	0.0232	<0.0001	0.0363	<0.0001	<0.0001	<0.0001	<0.0001
	Hot	<0.0001	<0.0001	0.0074	0.0053	0.0015	**0.1754**	0.0276
Methods		Slices			Summed versus Slices			
		TPB versus PROJSINE	VAOR versus PROJSINE	TPB versus VAOR	PROJSINE	TPB	VAOR	
p value	Cold	0.0003	**0.5055**	0.0035	<0.0001	**0.0971**	<0.0001	
	Hot	0.0046	**0.1418**	**0.3623**	**0.7078**	0.0125	**0.1323**	

Table 3. Summary of intra/inter-observer variability results

Method	Intra-observer		Inter-observer ICC3
	Average RC (range) (mm)	Average ICC1 (range)	
PROJSINE	0.89 (0.48–1.59)	0.91 (0.84–0.97)	0.83
TPB	0.77 (0.00–1.33)	0.80 (0.49–1.00)	0.71
VAOR	0.67 (0.00–1.38)	0.86 (0.58–1.00)	0.68
Downsampled PROJSINE	0.93 (0.72–1.48)	0.91 (0.83–0.97)	0.89
Downsampled TPB	1.96 (1.41–2.95)	0.36 (0.18–0.55)	0.40

3.2. Contiguous slice stacks

Contiguous 14-slice stacks of the same data were also included in the study to investigate any perceived differences compared to viewing reduced-noise summed slices. The resulting curves in figure 7 follow the same general trends as the summed slice data, but with an apparent degradation in observed detail of up to ∼1 mm for the cold rod images, and a slight improvement for the larger (10:1, inf:1) hot rod contrasts. Notably, for the infinite:1 ratio, the average reader values were 2.2 mm for multi-slice images versus 2.8 mm for the summed images. Readers appeared more able to separate the 2.2 mm rods when scrolling through multiple slices, which may have blurred together when the slices were summed due to inter-slice misalignment in the rods.

Linear regression of the three methods indicates that for contiguous slice stacks, the TPB acquisition method yielded the best results for cold contrasts, but no significant difference between TPB and VAOR scans for positive contrasts (table 2). When testing for statistical significance between summed and stacked data, observers saw significantly smaller objects for summed data for PROJSINE and VAOR, but no significant difference for TPB for cold contrast ratios. Conversely, for hot contrast ratios there were no significant differences between summed images and slices for PROJSINE and VAOR, but there was a significant difference for TPB.

For all of the breast phantom experimental conditions, the TPB acquisition method demonstrated significantly ($p < 0.05$) superior observer results than for data acquired with
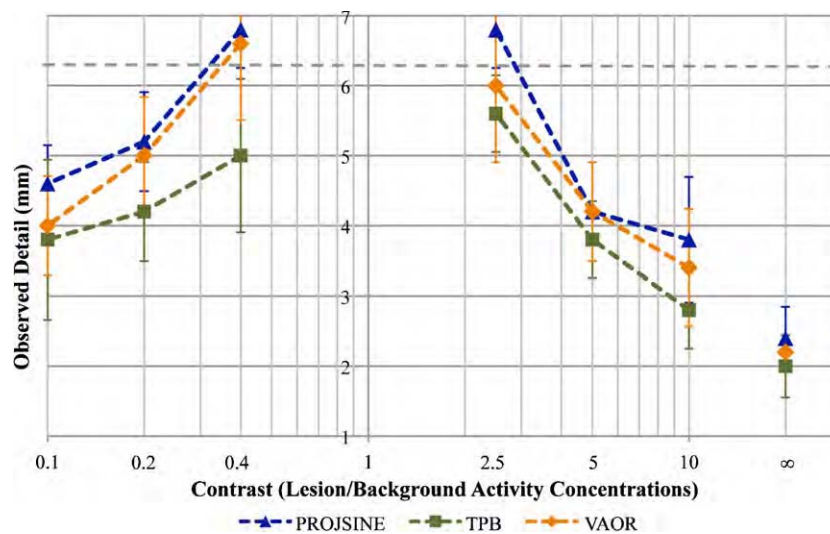
Figure 7. Contrast versus detail plots illustrating mean and standard deviation of independent observers comparing contiguous slice images of the rod phantom imaged in a cylinder with a standard trajectory and in a breast using PROJSINE and TPB trajectories. The upper limit of the phantom (6.2 mm) is indicated with a dotted line.

PROJSINE. This is likely due to the fact that the TPB acquisition orbit contained many views at a closer proximity to the phantom, while PROJSINE moved farther from the rods due to variations in both polar angle and ROR (table 1). One important caveat is that TPB demonstrated higher intra- and inter-observer variability compared to PROJSINE (table 3). The PROJSINE trajectory has been shown to have more complete sampling throughout the breast volume compared with TPB (Brzymialkiewicz *et al* 2006), and the symmetry of the rods in the phantom should have yielded a consistent trend in observer detection. With the development of automated object contouring on the SPECT system (Cutler *et al* 2008), we would expect better and more uniform overall resolution through the object of interest, which is additionally inferred from the high ICC3 value for the PROJSINE acquisitions (table 2).

3.3. Downsampled images

Downsampled 'high' noise data sets suffered from a lower number of total counts, and observer detection performance correspondingly degraded with decreasing contrast and increased noise. Figure 8 compares both contiguous and summed TPB acquisition downsampled data with the original data. For these analyses, if the reader (infrequently) could not see any rod at all, an estimated value of 7.0 mm was assigned. Thus, values located above the dotted 6.2 mm line are estimates, indicating that some of the observers saw no rods at all under those conditions. A value of 8.0 mm was also tested to assess the statistical sensitivity of the assigned value, with no substantial changes to the regression results in table 2. For higher noise data at low contrasts, further experiments with larger-diameter objects are warranted to verify the true lower limit of detectability. The gap between the full data and count-skimmed data is much wider for cold contrasts, because a greater number of counts were skimmed in order to normalize to the 10:1 contrast data. Count normalization additionally results in lower relative signal to noise ratios because in the cold contrasts, counts are spread across the background
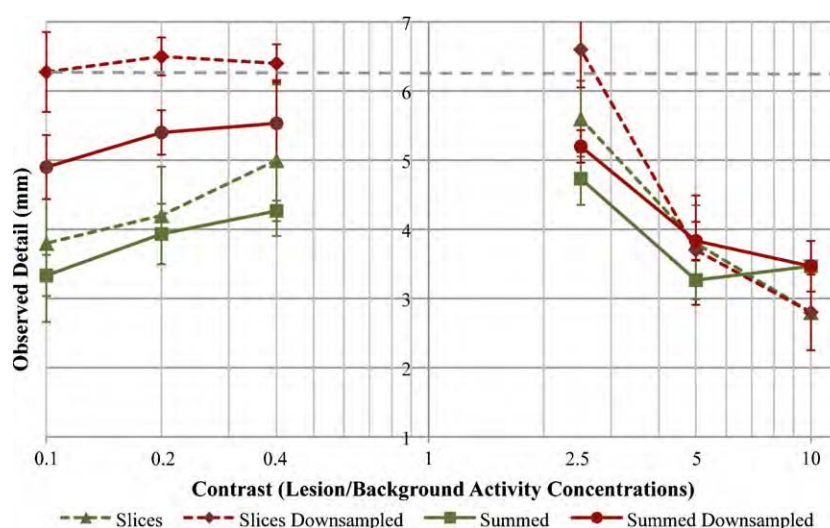
Figure 8. Contrast-detail plot for the TPB orbit for contiguous slice and summed slice images, original and 'high noise' downsampled data. The upper limit of the phantom (6.2 mm) is indicated with a dotted line.

instead of concentrating in the rods in the positive contrasts. PROJSINE acquisitions (not shown) followed a similar trend. TPB was prone to larger observer variability for the high noise data, demonstrated by the largest repeatability coefficients and ICC values (table 3). Though a definite separation in mean values between original and high noise data sets exists, the overall observer study results are still promising for clinical detection applications where detected count densities are more similar to the high noise data.

4. Conclusions

A high-performance clinical imaging system for dedicated SPECT breast imaging was successfully evaluated with a newly designed and constructed contrast-detail phantom. The average detail in a moderately sized 500 mL breast volume under relatively low noise conditions at 10:1 was ∼3.4 mm, degrading to ∼5.2 mm with the 2.5:1 concentration ratio. While far from the high resolution of radiographic imaging techniques, the spatial resolution of the system is better than whole body SPECT and PET detectors and comparable to other dedicated nuclear medicine based detectors (Schilling *et al* 2008). Compact CZT-based pixilated cameras are recently commercially available with even smaller pixels than those used on our current camera. Decreasing pixel sizes results in a further drop in sensitivity and increase in noise, which could potentially also affect lesion visibility for low contrast, low count (high noise) lesions. For example, More *et al* found that a larger pixelated (3.2 mm) NaI camera coupled with a high resolution collimator was better suited for 2D breast imaging than a smaller 1.4 mm pixilated NaI camera (More *et al* 2006); this corroborates our previous similar conclusions with NaI-based pixellated systems for 3D breast imaging (Tornai *et al* 2005a). Hruska *et al* use a high resolution 1.6 mm CZT gamma camera and have increased their overall sensitivity by optimizing (reducing) collimator length as well as adding a second camera head which images closer to the distal lesions of the first head (Hruska *et al* 2008, Weinmann *et al* 2009), so it is still unclear if a smaller pixel would benefit dedicated 3D imaging. If noise could be

normalized between 2D and 3D imaging, for example, then one of the main advantages of 3D imaging which is the inherently increased signal contrast due to the removal of overlapping tissues is still obtained. Additional advantages include potential for quantification as well as localization for biopsy targeting.

Overall, the observer study results are promising, demonstrating the potential of detecting sub-centimeter objects of various biological uptake, a critical target for effective functional breast imaging. For improved accuracy and less subjective results, a larger sample set of images is needed to more completely characterize the system. More realistic, 3D spherical lesions should also be evaluated at various contrasts for a variety of breast sizes in a broader observer study, since there are some advantages here using symmetric rods. Summing multiple planes to reduce noise improved detectability by up to ~1 mm smaller object visualization compared to objects in sliced-stacks, except for the highest 'hot' contrasts (>10:1), where multi-slice stacks improved visualization of the smallest rods. Spatial resolution correlated with the radius of rotation of the camera, highlighted for example by the observed finer resolution for TPB versus PROJSINE scans, because TPB contained more views at a closer proximity to the phantom. PROJSINE, however, had the most consistent combined intra- and inter-observer results, making it the best imaging approach for consistent results.

Acknowledgments

References

Archer C N, Tornai M P, Bowsher J E, Metzler S D, Pieper B C and Jaszczak R J 2003 Implementation and initial characterization of acquisition orbits with a dedicated emission mammotomograph *IEEE Trans. Nucl. Sci.* **50** 413–20

Barnhart H X, Haber M J and Lin L I 2007 An overview on assessing agreement with continuous measurements *J. Biopharm. Stat.* **17** 529–69

Brem R F, Rapelyea J A, Zisman G, Mohtashemi K, Raub J, Teal C B, Majewski S and Welch B L 2005 Occult breast cancer: scintimammography with high-resolution breast-specific gamma camera in women at high risk for breast cancer *Radiology* **237** 274–80

Brzymialkiewicz C N, Tornai M P, McKinley R L and Bowsher J E 2005 Evaluation of fully 3D emission mammotomography with a compact cadmium zinc telluride detector *IEEE Trans. Med. Imaging* **24** 868–77

Brzymialkiewicz C N, Tornai M P, McKinley R L, Cutler S J and Bowsher J E 2006 Performance of dedicated emission mammotomography for various breast shapes and sizes *Phys. Med. Biol.* **51** 5051–64

Buscombe J R, Cwikla J B, Holloway B and Hilson A J W 2001 Prediction of the usefulness of combined mammography and scintimammography in suspected primary breast cancer using ROC curves *J. Nucl. Med.* **42** 3–8

Coover L R, Caravaglia G and Kuhn P 2004 Scintimammography with dedicated breast camera detects and localizes occult carcinoma *J. Nucl. Med.* **45** 553–8

Cutler S J, Crotty D J and Tornai M P 2008 Dynamic laser-guided contouring for dedicated emission mammotomography *Nuclear Science Symp. Conf. Record, 2008. NSS' 08. IEEE* pp 4789–93

Faulkner K and Moores B M 1986 Contrast-detail assessment of computed tomographic scanners *Phys. Med. Biol.* **31** 993–1003

Hruska C B, Phillips S W, Whaley D H, Rhodes D J and O'Connor M K 2008 Molecular breast imaging: use of a dual-head dedicated gamma camera to detect small breast tumors *Am. J. Roentgenol.* **191** 1805–15

Khalkhali I *et al* 2002 ^{99m}Tc Sestamibi breast imaging for the examination of patients with dense and fatty breasts: multicenter study *Radiology* **222** 149–55

Madhav P, Bowsher J E, Cutler S J and Tornai M P 2009 Characterizing the MTF in 3D for a quantized SPECT camera having arbitrary trajectories *IEEE Trans. Nucl. Sci.* **56** 661–70

Maublant J, de Latour M, Mestas D, Clemenson A, Charrier S, Feillel V, Le Bouedec G, Kaufmann P, Dauplat J and Veyre A 1996 Technetium-99m-sestamibi uptake in breast tumor and associated lymph nodes *J. Nucl. Med.* **37** 922–5

More M J, Goodale P J, Majewski S and Williams M B 2006 Evaluation of gamma cameras for use in dedicated breast imaging *IEEE Trans. Nucl. Sci.* **53** 2675–9

Schilling K, Conti P, Adler L and Tafra L 2008 The role of positron emission mammography in breast cancer imaging and management *Appl. Radiol.* **37** 26–36

Spanu A, Cottu P, Manca A, Chessa F, Sanna D and Madeddu G 2007 Scintimammography with dedicated breast camera in unifocal and multifocal/multicentric primary breast cancer detection: a comparative study with SPECT *Int. J. Oncol.* **31** 369–77

Taillefer R 1999 The role of 99mTc-sestamibi and other conventional radiopharmaceuticals in breast cancer diagnosis *Semin. Nucl. Med.* **29** 16–40

Tofani A, Sciuto R, Semprebene A, Festa A, Pasqualoni R, Giunta S, Mottolese M, Benevolo M, Botti C and Maini C L 1999 99Tcm-MIBI scintimammography in 300 consecutive patients: factors that may affect accuracy *Nucl. Med. Commun.* **20** 1113–21

Tornai M P, Bowsher J E, Archer C N, Peter J, Jaszczak R J, MacDonald L R, Patt B E and Iwanczyk J S 2003 A 3D gantry single photon emission tomograph with hemispherical coverage for dedicated breast imaging *Nucl. Instrum. Methods Phys. Res.* A **497** 157–67

Tornai M P, Brzymialkiewicz C N, Bradshaw M L, Bowsher J E, Patt B E, Iwanczyk J S, Li J and MacDonald L R 2005a Comparison of compact gamma cameras with 1.3- and 2.0-mm quantized elements for dedicated emission mammotomography *IEEE Trans. Nucl. Sci.* **52** 1251–6

Tornai M P, McKinley R L, Brzymialkiewicz C N, Cutler S J and Crotty D J 2005b Anthropomorphic breast phantoms for preclinical imaging evaluation with transmission or emission imaging *Proc. SPIE* **5746** 825–34

Wackers F J *et al* 1989 Technetium-99m hexakis 2-methoxyisobutyl isonitrile: human biodistribution, dosimetry, safety, and preliminary comparison to thallium-201 for myocardial perfusion imaging *J. Nucl. Med.* **30** 301–11

Waxman A D 1997 The role of (99m)Tc methoxyisobutylisonitrile in imaging breast cancer *Semin. Nucl. Med.* **27** 40–54

Weinmann A L, Hruska C B and O'Connor M K 2009 Design of optimal collimation for dedicated molecular breast imaging systems *Med. Phys.* **36** 845–56

Characterizing the MTF in 3D for a Quantized SPECT Camera Having Arbitrary Trajectories

Priti Madhav, *Member, IEEE*, James E. Bowsher, *Member, IEEE*, Spencer J. Cutler, *Member, IEEE*, and Martin P. Tornai, *Senior Member, IEEE*

Abstract—The emergence of application-specific 3D tomographic small animal and dedicated breast imaging systems has stimulated the development of simple methods to quantify the spatial resolution or Modulation Transfer Function (MTF) of the system in three dimensions. Locally determined MTFs, obtained from line source measurements at specific locations, can characterize spatial variations in the system resolution and can help correct for such variations. In this study, a method is described to measure the MTF in 3D for a compact SPECT system that uses a 16×20 cm^2 CZT-based compact gamma camera and 3D positioning gantry capable of moving in different trajectories. Image data are acquired for a novel phantom consisting of three radioactivity-filled capillary tubes, positioned nearly orthogonally to each other. These images provide simultaneous measurements of the local MTF along three dimensions of the reconstructed imaged volume. The usefulness of this approach is shown by characterizing the MTF at different locations in the reconstructed imaged 3D volume using various (1) energy windows; (2) iterative reconstruction parameters including number of iterations, voxel size, and number of projection views; (3) simple and complex 3D orbital trajectories including simple vertical axis of rotation, simple tilt, complex circle-plus-arc, and complex sinusoids projected onto a hemisphere; and (4) object shapes in the camera's field of view. Results indicate that the method using the novel phantom can provide information on spatial resolution effects caused by system design, sampling, energy windows, reconstruction parameters, novel 3D orbital trajectories, and object shapes. Based on these measurements that are useful for dedicated tomographic breast imaging, it was shown that there were small variations in the MTF in 3D for various energy windows and reconstruction parameters. However, complex trajectories that uniformly sample the breast volume of interest were quantitatively shown to have slightly better spatial resolution performance than more simple orbits.

Index Terms—CZT detector, emission imaging, mammotomography, modulation transfer function, single photon computed emission tomography, three-dimensional trajectories.
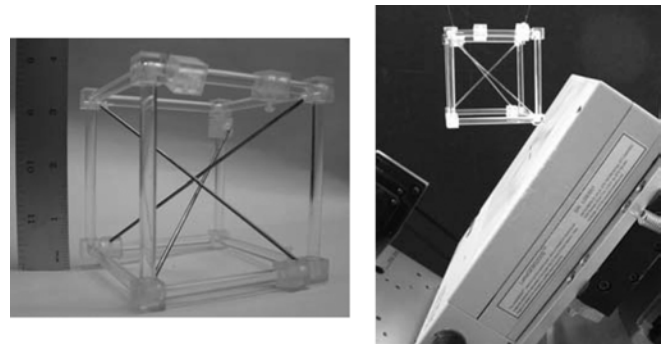

Fig. 1. (Left) Photograph of the acrylic phantom frame with three brass rods (brass rods were used in place of capillaries for the photo to clearly display the position of each tube). (Right) Photograph of the phantom suspended in front of the compact SPECT camera in air during a 360° acquisition.

I. INTRODUCTION

THE Modulation Transfer Function (MTF) can be used to characterize the frequency composition of spatial resolution. For emission imaging, the MTF can be determined via the line spread function (LSF) from images of a line source [1] (i.e. a capillary tube filled with radioactivity) or an edge source (i.e. radioactivity placed behind a lead plate) [2] in air. Measurements are usually taken at various distances from the camera face to determine spatial variations in resolution. MTF variations with respect to object-to-background ratio contribute to characterizing system linearity. Knowledge of these variations in the spatial resolution of an imaging system is important in understanding the reliability of information derived from an image, (i.e. gauging the minimum size of a lesion that could be detected).

In emission tomography, spatial resolution is determined quantitatively by measuring the LSF or point spread function (PSF), and semiquantitatively by assessing the reconstructed image quality of standard test objects such as the 3D disk and frequency-resolution (cold or hot) rod phantoms. In 2D, measurements of the LSF or PSF often assume that radiation detectors have a continuous response across their surface that is invariant within any given plane parallel to the detector's surface. However, this invariance assumption is questionable for recent medium- and small-field-of-view nuclear emission cameras having quantized detector elements, as are assumptions of approximately Gaussian response. Parallel hole or pinhole collimation, e.g. for small-animal imaging, involves significant nonstationarity in gamma camera response. It is also more common to describe the system performance in the frequency domain by obtaining the Fourier Transform of the PSF or LSF. Generally, image filtering is done in frequency space. The noise power spectrum (NPS), detective quantum efficiency (DQE), and other common parameters used in describing system response are also all measured in the frequency domain and

TABLE I
TRAJECTORY PARAMETERS USED FOR EACH ACQUISITION
OVER A 360° AZIMUTHAL RANGE

Trajectories	Acronym	Number of Projs	Polar Tilt Range (min-max degrees)	ROR Range (min-max cm)
Vertical Axis of Rotation	VAOR	128	0°	8.74
Tilted Parallel Beam	TPB	128	45°	4.05
Circle Plus Arc	CPA	139	0°-45°	4.05-6.48
Three-Lobed Sinusoid Projected onto a Hemisphere	PROJSINE	150	15°-45°	4.05-8.74

LSF. Therefore, by looking at the frequency response, measurement of the MTF in 2D or 3D can provide a quantitative insight into the full frequency response of the system regardless of the detector response function.

Previous line-source phantoms used to measure the MTF in 3D have been limited to measuring the spatial resolution one dimension at a time [3]–[5]. Arrays of point sources have also been used to assess spatial resolution in three dimensions at various locations throughout the image volume [6]. However, unlike line sources, 3D arrays of point sources are more difficult to manufacture and position uniformly, and also are more difficult to evaluate under different scatter and scatter-free conditions due to the nature of their support structure. For this work, a novel phantom was constructed to fully evaluate the three-dimensional MTF along three nearly orthogonal axes after a single tomographic acquisition. This phantom allows for the characterization of spatial resolution in three dimensions and at various locations throughout the imaged volume, providing insight into the total amount of blur and its spatial variation. This phantom can be especially useful for tomographic imaging systems capable of fully-3D acquisitions for SPECT or PET, though it could also be modified for use in transmission imaging systems [7].

Over the past few years, our laboratory has developed a dedicated emission mammotomography system [8]–[11]. Several 3D, non-traditional, noncircular trajectories about a pendant breast with various lesion sizes located in different areas have been implemented and assessed [9], [12]. Due to the spatially varying spatial resolution in SPECT and the nonlinear response of iterative ordered-subsets expectation maximization (OSEM) reconstruction, the system blur cannot be fully described by a single LSF or MTF. Instead, some indication of system blur can be provided by measuring the blur at several locations in the image, for several signal-to-background ratios, and for several sizes and shapes of structures of interest.

The purpose of this study is to describe the novel phantom and to use this phantom to characterize the local MTF in 3D and to identify parameters that can affect the overall spatial resolution of our current SPECT system. Here we focus on measuring the MTF in different locations in the 3D volume using several different energy windows, different reconstruction parameters and acquisition trajectories, and different object shapes. In the present paper, LSF refers to the image of a line source in zero
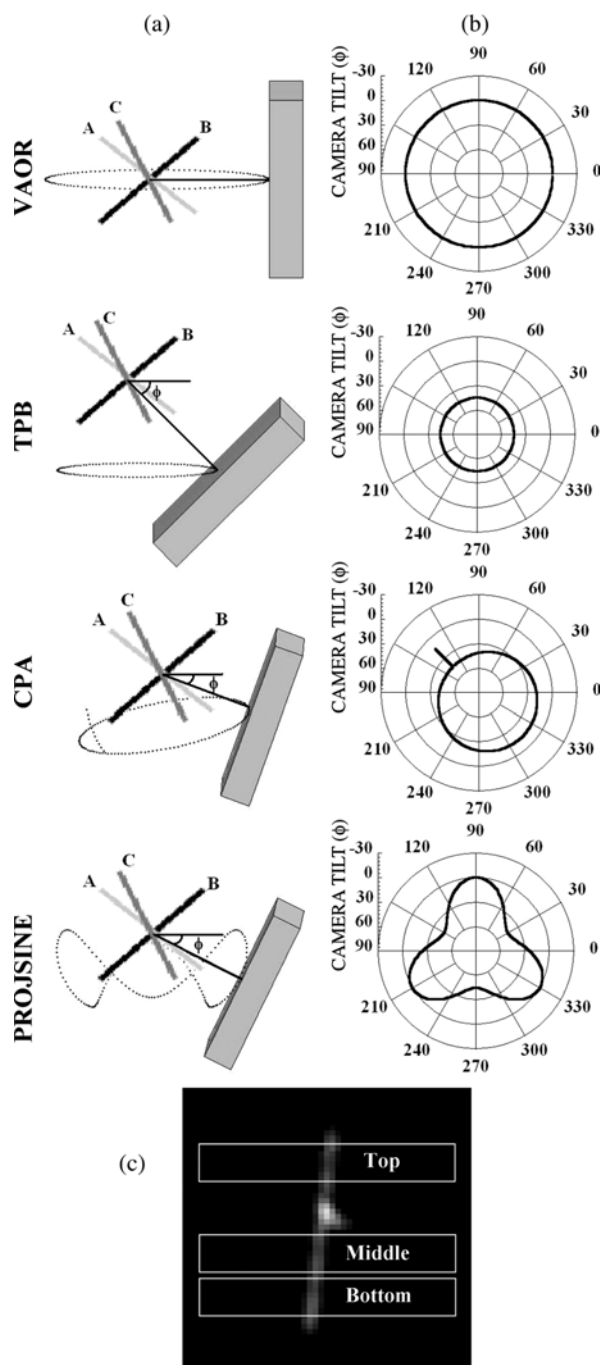
Fig. 2. (a) 3D setup of the phantom for all four trajectories. The SPECT camera (shown as a gray box) is facing left towards the phantom, placed at the center of the field-of-view. The phantom consists of three radioactivity-filled capillary tubes (labeled A,B,C). The shown placement of the tubes nearly matches the photograph of the phantom suspended in front of the SPECT camera in Fig. 1. The direction of increased polar camera tilt, ϕ, is also shown relative to the horizon. (b) Next to each 3D schematic is the corresponding polar plot (i.e. camera tilt) of the camera trajectory (plotted as a radius with $+90°$ at the center and $-30°$ at the edge) versus azimuth angle (plotted around the circle from 0° to 360°). (c) Reconstructed slice (5th iteration, 8 subsets, $80 \times 80 \times 80$ grid size, 2.5 mm) for one isolated capillary tube located in air acquired with a TPB orbit. "Top," "Middle," and "Bottom" of the capillary tube are defined for subsequently presented results, and span 11 cm along the length of the line source.

require the MTF in their calculations. Thus, there are various reasons for computing the MTF instead of simply the PSF or

Fig. 3. Photographs of the MTF phantom contained inside (Left) the 2000 mL cylinder and (Right) 850 mL breast phantom shell. (Bottom) Phantom was immersed in the water to the extent possible to quantify the effect of different object shapes along with various acquisition trajectories on the MTF, and (Top) is also shown in the phantoms without water present.

background and at a particular location. MTF refers to the absolute magnitude of the Fourier Transform of a particular LSF (i.e. at a particular location in the image) and thus throughout this paper the MTF will be referred to as the local MTF. In addition, isotropic in this paper is defined in terms of the MTF being uniform throughout the entire volume.

II. MATERIALS & METHODS

A. MTF Phantom

In order to quantify the spatial response of any imaging system including detector response, image acquisition procedures, complex 3D trajectories, scatter, and photon attenuation, a novel phantom was constructed (Fig. 1) to measure the local MTF in 3D. This phantom could be used for both emission (SPECT, PET, or even MRI) and transmission (X-ray CT) systems [7], [13]. A line source was chosen from which to obtain the MTF, since a radioactivity-filled capillary tube for emission imaging and solid tungsten wire for transmission imaging are easily interchangeable. Thus, this phantom would allow using a similar acquisition and quantification procedure for most imaging systems. More than one line source was necessary such that the MTF could be measured at different locations in the reconstructed imaged volume after a single tomographic acquisition. Using too many lines sources runs the risk of creating an overlap between the line sources in the reconstructed images, and so three lines were chosen. Additionally the phantom had very low scatter and attenuation characteristics, could be easily assembled, could be placed in any desired position in the camera's field of view, could be inserted into various fluid

filled containers, and could provide flexibility to reposition the line sources in order to image anywhere in the imaged volume.

Based on the desired features, acrylic rods (side length of 7.8 cm) are attached together into the shape of a box frame. Three capillary tubes ($\sim$11 cm long with 0.9 mm inner diameter) filled with 44.4–66.6 MBq of aqueous ^{99m}Tc (140 keV) were placed within the boxed frame such that each tube was held from one vertex to its corresponding opposite end, slightly away from another vertex. On its corresponding opposite end, the tube is attached to a slider piece which gives the flexibility to position the tube anywhere along the length of the side-rod to which it is attached. Once the desired position of the rod was set, the sliding support was fixed with an acrylic screw pressed against the side-rod. Depending on the size of the SPECT system, pixel size of the camera, and its minimum radius of rotation, smaller or larger capillary tubes could be used to encompass the entire field of view. The tubes were visibly separable in their positions such that they did not touch one another, and spanned the entire field of view. Also, they were not placed at exactly orthonormal planes in order to avoid interplay of measured responses from different directions near the center of the field of view.

B. Data Acquisition and Image Reconstruction

Our emission tomography system is composed of a compact 16×20 cm^2 field of view cadmium zinc telluride (CZT) LumaGEM 3200S gamma camera (*Gamma Medica, Inc.*, Northridge, CA) attached to a hemispherically positioning gantry. The camera uses a 64×80 array of $2.5 \times 2.5 \times 6$ mm^3 quantized CZT elements for a total of 5120 pixels. Measured mean energy resolution of the gamma camera at 140 keV is 6.7% FWHM and overall sensitivity is 37.9 cps/MBq [11]. A parallel-hole collimator with hexagonal holes (1.2 mm hole size flat-to-flat (inner diameter), 0.2 mm septa, and 25.4 mm height) is used in these studies. Due to the flexible gantry, the camera can be positioned anywhere in a hemisphere to facilitate acquiring projection data around a pendant uncompressed breast [8], [9], [11], [12].

Projections were collected over a 360° azimuthal rotation around the phantom suspended in air [Figs. 1 and 2(a)] using a vertical axis of rotation (VAOR), comparable to the simple circular orbits used by clinical SPECT systems (about their horizontal axis). Acquisitions were made at a radius of rotation (ROR) that corresponded to the minimum ROR possible when the MTF phantom was placed in different object shaped media (described in the next section). Data was collected in list mode and post-processed to obtain ±4% and ±8% wide symmetric energy windows about the 140 keV photopeak. Total scan time for each acquisition was 10 min, with increased acquisition times for subsequent scans to compensate for radioactive decay. Under these conditions, there were $\sim$28 k events per projection in the ±8% wide energy windowed data.

Images were iteratively reconstructed using 8 subsets of OSEM, and displayed at 1, 3, 5, and 10 iterations in all cases. These reconstructions were on a grid of $80 \times 80 \times 80$ voxels, for two different voxel widths—1.25 mm and 2.50 mm. The reconstructions were performed using the same ray-driven code as described earlier in [9], [10].

Three other trajectories were investigated: (1) tilted parallel beam (TPB) with 45° fixed camera tilt; (2) tilted circle plus (one) arc (CPA) with 45° max camera tilt, and (3) a three-lobed sinusoid projected onto a hemisphere (PROJSINE) with 0° to 45° polar camera tilting range (sinusoidal amplitude). These trajectories have been investigated elsewhere [9], [11], [12], but not for their frequency response characteristics. These trajectories and the direction of polar camera tilt are illustrated in Fig. 2. Specific parameters that were used for all four trajectories are given in Table I. The increased number of projections is due to the use of polar (ϕ) sampling along with azimuthal (θ) sampling, necessitating $\Delta\phi$ steps along with $\Delta\theta$ steps to reach 360° azimuthally.

C. MTF Phantom in Different Object Shapes

The degrading effects of different object shapes on the MTF were also evaluated by placing the line source phantom in two different environments: 2000 mL water-filled glass-walled cylinder (12 cm diameter) and 850 mL water-filled plastic-walled breast-shaped container (nipple-to-chest distance of 11 cm, medial-lateral distance of 17 cm, and superior-inferior distance of 18 cm) (Fig. 3). All four trajectories were investigated except for the cylinder where only VAOR was used. The local MTF was calculated for all trajectories measured with the phantom placed in the cylinder and breast. Data was collected using an ±8% wide symmetric energy window and was post-processed to also obtain ±4% wide symmetric energy windows. Energy window width for dedicated, uncompressed breast imaging has been shown to affect image quality under various acquisition conditions [14]. The ±8% wide energy window, while not exploiting the fine resolution capability of CZT (6.7% intrinsic FWHM), corresponds to that used in standard, clinical nuclear medicine camera systems (15% wide), and is substantially narrower than that of scintillator based compact, quantized detector element gamma cameras (30% wide). Furthermore, early contrast-detail observer studies with this system have shown that energy windows near but above the intrinsic system resolution allow for visualization of small objects [14]. The ROR was determined by placing the breast 1 cm or less away from the camera face at all camera orientations. For all four trajectories tested, acquisitions were obtained at the same RORs used for the phantom in air (shown in Table I). Scans were also performed over 10 min, with increased acquisition times for subsequent scans to compensate for radioactive decay. Under these conditions, approximately 13 k counts were collected in each ±8% wide energy windowed projection of the MTF phantom measured in the scatter media. Iterative reconstruction was performed using the same parameters for the projections of the phantom suspended in air.

D. Local MTF Determination

The overall local MTF calculation was computed based on an algorithm presented elsewhere [15], and has been successfully applied in the preliminary local MTF measurements of our 3D X-ray computed mammotomography (CmT) system as well [7]. Once the images were reconstructed, the first step was to manually rotate the images such that each tube could be isolated onto a single slice [Fig. 2(c)]. A binary line image of the outline of
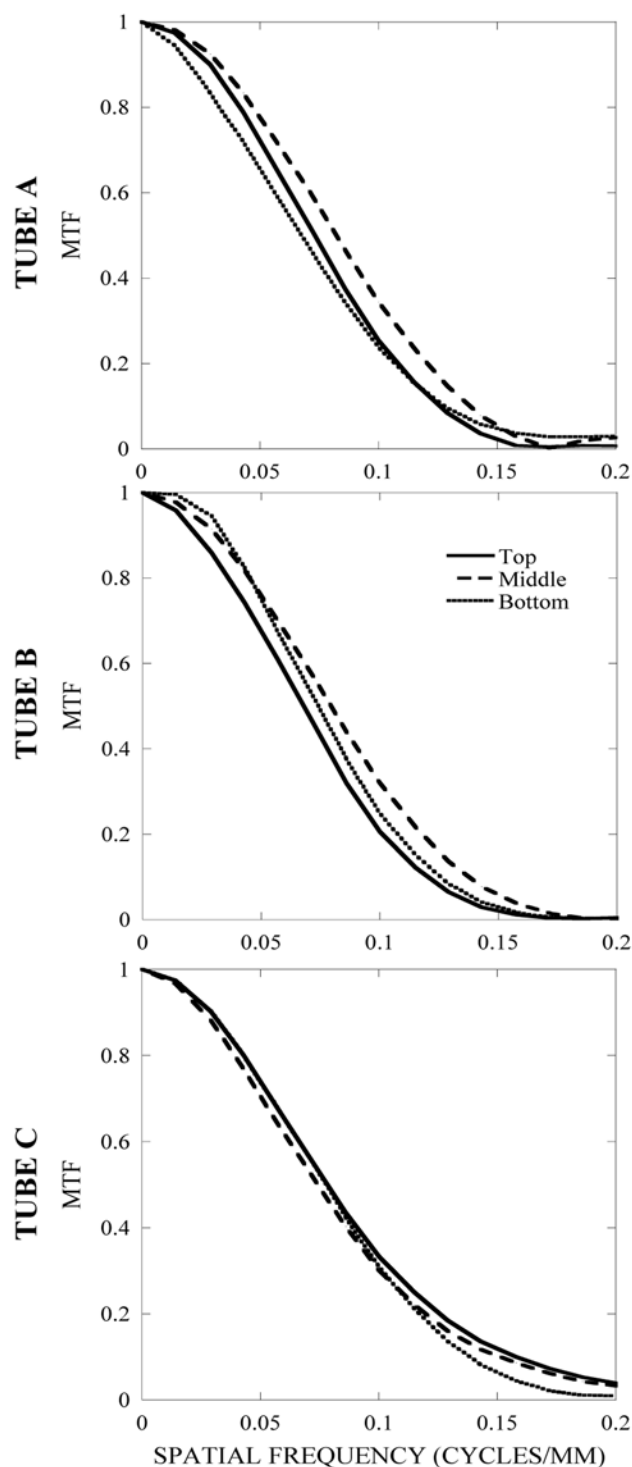

Fig. 4. Results for tube A (top), B (middle), and C (bottom) show little variation in MTFs at different portions along the capillary line source for a 360° SPECT acquisition. MTF measurements were obtained from measurements taken of the phantom in air using a simple VAOR orbit. Nyquist frequency is at 0.2 mm^{-1}.

the tube was acquired by using a Sobel edge detection method [16]. The angle and position of the tube was determined by the Radon transform. Based on the resulting curves in polar coordinate space, the location of the curves' intersection (i.e. maximum intensity) gave an estimate of the angle and spatial position of the line source [17]. Inaccuracy in estimating the true
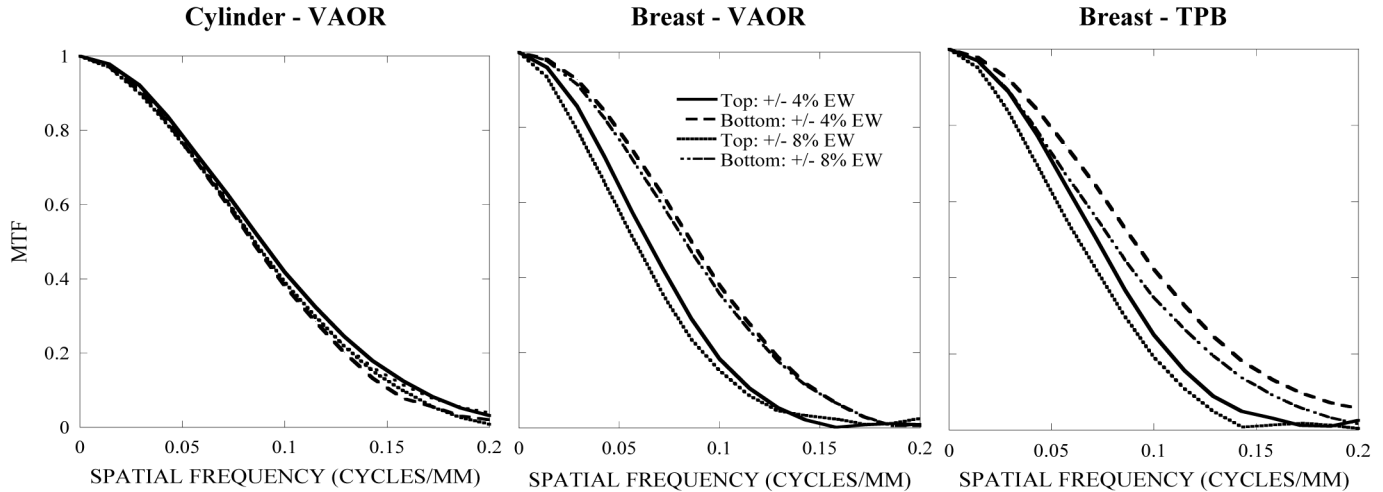
Fig. 5. MTF of the top and bottom segment of the capillary source B placed in a water-filled cylinder (Left) and a water-filled breast shape phantom acquired using VAOR (Middle) and TPB (Right) orbits at $\pm 4\%$ and $\pm 8\%$ energy windows. Tighter energy windows appear to have a slight improvement in resolution especially at the TPB case.
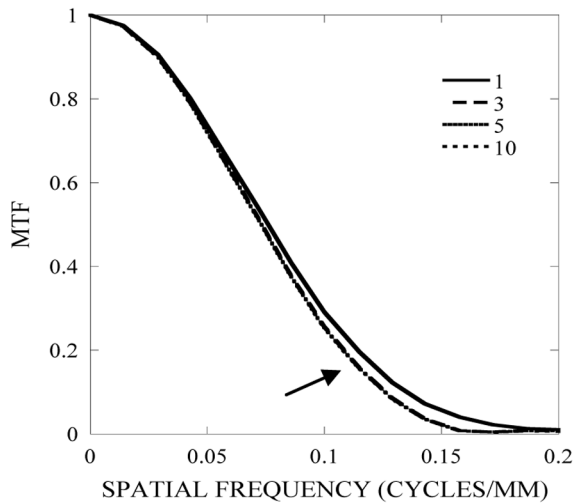

Fig. 6. MTF at several iterations of the phantom in air using VAOR. MTFs overlap for iterations 3, 5 and 10 (shown by arrow). MTF was obtained using the top portion of capillary A.

angle of a line can give an unsmooth LSF and degrade the MTF, especially in higher frequency regions. A composite local LSF was generated by reprojecting and resampling a small region of interest around the line source onto a one-dimensional array of sub-pixel bins positioned perpendicular to the calculated angle of the tube. Use of subpixel bins was necessary since the samples were not uniformly distributed along the one-dimensional array [18]. Different subpixel bin sizes (0.1, 0.3, and 0.7) were initially tested to find an optimal bin size. For smaller bin sizes, such as 0.1, high frequency components were exaggerated in the MTF due to the increased noise. At larger bin sizes, such as 0.7, the zero of the MTF occurred below the Nyquist frequency. Therefore, for this work 0.3 subpixel bin size was found to be the optimal size. The samples were thus binned to 1/3 of the

original pixel size of 2.5 mm. This result was then smoothed by averaging neighboring pixels within a three pixel moving average window to get the final local LSF $(\mathrm{LSF_f})$

$$\mathrm{LSF_f(x)} = \frac{\mathrm{LSF(x-1) + LSF(x) + LSF(x+1)}}{3} \quad (1)$$

where x is the spatial location of the pixel. Smoothing is necessary to reduce the noise and effect of the high-frequency response in the MTF. Zero padding and a Hanning filter were also applied to the local LSF to eliminate other high frequency artifacts.

Corresponding local MTFs were calculated by taking the absolute value of the one-dimensional discrete Fourier Transform of the $\mathrm{LSF_f}$

$$\mathrm{MTF(f)} = |\Im\{\mathrm{LSF_f(x)}\}| \quad (2)$$

where f represents the spatial frequency. The local MTF here describes the magnitude of the component response of the system to the known input. Since an infinitely small line source is not being used, the effects of the finite width of the capillary tube, a, is corrected for by dividing the MTF by $a\,\mathrm{sinc}\,(\pi a f)$. This MTF was finally normalized to yield the final MTF. The MTFs along various parts of the tube (e.g. a "local MTF") were calculated in order to evaluate the response at different locations in the sampled volume [Fig. 2(c)].

For each tube, an average MTF, its standard deviation, and upper and lower bounds for the estimated average MTF was calculated from the measured MTF along different segments of the tube. Using these results, the root mean square difference (RMSD) was calculated by subtracting the upper and lower bounds, squaring the difference, finding the average of all these squared differences, and taking the square root. The measured RMSD values help to evaluate the amount of uniformity in the MTF along different portions of a single line source.
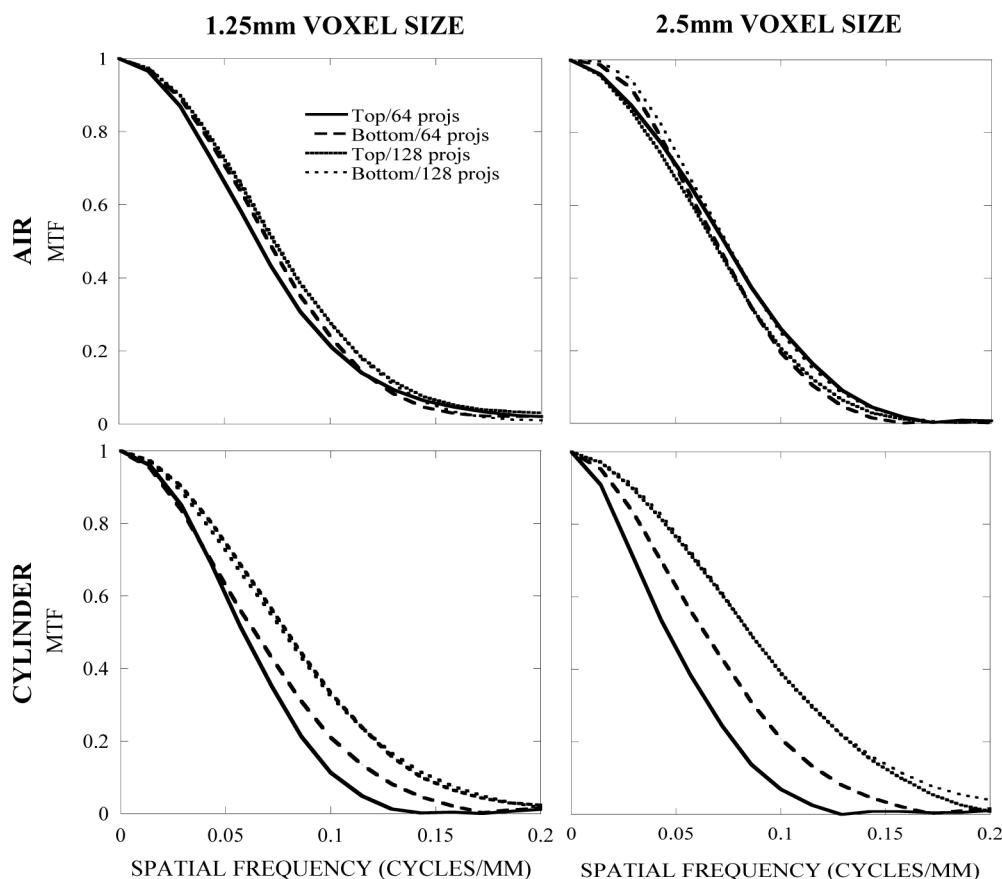
1.25mm VOXEL SIZE **2.5mm VOXEL SIZE**

Fig. 7. (Top row) MTF obtained of the phantom in air at a reconstructed voxel size of (Left column) 1.25 mm (160 × 160 × 160 grid size) and (Right column) 2.5 mm (80 × 80 × 80 grid size). Plots indicate very slight difference between the different numbers of indicated projections. (Bottom row) Unlike in air, the MTF obtained from the phantom in the water-filled cylinder, for both voxelizations, has a greater decrease and more anisotropy in MTF for the 64 projection data set. MTFs shown here were obtained using capillary tube B and VAOR orbital acquisition (see Fig. 2).

III. RESULTS AND DISCUSSION

A. MTF Along Different Line Location

Fig. 4 shows the local MTFs measured in air with the ±8% wide energy window at different locations along each of the nearly orthogonal capillary tubes. Measurements were derived from images collected of the phantom in air using the VAOR orbit. For all three orientations, there was only a small variation in the MTF along the lines, indicating uniform 3D resolution throughout the imaged volume. VAOR orbits are known to be the largest uniformly sampled volumes for both conventional and compact, versatile 3D SPECT cameras [9]. The uniformity of these results is not surprising since the SPECT scan was collected over a 360° azimuthal orbit. Hence, projection "averaging" throughout this reconstructed volume may be expected to yield a nearly uniform response.

B. MTF at Different Energy Window

The MTF was also determined at ±4% and ±8% energy windows to see if different amounts of object scatter would affect the resolution of the reconstructed images. Fig. 5 shows the MTF for one of the capillary tubes in the MTF phantom suspended in the water-filled cylinder and the water-filled breast,

with data acquired using VAOR and TPB orbits at both energy windows. For the cylinder, there is no difference in the MTFs measured anywhere along the line.

For the breast phantom, the MTF results are somewhat different. There are differences in the measured MTFs at different locations, which correspond to the thicker posterior breast (top) or narrower anterior breast near the nipple (bottom), but only slight differences in these locations due to energy window width. Furthermore, using a smaller energy window with incomplete sampling and the TPB orbit also had a very slight effect on the local MTF.

C. MTF With Various Reconstruction Parameters

In OSEM, the projection data is grouped into subsets and the EM algorithm is applied to each subset to get an estimate of the image. In principle, more iterations are performed until the algorithm has converged to a true (or near) optimum value. However this can yield images of poor quality. Previous studies for emission mammotomography imaging breast lesions have shown that there is a trade-off between the rate of contrast improvement and SNR degradation in the reconstructed images [8], [9], [12]. This contrast-SNR roll-over is similar to the minimum of a bias-variance metric. For SPECT mammotomography imaging this roll-off is often best between 2 and 3 iterations.

In a similar way, the measured local system MTF appears to have stopped changing after only a few iterations. Fig. 6 shows the MTF at 1st, 3rd, 5th, and 10th iterations along a single dimension. The slow-down in MTF improvement is probably similar to the slow-down in contrast improvement with increasing iterations. At the 5th and 10th iteration, it appears that there is no change in the MTF beyond the 3rd iteration. The results are similar (not shown) for the other portions of each of the three capillary sources for a uniform orbit such as VAOR.

Using smaller voxel sizes and fewer projection images during iterative reconstruction can also have an effect on the measured resolution (Fig. 7). As voxel size decreases and number of projections increase, the MTF expectedly improves and remains consistent (less anisotropic), especially under non-ideal conditions (i.e. water-filled cylinder) (Fig. 7, BOTTOM). From these plots, it can be inferred that when acquiring fewer projections under non-ideal conditions, the MTF varies significantly due to incompleteness of sampling the scatter distribution and can introduce artifacts in the reconstructed images. However, very small differences are seen in the MTF for conditions without scatter (Fig. 7, TOP). The MTF obtained at 128 projections in the water-filled cylinder appears to be better than in air. This could be due to the increased attenuation and noise in the scatter images which made it more difficult to localize the signal.

D. MTF With Various 3D Trajectories

Other than VAOR, three different trajectories, TPB, CPA, and PROJSINE, were also evaluated by measuring the MTF at three different locations along the capillary tube in air (Fig. 8). RMSD results in Table II indicate small but similar variations in the MTF for VAOR and PROJSINE. The importance of this is that the complex trajectory will likely be necessary for clinical breast imaging [8], [9], while VAOR provides a completely sampled region with the largest volume. The TPB and CPA trajectories yielded a worse MTF in the top portion, but had a better MTF at the bottom portion due to the relative position of the camera to the line sources (Fig. 8). This is most likely due to a combination of incomplete sampling, attenuation, and distance related degradations associated with SPECT imaging.

Fig. 9 shows the difference in spatial resolution among each of the four orbits for the top segment of the capillary tube. Previous studies have shown that insufficient sampling can cause the reconstructed slices to be distorted [9], [12]. For the TPB orbit, in contrast to the bottom segment of the capillary source, the top segment of the capillary tube [shown in schematic in Fig. 2(a)] is never close to the face of the SPECT camera, causing a difference in the measured spatial response.

E. MTF Within Different Object Shapes

Using a VAOR orbit, the MTF was determined for the line phantom suspended in (1) air; (2) a water-filled cylinder; and (3) a water-filled breast phantom using the same, fixed ROR for all three cases. Images reconstructed with 5 iterations and 5 subsets of an OSEM algorithm produced minimal differences between
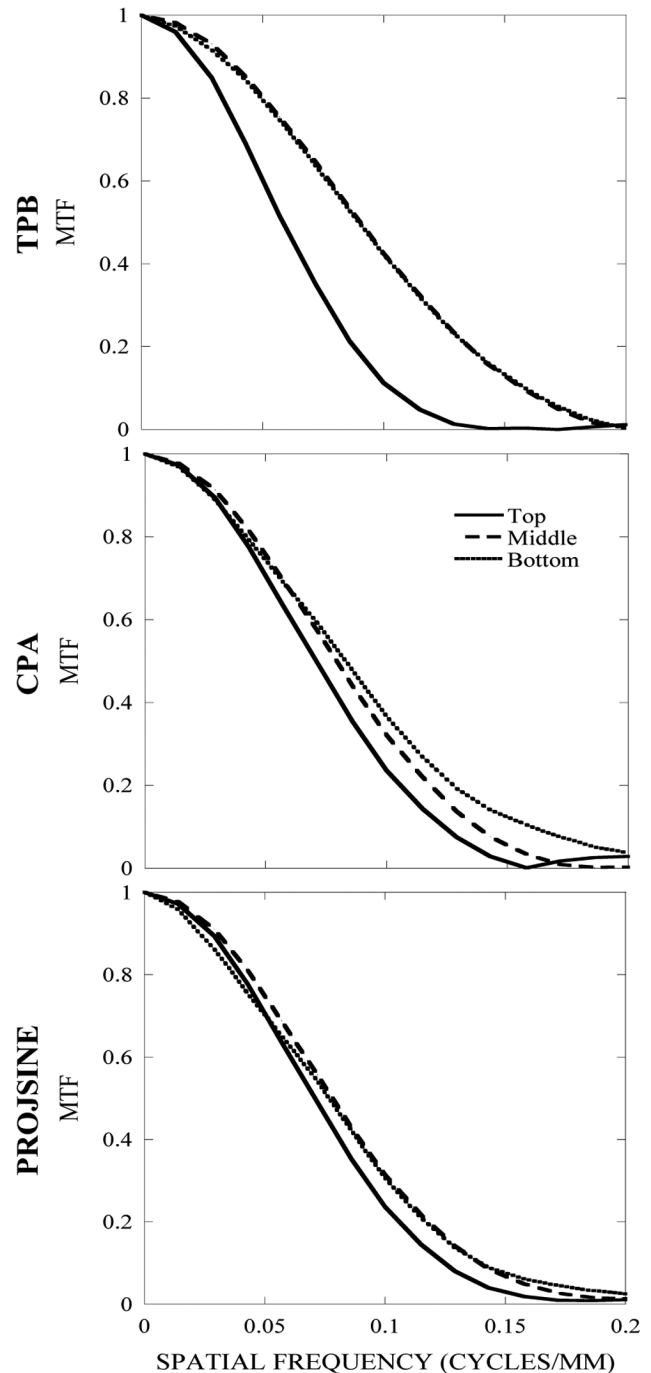

Fig. 8. Using TPB (top), CPA (middle), and PROJSINE (bottom) trajectories, the MTFs were obtained from the top, middle, and bottom segment of the reconstructed line source B. The MTFs for TPB and CPA have more variation among different segments along the tube compared to VAOR (Fig. 4, middle) and PROJSINE. For the bottom line segment, both TPB and CPA actually give a higher MTF than VAOR and PROJSINE due to the bottom segment being closest to the camera throughout the trajectory, as seen in the schematic in Fig. 2(a).

the MTF obtained in air and in the cylinder (Figs. 4 and 7), but showed a slight difference in comparison to the MTF obtained with the breast phantom (Fig. 10) mostly likely due to the differences in object shape (i.e. breast phantom versus a cylinder) and a slight difference in the measured location relative to the measurement in air or with the cylinder. RMSD values for capillary

TABLE II
RMSD VALUES FOR EACH CAPILLARY TUBE ACQUIRED
USING VARIOUS TRAJECTORIES

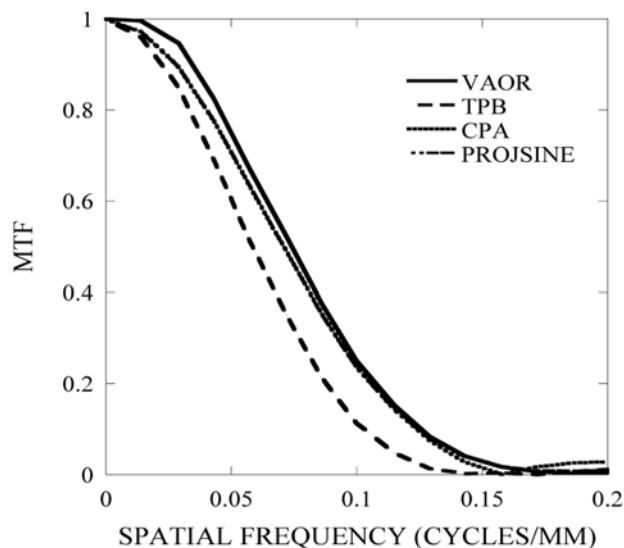| Trajectories	Tube A	Tube B	Tube C
VAOR	0.049	0.044	0.039
TPB	0.145	0.123	0.042
CPA	0.103	0.093	0.091
PROJSINE	0.041	0.032	0.040

Fig. 9. MTFs were obtained from the top segment of the reconstructed line source B for each of the three orbits. TPB produces slightly worse MTFs than VAOR and PROJSINE since the top segment is farther away from the camera for those trajectories.
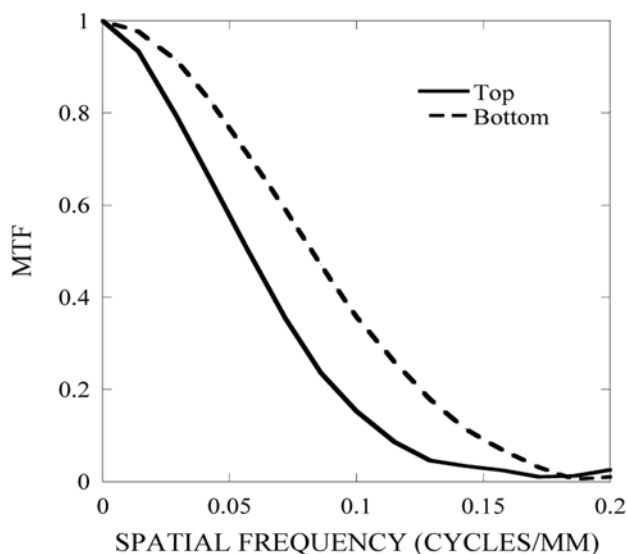

Fig. 10. MTF obtained from the line phantom (capillary tube B) placed in the breast using the VAOR orbit. Unlike MTF curves obtained in air and a cylinder, there is more variation in MTF in a breast phantom.
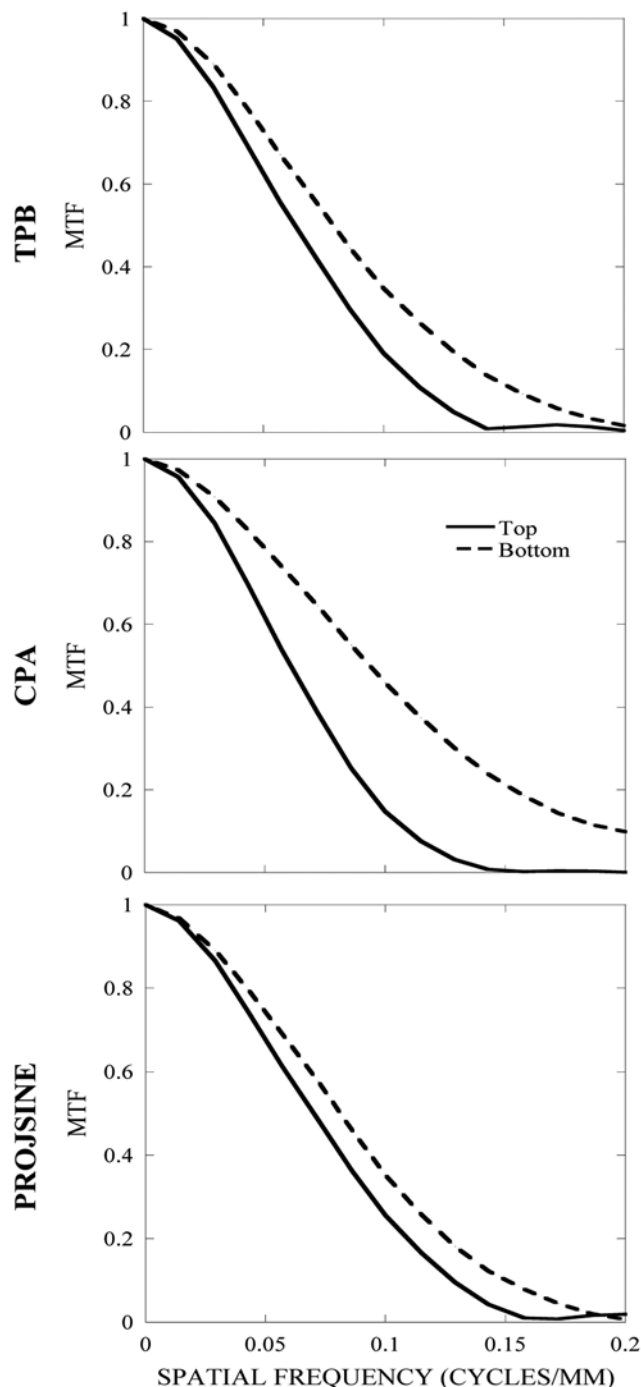

Fig. 11. MTF obtained from the phantom (top and bottom segment of capillary tube B) placed in the breast using TPB (top), CPA (middle), and PROJSINE (bottom) trajectories. Results are very similar to results measured in air.

tube B acquired in air, cylinder, and breast are 0.044, 0.048, and 0.064, respectively. This slight degradation in resolution seen with VAOR in a breast phantom illustrates the necessity of using novel trajectories that use increased camera tilt angles to improve sampling and also achieve a closer ROR. As shown in Figs. 10, 11, and Table III, there is slight variation in the MTFs with VAOR, TPB and CPA trajectories, consistent with earlier results using these trajectories. There is considerably less variation with PROJSINE. Comparisons of all four trajectories are plotted together for the top and bottom segment of the capillary tube (Fig. 12).
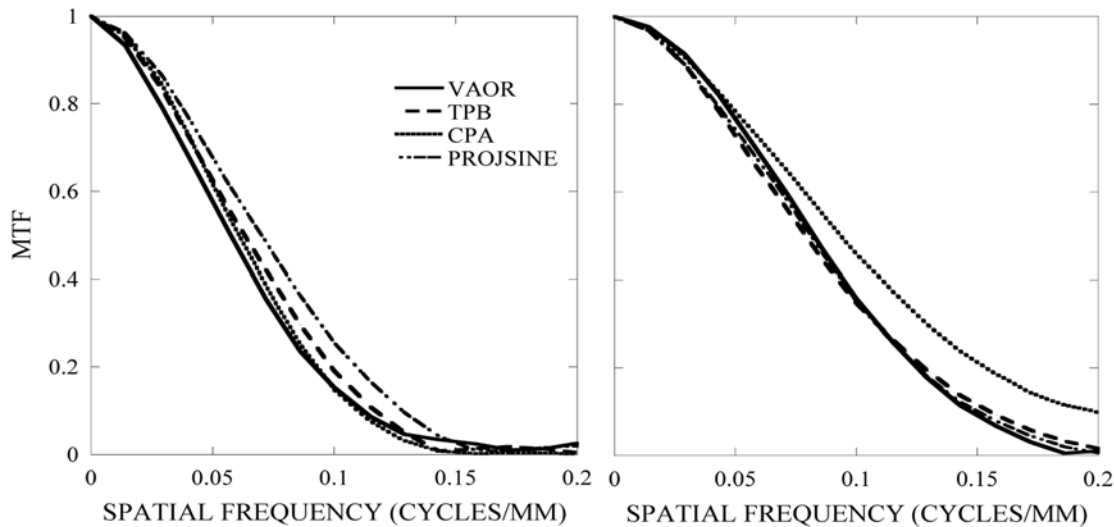
Fig. 12. MTF of the top (left) and bottom (right) segment of capillary source B placed in the breast for all four trajectories.

TABLE III
RMSD VALUES FOR EACH CAPILLARY TUBE IN BREAST ACQUIRED
USING VARIOUS TRAJECTORIES

Trajectories	Tube A	Tube B	Tube C
VAOR	0.056	0.064	0.086
TPB	0.103	0.092	0.122
CPA	0.092	0.119	0.096
PROJSINE	0.050	0.052	0.046

IV. CONCLUSION

In this work, we have developed a novel phantom for use in measuring the local MTF in 3D to evaluate versatile, novel-trajectory emission tomographic systems and provide an insight into the degrading effects caused by different orbital acquisitions, different shaped geometries, and the reconstruction process. This initial study demonstrated that energy window has a secondary effect on resolution, in contrast to incomplete sampling. The relatively small number of OSEM iterations also had little effect on the MTF, and that more projections are necessary in non-ideal conditions (i.e. with attenuation media) to yield an improved and more isotropic MTF. Also, it was shown that unlike for simple circular (VAOR) and more complex (PROJSINE) trajectories, asymmetric acquisition trajectories (e.g. TPB and CPA) have more variations in the MTF between different locations in 3D space. Differences between the curves are caused both by trajectories having fixed polar tilt and subsequently incomplete sampling. This implies that a complex trajectory like PROJSINE more uniformly samples the breast volume of interest and may be necessary for clinical breast imaging. Having flexible 3D positioning about the breast yielded minimal RMSD differences, which is important for high resolution molecular emission imaging.

This study also demonstrates the benefit of using a local 3D MTF phantom to evaluate a tomographic imaging system. With such a phantom, the effect of attenuation, scatter, energy windows, reconstruction process, and 3D trajectories can be easily evaluated to get a better understanding on how these different parameters can affect image quality.

REFERENCES

[1] M. L. Nusynowitz and A. R. Benedetto, "Simplified method for determining the modulation transfer function for the scintillation camera," *J. Nucl. Med.*, vol. 16, pp. 1200–1203, 1975.

[2] T. Väyrynen, U. Pitkänen, and K. Kiviniitty, "Methods for measuring the modulation transfer function of gamma camera systems," *Eur. J. Nucl. Med.*, vol. 5, pp. 19–22, 1980.

[3] M. Coleman, M. A. King, S. J. Glick, K. Knesaurek, and B. C. Penney, "Investigation of the stationarity of the modular transfer function and the scatter fraction in conjugate view SPECT restoration filtering," *IEEE Trans. Nucl. Sci.*, vol. 36, pp. 969–972, 1989.

[4] S. J. Glick, M. A. King, K. Knesaurek, and K. Burbank, "An investigation of the stationarity of the 3D modulation transfer function of SPECT," *IEEE Trans. Med. Imag.*, vol. 36, pp. 973–977, 1989.

[5] S. J. Glick, W. G. Hawkins, M. A. King, B. C. Penney, E. J. Soares, and C. L. Byrne, "The effect of intrinsic attenuation correction methods on the stationarity of the 3-D modulation transfer function of SPECT," *Med. Phys.*, vol. 19, pp. 1105–1112, 1992.

[6] L. R. Furenlid, D. W. Wilson, Y. Chen, H. Kim, P. J. Pietraski, M. J. Crawford, and H. H. Barrett, "FastSPECT II: A second-generation high-resolution dynamic SPECT imager," *IEEE Trans. Med. Imag.*, vol. 51, pp. 631–635, 2004.

[7] P. Madhav, R. L. McKinley, E. Samei, J. E. Bowsher, and M. P. Tornai, "A novel method to characterize the MTF in 3D for computed mammotomography," in *Proc. SPIE Med. Imag. Conf.*, Feb. 11–17, 2006, vol. 6142.

[8] M. P. Tornai, J. E. Bowsher, C. N. Archer, J. Peter, R. J. Jaszczak, L. R. MacDonald, B. E. Patt, and J. S. Iwanczyk, "A 3D gantry single photon emission tomograph with hemispherical coverage for dedicated breast imaging," *Nucl. Instrum. Meth. Phys. Res. A*, vol. 497, pp. 157–167, 2003.

[9] C. N. Archer, M. P. Tornai, J. E. Bowsher, S. D. Metzler, B. C. Pieper, and R. J. Jaszczak, "Implementation and initial characterization of acquisition orbits with a dedicated emission mammotomograph," *IEEE Trans. Nucl. Sci.*, vol. 50, pp. 413–420, 2003.

[10] C. N. Brzymialkiewicz, M. P. Tornai, R. L. McKinley, S. J. Cutler, and J. E. Bowsher, "Performance for dedicated emission mammotomography for various breast shapes and sizes," *Phys. Med. Biol.*, vol. 51, pp. 5051–5064, 2006.

[11] C. N. Brzymialkiewicz, M. P. Tornai, R. L. McKinley, and J. E. Bowsher, "Evaluation of fully 3D emission mammotomography with a compact cadmium zinc telluride detector," *IEEE Trans. Med. Imag.*, vol. 24, pp. 868–877, 2005.

[12] C. N. Brzymialkiewicz, M. P. Tornai, R. L. McKinley, and J. E. Bowsher, "3D data acquisition sampling strategies for dedicated emission mammotomography for various breast sizes," in *Proc. IEEE Nuclear Science Symp. Medical Imaging Conf.*, Oct. 16–22, 2004, vol. 4, pp. 2596–2600.

[13] P. Madhav, C. N. Brzymialkiewicz, S. J. Cutler, J. E. Bowsher, and M. P. Tornai, "Characterizing the MTF in 3D for a quantized SPECT camera having arbitrary trajectories using a novel phantom," in *Proc. IEEE Nuclear Science Symp. Medical Imaging Conf.*, Oct. 23–29, 2005, pp. 1722–1726.

[14] S. J. Cutler, C. N. Brzymialkiewicz, and M. P. Tornai, "Investigating the effects of energy resolution in dedicated emission mammotomography," in *Proc. IEEE Nuclear Science Symp. Medical Imaging Conf.*, Oct. 23–29, 2005, vol. 5, pp. 2537–2541.

[15] E. Samei and M. J. Flynn, "A method for measuring the presampled MTF of digital radiographic systems using an edge test device," *Med. Phys.*, vol. 25, pp. 102–113, 1998.

[16] J. S. Lim, *Two-Dimensional Signal and Image Processing*. Englewood Cliffs, NJ: Prentice-Hall, 1990.

[17] R. C. Gonzalez, *Digital Image Processing*, 2nd ed. Reading, MA: Addison-Wesley, 1987.

[18] H. Fujita, D. Tsai, T. Itoh, K. Doi, J. Morishita, K. Ueda, and A. Ohtsuka, "A simple method for determining the modulation transfer function in digital radiography," *IEEE Trans. Med. Imag.*, vol. 11, pp. 34–39, 1992.

Novel Patient Optimized Acquisition Trajectories for Dedicated Breast SPECT Imaging

KL Perez[1,2], SJ Cutler[1,3], P Madhav[1,3], MP Tornai[1,2,3]

[1] *Department of Radiology, Duke University Medical Center, Durham, NC 27710*
[2] *Medical Physics Graduate Program, Duke University Medical Center, Durham, NC 27710*
[3] *Department of Biomedical Engineering, Duke University, Durham, NC 27708*

Novel acquisition trajectories developed for our dedicated breast SPECT camera move 3 dimensionally within a hemispherical volume, fully contouring a patient's pendent breast and provide a high quality, high resolution 3D functional image. These unique trajectories, created in under a minute, are personalized for each breast of each patient and thus can be altered to maximize the image quality for a particular study. If a suspected lesion location is known prior to the scan, a trajectory can be created with many close and direct views of the lesion. A torso phantom with an attached 1730 mL breast phantom containing a 2.1 mL (0.8cm radius) spherical lesion was filled with clinical levels of activity: heart:liver:torso:breast:lesion concentration ratio 12:12:1:1:6. A variety of acquisition trajectories were employed to image the lesion. Sequential tilted parallel beam trajectories studied the maximum polar angle for imaging the breast and chest wall without views of the heart and liver. Other trajectories were created to obtain the best lesion signal. This study shows PROJSINE trajectories can recover the breast's shape and image into the chest wall. Altering the camera's starting position or subtracting projection views can reduce cardiac and hepatic contamination in the reconstructed image. However, more than one trajectory may provide equivalent image quality. Acquisition trajectories can be created to meet specific imaging goals which consider certain patient factors, such as breast size, lesion location and cardiac and hepatic uptake.

Presented at the
2008 International Workshop on the Molecular Radiology of Breast Cancer
Dresden, Germany
20-21 October, 2008
and published in *2008 IEEE Medical Imaging Conference Record*, 5629-5634.

Improved Chest Wall Imaging through Combined Complex Trajectories in Dedicated Dual Modality SPECT-CT Breast Molecular Imaging

Dominic J. Crotty[1,2], Spencer J. Cutler[1,2], Randolph L.McKinley[3]
Priti Madhav [1,2], Kristy L. Perez[1,4], Martin P. Tornai[1,2,4]

[1]Department of Radiology, Duke University Medical Center, Durham, NC 27710
[2]Department of Biomedical Engineering, Duke University, Durham, NC 27708
[3]Zumatek Incorporated, Chapel Hill, NC 27519
[4]Medical Physics Graduate Program, Duke University Medical Center, Durham, NC 27710

ABSTRACT

In the hybrid SPECT-CT breast molecular imaging system currently in development in our lab, patient positioning is a practical compromise between comfort and a need to maximize the imaged volume of breast and chest wall. While the integrated system rotates under the patient, the CT system is restricted to azimuthal trajectories at a fixed height, but the flexible SPECT system is capable of fully 3D positioning around the pendant breast. The current bed design separates the top of the CT cone beam from the chest wall, thus limiting the system's ability to image this area. This study examines combined complex trajectories, including limited angle tomography for both modalities and raising the entire imaging system during the scan, to more effectively image lesions in or near the chest wall. While emphasizing new CT system trajectories, novel asymmetrical SPECT trajectories are also developed to maximize the imaged volume while avoiding contact with the bed or patient. Various sized lesions filled with low and medium concentrations of ^{99m}Tc activity (10:1 to 3:1) and CT contrast are imaged using a range of trajectories. Dual modality projections are post-processed to mimic limited angle trajectories or trajectories that raise the CT system for a portion of the scan. Reconstructed image metrics including SNR, contrast, attenuation coefficients and lesion profiles are quantified to understand the effect of these trajectories; image registration effects are also examined in addition to the effect that raising the system has on acquisition sequencing for the orthogonally placed sub-systems. Initial reconstructed images from data sets with trajectories that removed 60° of SPECT and CT azimuthal data and trajectories combining limited angle acquisition with vertical system shift qualitatively show a significant increase in observed volume while maintaining lesion visibility. Simple system shifting in mid-scan thus appears to improve chest wall imaging for both modalities.

Initial Investigation of Novel Trajectories to Improve Chest Wall Imaging in a Dedicated Breast Computed Tomography System

Dominic J. Crotty[a,b], Randolph L. McKinley[c], Priti Madhav[a,b], Spencer J. Cutler[a,b], Martin P. Tornai[a,b]

[a] Department of Radiology, Duke University Medical Center, Durham, NC 27710
[b] Department of Biomedical Engineering, Duke University, Durham, NC 27708
[c] Zumatek Incorporated, Chapel Hill, NC 27514

In current dedicated breast computed tomography (mammotomography) systems, comfortable patient positioning on a stationary bed restricts the practicable range of source-detector trajectories, thus compromising the system's ability to adequately image the patient's anterior chest wall. This study examines the effect on detecting small, low-contrast lesion-like-spheres using limited angle x-ray source-detector trajectories and trajectories that intentionally raise the tomographic imaging system mid-acquisition. These modified acquisition paths may increase chest wall visualization, simplify the design of the imaging system and increase patient comfort by allowing the design of an improved patient bed. Thin walled balloons of various volumes filled with iodine act as surrogate high contrast lesions to initially investigate the effect of these novel trajectories. Then, stacks of 5mm acrylic spheres regularly spaced in concentric circles are placed in water to simulate a low contrast environment in a uniform scatter medium. 360° azimuthal scans are acquired at various bed heights with contiguous projections subsequently removed to create limited angle acquisitions from 240-360°. Projections from the different bed heights are interwoven to form trajectories that mimic discontinuously raising the imaging system mid-acquisition. The resulting iteratively reconstructed volumes are evaluated with an observer study. Initial images suggest that using limited angles and raising the system is possible while increasing the observer's ability to visualize objects near the chest wall. Based on the results of this study, an improved patient bed to facilitate chest wall imaging will be designed, and the feasibility of vertical system motion to increase imaged breast volume explored.

Keywords: CT, CTCB, MG, PER, breast CT, mammotomography, complex trajectory, cone beam CT

Presented at the
2009 SPIE Medical Imaging Conference,
Orlando, FL,
and published in *2009 Proc. SPIE: Physics of Medical Imaging*, 72585L-10.

Towards Quantification of Dedicated Breast SPECT Using Non-Traditional Acquisition Trajectories

Kristy L. Perez[1,2], Spencer J. Cutler[1,3], Priti Madhav[1,3], Martin P. Tornai[1,2,3]

[1] *Department of Radiology, Duke University Medical Center, Durham, NC 27710*
[2] *Medical Physics Graduate Program, Duke University, Durham, NC 27710*
[3] *Department of Biomedical Engineering, Duke University, Durham, NC 27708*

Quantification of radiotracer uptake in lesions gives valuable information to physicians in deciding patient care or determining treatment efficacy. While more routinely done in PET, quantification is still less common for routine SPECT imaging. Physical processes and, with systems capable of 3D trajectories, reconstruction artifacts can yield an incorrect absolute activity of the tracer. Differences in the obtained activity value from each trajectory are investigated to determine if the acquisition trajectory can be used for quantification. For these experiments, a fillable 600mL breast and 2.3mL lesion phantoms containing aqueous ^{99m}Tc pertechnetate were imaged with a dedicated dual-modality SPECT-CT scanner. SPECT images were collected using a compact CZT camera with various 3D acquisitions including vertical (VAOR), 45 degree tilted (TPB), and complex sinusoidal (PROJSINE) trajectories. Collimator and detection efficiencies of the SPECT camera were incorporated into the OSEM iterative reconstruction. Attenuation correction was implemented using a uniform attenuation coefficient matrix, but in the next steps will be done with scaled volumetric CT images. In addition, a Compton Window scatter correction method was applied with an empirically determined k value of 0.3 and a scatter window ranging from 113 to 133 keV, abutting and below the 8% photopeak window. A line source was used to determine a scaling factor of 0.07 to correct reconstructed data to activity. The resulting calculated lesion activity in the image was found to be within 20.5% (+/- 9.9%) of the dose calibrator measured activity value. The scaled breast background values were double the dose calibrator measured activity value indicating that further investigation of the linearity of the method is needed. As far as we are aware, this is the first time that absolute quantification has been applied to SPECT data acquired with non-traditional, non-circular trajectories.